João Miguel Macau da Maia

Licenciado em Ciências da Engenharia Química e Bioquímica

Molecular Simulation of Gas Adsorption Equilibria in Nanoporous Materials

Dissertação para obtenção do Grau de Mestre em
Engenharia Química e Bioquímica

Orientador: José Paulo Barbosa Mota, Professor Catedrático, FCT/UNL

FACULDADE DE CIÊNCIAS E TECNOLOGIA
UNIVERSIDADE NOVA DE LISBOA

Setembro, 2014

Molecular Simulation of Gas Adsorption Equilibria in Nanoporous Materials

Dissertação para obtenção do Grau de Mestre em

Engenharia Química e Bioquímica

Orientador: Professor Doutor José Paulo Barbosa Mota

Monte da Caparica, Faculdade de Ciências e Tecnologia, Universidade de Lisboa

Setembro 2014

Molecular Simulation of Gas Adsorption Equilibria in Nanoporous Materials

Acknowledgements

Although the elaboration of this thesis consists in an individual work, its completion couldn't be possible without the help of innumerous people. The fundaments and constructive critics given in more complicated time, was a real help to overcome some problems and to in light some lack of understanding. For that I would like to focus my gratitude towards my thesis supervisor, Doctor Prof. José Paulo Mota, for his support and especially for teaching me types of knowledge that are very useful in terms of time and money. In my opinion, engineering is a question of efficiency and those two terms, have a very significant role.

I also want to express my gratitude to Professor Mário Eusébio for his support during and before this thesis. I have learned that the difference between a real project and the theoretical one, relies on real simple details.

Regarding my group coworkers, Fernando Cruz, Isabel Esteves, Rui Ribeiro, Alison Setim and Bárbara Camacho, I would like to acknowledge their their support and friendship and the opportunity given to collect real experimental data.

I want to acknowledge the Faculdade de Ciências e Tecnologia, UNL, and in particularly the Chemistry Department, for all that I've learn in where, my degree and for the all the possibilities that it opens for my future.

I want to thank all my friends for their support and concern. I Also want to thank them for their great advices. They helped me to keep focus on what is, and what is not important, and they showed me that science is not only numbers and words; science is real world changes.

Finally I want to thank all my family! To all my cousins, to all my uncles and aunts, to my sister in law and to my brother, thank you for never doubting me! For that reason I hope to one day correspond to all of your expectations and give back to you as much as you have given me. The dearest thanks go to my mother and to my grandparents. Without you, none of what I have achieved could have been possible and for that no words can express my gratitude. I can only say that, there are no good or bad, easy or difficult paths, only exists numerous ways of facing it.

To all, without exception, a great thanks!

João Macau Maia

Abstract

This work is divided into two distinct parts. The first part consists of the study of the metal organic framework UiO-66Zr, where the aim was to determine the force field that best describes the adsorption equilibrium properties of two different gases, methane and carbon dioxide. The other part of the work focuses on the study of the single wall carbon nanotube topology for ethane adsorption; the aim was to simplify as much as possible the solid-fluid force field model to increase the computational efficiency of the Monte Carlo simulations.

The choice of both adsorbents relies on their potential use in adsorption processes, such as the capture and storage of carbon dioxide, natural gas storage, separation of components of biogas, and olefin/paraffin separations.

The adsorption studies on the two porous materials were performed by molecular simulation using the grand canonical Monte Carlo (μ,V,T) method, over the temperature range of 298-343 K and pressure range 0.06-70 bar. The calibration curves of pressure and density as a function of chemical potential and temperature for the three adsorbates under study, were obtained Monte Carlo simulation in the canonical ensemble (N,V,T); polynomial fit and interpolation of the obtained data allowed to determine the pressure and gas density at any chemical potential.

The adsorption equilibria of methane and carbon dioxide in UiO-66Zr were simulated and compared with the experimental data obtained by Jasmina H. Cavka et al. The results show that the best force field for both gases is a chargeless united-atom force field based on the TraPPE model. Using this validated force field it was possible to estimate the isosteric heats of adsorption and the Henry constants.

In the Grand-Canonical Monte Carlo simulations of carbon nanotubes, we conclude that the fastest type of run is obtained with a force field that approximates the nanotube as a smooth cylinder; this approximation gives execution times that are 1.6 times faster than the typical atomistic runs.

Keywords: metal organic framework, carbon nanotubes, adsorption, gas, molecular simulation, Grand Canonical Monte Carlo (GCMC).

Resumo

O trabalho realizado pode ser dividido em duas partes distintas. A primeira parte, baseia-se no estudo de uma estrutura organo-metálica porosa, o UiO-66Zr, onde o principal objectivo foi encontrar o melhor campo de forças que traduz, com mais exatidão, as propriedades de adsorção dos dois gases em estudo, metano e dióxido de carbono. A segunda é relativa ao estudo de adsorção de etano num nanotubo de carbono de parede única, em que o objectivo foi encontrar um campo de forças simplificado que originasse tempos de computação mais curtos.

A escolha de ambos os adsorventes baseia-se nas suas capacidades para o processo de adsorção, em quer ambos mostraram ser bastante promissores. Processos como: Captura e armazenamento de dióxido de carbono; armazenamento de gás natural; separação de componentes provenientes de biogás; separação de olefinas/parafinas, entre outros.

Os estudos de adsorção feitos nos dois adsorventes, foram feitos através de simulação molecular, utilizando o método de Monte Carlo no conjunto grande canónico (μ,V,T). Para uma gama de temperaturas que vão destes os 398-343 K e num range de pressão 0.06-70 bar. Em relação às calibrações realizadas para os três tipos de adsorbatos, essas, foram obtidas através de simulação de Monte Carlo no conjunto canónico (N,V,T), onde uma interpolação de uma equação polinomial foi feita com os dados recolhidos.

Tendo em conta o UiO-66Zr, foi obtida a quantidade total adsorvida em função da pressão do sistema e comparada com os dados experimentais obtidos por Jasmina H. Cavka et al.. Conclui-se que o campo de forças que melhor representa o fenómeno de adsorção, para os dois gases, no UiO-66Zr foi o campo de forças de átomos agregados sem cargas. Com esse campo foram também recolhidas informações acerca do calor isosterico e das constantes de Henry.

Para as simulações de Monte Carlo (GCMC) com um único nanotubo de carbono, conclui-se que o campo de forças mais rápido é campo de forças que assume que a parede to nanotubo é lisa..Este campo de forças é 1.6 vezes mais rápido que as simulações atomísticas.

Palavras-chave: estrutura metálica orgânicos, nanotubos de carbono, adsorção de gás, simulação molecular, o Grand Canonical Monte Carlo (GCMC).

List of Abbreviation, Variables and Notations

Abbreviations

BET	Brunauer–Emmett–Teller Isotherm Model
BIF	Boron-Imidazolate Frameworks
BTC	Benzenetricarboxylate
C_2H_6	Ethane
CH_4	Methane
CNT	Carbon Nanotubes
CO_2	Carbon Dioxide
COF	Covalentorganic Frameworks
CVD	Chemical Vapor Deposition
DFT	Density Functional Theory
DOE	U.S. Department Of Energy
DREIDING	Force Field
GCMC	Grand Canonical Monte Carlo
IRMOF	Isoreticular Metal Organic Framework
IUPAC	International Union Of Pure And Applied Chemistry
LJ	Lennar Jones
MANIAC	Mathematical Analyzer, Numerical Integrator, And Computer
MC	Monte Carlo
MD	Molecular Dynamics
MIL	Materials Of Institute Lavoisier
MOF	Metal Organic Frameworks
MWNT	Multi Walled Nanotube
NLO	Non-Linear Optical
NOAA	U.S. National Oceanic And Atmospheric Administration
OPLS	Optimized Potentials For Liquid Simulations
SWNT	Single Walled Nanotube
TIF	Tetrahedral-Imidazolate Frameworks
TraPPE-UA	Transferable Potentials For Phase Equilibria-United Atom
TraPPE-EH	Transferable Potentials For Phase Equilibria-Explicit Hydrogens
UFF	Universal Force Field
UiO	Universitetet I Oslo
XRPD	X-Ray powder diffraction
ZIF	Zeolitic-Imidazolate Frameworks
ZMOF	Zeolitelike Metal-Organic Frameworks

Variables and Notations

μ	(kJ mol^{-1})	Chemical Potential
ε	(J)	Lennar Jones Parameter. Well Depth
θ		Fractional Filling Of The Micropore
Λ	(nm)	Thermal de Broglie Wavelength
ρ_{ai}	(nm^{-1})	Apparent Density Of The Adsorbate Phase
ρ_P	(nm^{-1})	Apparent Density Of Solid Phase
σ	(K)	Lennard-Jones Parameter. Distance at which the potential between the two particles is zero
ϕ	(K)	Dihedral Angle
Ω		Total Multiplicity Of States
<...>		The Ensemble Average Number
C_h	^{o}	Chiral Vector
F	J	Free Helmholtz Energy
G	($J.mol^{-1}$)	Free Gibbs Energy
H	J	Enthalpy
K		Equilibrium Constant
k_a		Adsorption Constant
k_B	($J.K^{-1}$)	Boltzmann Constant = 1.38066x10-23 J/K
k_d		Desorption Constant
K_H	($mol.kg^{-1}.bar^{-1}$)	Henry Constant
K_L		Freundlich Constant
N/n		Number Of Particles
P	(bar)	Pressure
Q	($kJ.mol^{-1}$)	Heat
q_s	($mol.kg^{-1}$)	Saturation Loading
Q_{st}	($kJ.mol^{-1}$)	Isosteric Heat Of Adsorption
q_T	($mol.kg^{-1}$)	Total Amount Absorbed
R		Ideal Gas Constant
r	(Å)	Position
r_{cut}	(Å)	Cutoff Radius
S	(J/K)	Entropy
T	(K)	Temperature
U	(kJ)	Internal Energy
U^{bend}	(kJ)	The Bond Bending Energy For The Angle Formed By Two Successive Chemical Bonds
U^{bond}	(kJ)	Potential energy of a single chemical bond
U^{el}	(kJ)	The Columbic Interaction Energy
$U^{torsion}$	(kJ)	The Torsional Energy Due To The Dihedral Angles Formed By Four Successive Atoms In A Chain
U^{VW}	(kJ)	The Van Der Waals Interaction Energy
V		Volume
W		Work
Z		Partition Function

Table of contents

List of Figures

List of Tables

1 Background

1.1 Motivation

The continue increase of the energy demand and its effect on the world economy and environment are the main impulse for new studies and technologies. A sustainable and efficient process to harvest and sustain many forms of energy is fundamental to ensure the reliable and sustainable use of such new technologies. Nowadays many forms of energy can be used; they can be divided into two major classes: non-renewable energy sources and renewable energies sources. Until now the use of non-renewable energy sources has been very important for human development, due to their high energy density and the innumerous sub-products that can be obtained from them. However, the improper consumption of such forms of energy results in severe effects on the environment.

The burning of non-renewable fuels, such oil and its derivatives, results in tremendous amounts of carbon dioxide released to the atmosphere. Carbon dioxide absorbs easily the infrared radiation and thus contributes intensely to the greenhouse effects. It is clear that the proper choice of the type of fuel that can be used has a significant impact on the environment. Today many developed countries are adopting new policies in term of the amounts of carbon dioxide released.

The investment that is made on new technologies depends on the world economics and for that, technologies must be not only be efficient and less polluting but also economically viable [1].

The large reserves of natural gas, as well as the increasing interest in shale gas, and the fact that methane is considered and as an environmentally friendly fuel gas, is leading investors to bet on this type of fuel. Although methane production derives from nonrenewable energy sources, it emits much less carbon dioxide than liquid hydrocarbon fuels due to his high hydrogen/carbon ratio. The problem with methane is that it is a gaseous fuel and thus it is not easy to store it compactly and safely [2].

One method that is attracting much attention is the adsorptive storage and the separation and purification of gas mixtures by adsorption. Physisorption methods can be used with relative simplicity and by choosing the proper adsorbent and the right conditions it is possible to separate and store a wide variety of compounds [3].

The development of new adsorbent materials, such as metal organic frameworks and carbon nanotubes, has originated many new adsorbents with different properties, which can be tailored to enhance their adsorption capacity and/or selectivity. The metal–organic frameworks have recently shown a strong research interest because of their rigid structures, large pore volumes, tunable pore sizes, large surface areas, and potential applications as novel adsorbents. Regarding the adsorption properties of the carbon nanotubes, their large surface areas and 1-D nature of their porous topology are setting the carbon nanotubes as a very promising adsorbent. [4] [5]

The experimental study of numerous porous materials can be time consuming and many times not cost effective. In order to overcome that handicap, computer simulation has been steadily developed and matured since the 1950's, with the aim of replacing many experiments with accurate precision. For the study of adsorption, computer simulation offers many possibilities, since it is easy to experiment with many materials under different thermodynamic conditions.

To properly perform a computer simulation it is important to understand what is a computer simulation, how it works, and what method it is based on.

The study and work in thermodynamics made by many scientists since sixteen century, proved to be one of the most importance of all fields of science. Driven by the invention of the steam engine, it represents an important role in the history of physics, chemistry, classical mechanics and quantum mechanics, which allow making great discoveries that have change the world for what we know today. Therefore it is of most importance to understand the basis of the innumerous concepts that forms thermodynamics, facilitating the conjugation between the real world changes and its mathematical expression.

In this thesis the comprehension of thermodynamics will focus on the process of adsorption and the variables that govern this phenomenon. Their mathematical expression will able us to compute data and simulate adsorption, not only for a single adsorbent and adsorbate, but for a variable range of compounds. This is a real advantage compared to the experimental process, where the measurement of an isotherm is a time consuming task whereas its simulation only takes a fraction of it. So, in order to obtain a very good molecular simulation it is fundamental to have all terms correctly and understand how they will change with the variation of some parameters, such as: temperature; pressure; volume and number of particles in the system under study.

In this chapter, we try to give the fundamental aspects of thermodynamics and how they are related to the simulation performed. The objective is to obtain the total of molecules present in the simulation box that is defined by the equilibrium state. This state of equilibrium in the simulation box is a function of a series of intensive and extensive variables that are related to the average of molecular kinetic and potential energy.

We consider the concept called *Ergodicity*, introduced by Boltzmann in 1887 and developed later by J.Willard Gibbs in 1902, where it is proposed that the mean of a certain property in space, regarding to the position in the system, is equal to the average of that property over time. For this matter it is possible to obtain statistical averaged properties by two different methods: one that computes averages over the simulated time, called Molecular Dynamics, and other that computes averages over a number of trial configurations of the system, called Monte Carlo simulation. Both have advantages and disadvantages; the one selected for a particular problem depends on the type of properties that we wish to compute and the time of the computation.

Conjoining the work done by Boltzmann and Gibbs in statistical thermodynamics and using some slapping methods it is possible, choosing the proper force field for each single molecule and the excitations that will occur in the neighborhood of these molecules, to find the lower energy level in a system and consequently the equilibrium, being this, the basis to the Monte Carlo (MC) simulation.

That equilibrium can only be obtained after a sufficiently long time. The concept of time in this type of simulations consists in a certain number of steps that are defined initially. It's also important to mention that in the statistical thermodynamic, properties are calculated on the probability of finding the system in a specific state and so it is expected so observe a stabilization of the averages as time passes once the most probable state is the one wich has more significance to the final results. The stabilization observe, results in the algorithms and slapping methods employed in MC simulation and does proved to have an important role in the final estimation [6] [7].

1.2 Fundamental Concepts in Thermodynamics

The thermodynamics name result in the combinations of two Greek word, *therm* and *dynamis*, heat and power respectively. It's the science of energy where the temperature has a very important role. Emerging after the construction of the steam engines, many developer and scientists, such as Thomas Savery, Thomas Newcomen, Carnot, Rankine, Clausius, Kelvin, Gibbs, contribute to the formulation of thermodynamic principles that describe the conservation and conversion of energy. For this, many formulations, concepts and laws where introduced to explain a field of science that is based entirely on logic, and so, it is essentially to understand the most important definitions.

1.2.1 Systems

In thermodynamics a system is a part of the physical universe and it is delimited by a specified boundary. In order to make good predictions on the thermodynamics properties of the system, the system must be composed by a large number of particles, in the order of the 10^{23} - 10^{25}. Because thermodynamics is an average of the microscopic properties a large number of particles have a benefic effect of the statistical values, there for is pre-establish that a number of particles N, must be higher than 10^{15} order.

A thermodynamic system has a well-defined geometric volume and its boundaries separates the inside from the outside, that system can also be continuous, discontinuous, or discrete. In the simulation performed we use a simulation box that corresponds to a part of a discrete system. The simulation tool uses then the data from that box and replicates that box into others that will form the surrounding environment, simulating then a discrete system.

In any case, a thermodynamics system is a very dynamic system and so there are innumerous degrees of freedom that it should take into account. Because of that, determination of the properties becomes a very stiff process and for that, there is the need to characterize ideals systems in various types. Mainly a system can be divided into three major types: isolated system; close system; open system.

Isolated systems cannot exchange energy and matter with the exterior, therefor there is no interaction with is neighborhood. Their walls are restrictive to the change of energy, volume and number of particles. So heat (Q), volume (V) and number of particles (N) are constant true time.

Close systems are the systems that can change energy with the exterior but not matter. So the only thing that remains constant is the number of particles.

Open systems allow the exchange of matter and energy. These systems are the most related to real exchanges and therefor heat, volume and the number of particles are not constant. For that reason, predicting their thermodynamics properties is a more complex process. Classical thermodynamics deals especially with close systems, for open systems statistical thermodynamics is the most suitable.

1.2.2 Thermodynamic properties

Thermodynamics properties consist in the physical or chemical attributes that specify the macroscopic characteristic properties of a system. These macroscopic properties result from the statistical averages of the observable microscopic coordinates of motion and position, being that motion set by a momentum or kinetic energy and position by potential energy.

It is possible to define two types of thermodynamics properties: intensive and extensive properties. Extensive properties are dependent on the size of the quantity of matter in a system. Mass, energy, entropy are just a few examples, and such properties are additives. On the other hand, properties like temperature, pressure and others are intensive properties and are not dependent on the size of the quantity of matter in a system, and some, can be express as derivatives of extensive properties. Thermodynamics properties can also be conservative and non-conservative. Conservative properties in isolated system do not change, that also means that besides the path that a certain properties takes to point A to point B, and then returns to point A by other path is initial values will remains de same. Properties like energy, mass, momentum, and others, are conservative properties. A very simple example of a conservative property is the potential energy, where it value only depends on the height of the object and not the path that he made to get there. Non-conservative properties change their energy to the system as they move along the point A to the point B, that energy is converted into a form which can't be used by these properties again one example is the work done by friction.

A system will be defined by a set of extensive and intensive thermodynamics properties, being the most usual the heat (Q), the entropy (S), the volume (V), the number of particles (N), the temperature (T), the pressure (P) and the chemical potential (μ).

1.2.3 Energy

Energy is a conservative and extensive property of every system and it can be transferred between systems by the flow of heat and mass or by work exerted by one system on the other. There are also different forms of energy, the most common being internal, potential, kinetic. Depending of the type of the system that is under study, it is possible to obtain different types of variations of energy in the system. In order to fully calculate the parameter of interests, it is more useful to measure the variation of the energy than the total energy of the system. That calculation is done taking into account a reference state and so, the final energy of the system after a perturbation is the sum of the reference state plus the variations that occur in the systems. It is important to refer, that to occur a variation in the system some energy must be spent doing work or to transfer heat; by definition this energy is called free energy of the system. The variations of energy depend not only of the type of the system and boundaries, but also depend of the different types of forms. When the free energy reaches a minimum value, the the system is under thermodynamic equilibrium.

1.2.4 Boundaries

Systems are separated from the exterior by a boundary and so all the work and heat done to the systems have to cross that boundary. In order to simplify the process and diminish the degrees of freedom it is establish some restrains on these boundaries. The types of boundaries also have a very important role to the determination of the thermodynamics properties, and depending of the types of boundaries that are in study it's possible to relate them to real working conditions. So in order to do that, it's used the extensive and intensive thermodynamics properties present earlier, given them some restrain and creating then, the various types of boundaries for each types of system. Next, its present the major types of boundaries and how they affect the change of the thermodynamics properties.

1.2.4.1 Adiabatic Boundaries

Adiabatic Boundaries are restrictive only to the change of heat and so any of the other major properties aren't constant.

(Q = const, S ≠ const, U ≠ const, V ≠ const, N ≠ const T ≠ const, P ≠ const,)

1.2.4.2 Rigid Boundaries

Rigid Boundaries don't allow the variation of the volume, therefor the introduction of particles in the systems will result in the increase of pressure.

(V = const, P ≠ const, Q ≠ const, S ≠ const, U ≠ const, N ≠ const T ≠ const,)

1.2.4.3 Moving Boundaries

Moving Boundaries basically are the reverse of a rigid Boundary. They don't allow the variation of pressure and therefor the introduction of particles in the systems will result in the increase of volume.

(P = const, V ≠ const, Q ≠ const, S ≠ const, U ≠ const, N ≠ const, T ≠ const,)

Choosing then the right system and the right boundaries, it's possible to represent correctly the real system in study and construct the correct mathematical expression for the free energy. However not only the characterization of the system and is boundaries it's enough and for that reason it was necessary to formulate the laws of thermodynamics.

The choice of the types of boundaries will depend of the conditions of experimental work that is being done. In chemistry it's easier to maintain the system at constant pressure than the volume and for that reason it's often chosen moveable boundaries.

1.2.5 Laws of thermodynamics

Only with the formulations of the laws of thermodynamics it was possible to predict the behavior of macroscopic systems. Those laws result in a large amount of equations and axioms based entirely on logic, attached to well-defined constraints. These laws are the building block to all thermodynamics and the concept of energy and their conservation couldn't be possible to express without them.

1.2.5.1 The zeroth law of thermodynamics

The zeroth law, allow to build up a universal temperature scale and it states that if a system A is in equilibrium with system B, and if system B is in equilibrium with system C, then system A is in equilibrium with system C. If a system is in thermal equilibrium, it is assumed that the energy is distributed universally all over the volume. Also state that if the energy of a system increases the temperature of that system also increases

1.2.5.2 The first law of thermodynamics

Energy is defining as a conservative force so depends only on the initial and final states, not on the path between these states and so it's is possible to arrange a mathematical expressing to the internal energy. The use of a cyclic integral assures, Eq. 1.1, that when a specific variable returns to the initial state their value will be the same. This condition ensures the conservation of energy in the universe. [8]

$$\oint \boldsymbol{U} = \mathbf{0} \qquad \textbf{Eq. 1.1}$$

The first law considers then, that the variation of the internal energy depends on the work done by the environment into the system, by definition it's a positive value and, depends on the heat receive into the system, that by definition it's is a positive value as well.

$$\boldsymbol{dU} = \boldsymbol{dQ} + \boldsymbol{dW} \qquad \textbf{Eq. 1.2}$$

In general, the term δW represents all different forms of work, being the most commonly used the work done by compression, by surface deformations and by and chemical work (μdni).

$$\boldsymbol{\delta W} = -\boldsymbol{PdV} + \boldsymbol{\sigma dA} + \mu\boldsymbol{dni} \qquad \textbf{Eq. 1.3}$$

Where (-PdV) is the compression work, related with the pressure and volume, (σdA) is the surface deformations work, related to the surface tension and the area and (μdni) the chemical work, related with the chemical potential and the number of molecules.

1.2.5.3 The second law of thermodynamics

The second law results of the empirical observation of some process that occurs in nature, and it's very important to define the direction of the flow of energy and when it's stops. This, states that in a process containing two systems, the flow of energy will goes in the direction of the hotter system to the colder system until they reach the equilibrium. To express this occurrence correctly, it was needed to formulate a new property named entropy. This property was introduced by Carnot in 1824 and further developed by Clausius and Kelvin in mid-1850. [7]

1.2.6 Entropy

Whit the formulation of the second law and whit the use of statistical mechanics it was possible to define Entropy (S). This property is a non-conserved and extensive property of a system in any state and its value is part of the state of the system. The change of energy in the system will results then in the destruction of creation of entropy.

It's often said that entropy is a disorder of a system however this definition it's not the best one to express this property properly. So entropy is actually a function of a natural logarithm of the total multiplicity of states (Ω). Analyzing the probability of the multiplicity of given state, it is observed that the most likely value is one that has a higher multiplicity for a given state and so the entropy will have a maximum value when it's in equilibrium. That probability is depend of the quantity of energy in the system and is increase will allow reaching higher states of energy.

The expression of the entropy related to the multiplicity of states was formulated by Boltzmann.

$$S \equiv k_B * \ln \Omega_T \qquad \textbf{Eq. 1.4}$$

Where kB is the Boltzmann constant and represents the ratio of the ideal gas constant with Avogadro's number (k_B=1.38066x10-23 J/K), this constant give the dimension requires and the use of the natural logarithm allow a value to Ω more suitable.

Analyzing then the dimensions of the variation of the entropy in function of the variation of the internal energy (U in Joules), it is possible to arrange the following function:

$$\left(\frac{\delta S}{\delta U}\right)_{V,N} = \frac{1}{T} \qquad \textbf{Eq. 1.5}$$

Writing the entropy as a function of the internal energy and temperature gives:

$$dS = \frac{dU}{T} \qquad \textbf{Eq. 1.6}$$

Considering the first law and assuming that volume is constant i.e. the work done in the system is equal to zero, the expression of the entropy takes the most common way.

$$dS = \frac{dQ}{T} \qquad \textbf{Eq. 1.7}$$

1.2.7 Thermodynamic Potentials

Thermodynamic potentials are state functions of energy that differ according to different properties. The types of property chosen to represent the system have a significant and different impact and therefore different types of energy can be obtained. Those properties can be a set of extensive and intensive properties and with the help of the Maxwell relation and the Legendre transforms it is possible to obtain the different types of energy, and expressions for different experimental conditions, such as changes in volume, temperature, pressure, composition.

The most common thermodynamic potentials are the Internal Energy (U), Enthalpy (H), the free Helmholtz Energy (F) and the free Gibbs Energy (G).

1.2.7.1 Internal Energy (U)

Internal energy represents the energy needed to create the system. As previously present in the definition of the first law of thermodynamics, energy is the sum of the heat and work done in a closed system. If the system is open to material, then it must be consider the energy of particles added. Combining the second law, obtains the expression to internal energy in function of extensive variables as volume, entropy, and number of interchange in chemical species. [8]

$$dU = TdS - PdV + \sum_i \mu dni \qquad \textbf{Eq. 1.8}$$

Considering that entropy and volume remained constant:

$$\mu_i = \left(\frac{\delta U}{\delta ni}\right)_{S,V,n_i} \qquad \textbf{Eq. 1.9}$$

Other combinations can be made in order to represent internal energy in a more practical way. One, used in the simulations performed, consists in the sum of different types of potentials that are function of the position (r) in the simulation box and represented the heat and work done in the system.

In classical molecular simulation the total interaction potential is considered to be the additive interactions with other atoms on the same molecule (bonded, bending angles, torsion, improper torsion, and intramolecular nonbonded terms) and interactions with other molecules (intermolecular nonbonded terms).

$$\boldsymbol{U(r) = U_{non\,bond} + U_{bond} + U_{bend} + U_{torsion} + U_{imp.torsion} + \varepsilon_K} \qquad \textbf{Eq. 1.10}$$

1.2.7.2 Free Helmholtz Energy (F)

The free Helmholtz energy considers that if a system created with rigid boundaries, where no variations on volume occur, in an environment with a certain temperature, higher than the temperature of the system created, it's possible to gain some energy from the environment and so the amount of energy need to create a system will be less. Other possible way to obtain this is considering that we have a Legendre transformation on the variation of the internal energy, replacing in the correct way the entropy by the temperature. The Helmholtz free energy can be written as:

$$\boldsymbol{F = U - TS} \qquad \textbf{Eq. 1.11}$$

Taking the direct differential on F, and replace dU, obtained:

$$\boldsymbol{dF = TdS - PdV + \sum_i \mu dni - TdS - SdT} \qquad \textbf{Eq. 1.12}$$

$$\boldsymbol{dF = -SdT - PdV + \sum_i \mu dni} \qquad \textbf{Eq. 1.13}$$

Considering that temperature and volume remained constant:

$$\mu_i = \left(\frac{\delta F}{\delta ni}\right)_{T,V,n_i} \qquad \textbf{Eq. 1.14}$$

1.2.7.3 Enthalpy (H)

The enthalpy consists in the internal energy plus the energy necessary to create room for the system in the environment, so in these conditions there are no changes in the pressure and the boundaries are moveable. To obtain this type of energy with the Legendre transformation it is needed to replace the volume by the pressure as an independent variable. The enthalpy can be written as

$$\boldsymbol{H = U - (-PV)} \qquad \textbf{Eq. 1.15}$$

Note in this case, the variations of the work done is negative, this appends because is the systems that is making work to the environment and not the contrary.

Taking the direct differential on H, and replace dU, obtained:

$$dH = TdS - PdV + \sum_i \mu dni + PdV + VdP \qquad \textbf{Eq. 1.16}$$

$$dH = TdS + VdP + \sum_i \mu dni \qquad \textbf{Eq. 1.17}$$

Considering that entropy and volume remained constant:

$$\mu_i = \left(\frac{\delta H}{\delta ni}\right)_{S,V,n_i} \qquad \textbf{Eq. 1.18}$$

1.2.7.4 Free Gibbs Energy (G)

The free Gibbs energy considers that if a system crated whit moveable boundaries, where no variations on the pressure occur, in an environment whit a certain temperature higher than the temperature of the system created, it's possible to gain some energy from the environment and, because the system needs to create room for itself this will consist in an energy loss as well. To obtain the free Gibbs energy with the Legendre transformation it is needed to replace the volume by the pressure as an independent variable and the entropy by the temperature. The free Gibbs energy can be written as:

$$G = H - TS \qquad \textbf{Eq. 1.19}$$

$$G = U + PV - TS \qquad \textbf{Eq. 1.20}$$

Taking the direct differential on G, and replace dU, obtained:

$$dG = TdS - PdV + \sum_i \mu dni + PdV + VdP - TdS - SdT \qquad \textbf{Eq. 1.21}$$

$$dG = VdP - SdT + \sum_i \mu dni \qquad \textbf{Eq. 1.22}$$

Experimentally in chemistry it is easier to obtain thermodynamic data from variables that are easy to measure and control; these variables are the temperature and pressure. For this reason, in chemistry the free Gibbs energy is the most interesting form of energy to calculate. Considering the pressure and volume constant: [7] [9]

$$\mu_i = \left(\frac{\delta G}{\delta ni}\right)_{P,T,n_i} \qquad \textbf{Eq. 1.23}$$

1.2.8 Ensembles

Ensembles are different conditions imposed on a system, and are developed in the field of statistical thermodynamics, they are particular useful when computing a system with a large number of particles, making the calculation performed much easier.

In statistical thermodynamics, the collection of possible states dependable of some constraints is referred to an ensemble of states. Depending on the constraints, special names are given to these ensembles.

1.2.8.1 Microcanonical (U,V,N)

This ensemble considers an isolated system with rigid boundaries, where the total energy, the volume and the number of particles in the box remain constant. A micro-canonical ensemble is an assembly of innumerous copies of an isolated system where they have all the same energy.

Since isolated systems are difficult to realize in practice, the microcanonical ensemble is not often used. The image below demonstrated the many copies of the system separated from each other.

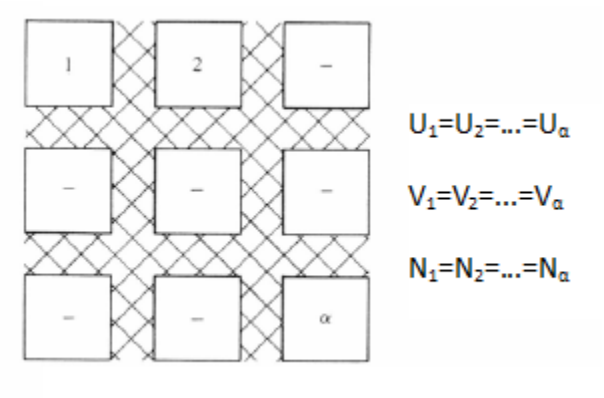

Figure 1.1 – Microcaninical ensemble. Systems 1 trough α, are isolated from each other. Adapted from [10]

1.2.8.2 Canonical (N,V,T)

This ensemble considers a closed system with rigid boundaries, where the number of particles, the volume and temperature remain constant. In other words, it's similar to have a system in a thermal bath where the change of energy occurs between the many copies created of the system in study. Those copies are created in order to represent the many possible energy states and find the most probable one.

Unlike the microcanonical ensemble where there isn't any change in the energy of the system and consequently no changes in ground state, in the canonical ensemble is necessary taking into account the variation of energy and find the ground state at equilibrium. That is done according to the metropolis scheme, where a random walk is constructed trough a region of space. That random walk is constructed through trial moves, in order to find a lower energy in the system. The trial moves are done randomly, by sampling methods and when one generates an energy level higher than the previous that trial move is reject.

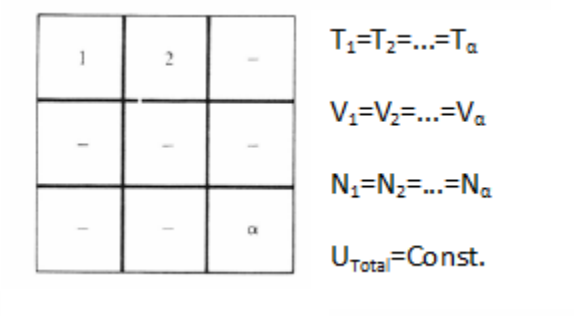

Figure 1.2 – Canonical ensemble. Systems 1 trough α, are complete closed from each other. Adapted from [10]

1.2.8.3 Grand canonical (μ, V, T)

This ensemble considers an open system with rigid boundaries where the temperature, volume and chemical potential remain constant. For this type of ensemble it is possible to have changes of heat as well changes in the number of particles.

Similar to the Canonical ensembles, the Grand canonical ensemble uses a modified metropolis method to compute thermodynamics averages, where the difference it is in the variables used. Since the number of particles is deeply related with the chemical potential it is possible to shift a variable to another, and so for a particular chemical potential imposed, in equilibrium, will be a specific number of particles in the simulation box.

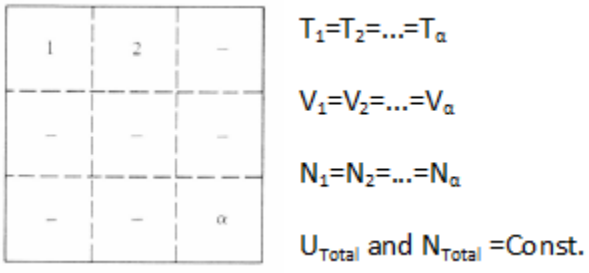

Figure 1.3 – Canonical ensemble. Systems 1 trough α, are complete open from each other. Adapted from [10]

This type of ensemble is the ideal one when simulating systems that require adding or removing some particles, for example the study of adsorption phenomena or phase transitions. For that reason this will be the type of ensemble used in the simulation performed.

1.3 Adsorption phenomenon

Adsorption is the phenomenon of accumulation of a gas or liquid on a surface of a solid or liquid. By definition the component being adsorbed is call adsorbate and the solid is called adsorbent. This phenomenon takes place at the presence of two distinguishesD phases where at the boundaries the accumulation of particles occurs.

Adsorption has been used since the ancient Egyptian and Sumerians but its study only started with the observations carried by Scheele in 1773, experimenting adsorptions of gases in charcoal and clays.

For large scales process, major development were made in systems that have in is present two distinguish phase, solid-gas and solid-liquid. Many processes were driven by the developments made and today many applications for adsorption can be found, for example, separation processes of gaseous and liquid mixtures, heterogeneous catalysis, chemical analyses, biological process, such drug delivery, separation and purification of gases.

Adsorption process is recognized as the most efficient, promising and widely used essentially because of its simplicity, economically viable and technically feasible. Despite of is abundant use in large industries, the biggest barrier of its application by the industries is the cost-prohibitive adsorbent and difficulties associated with regeneration. [11]

In the effort to explore novel adsorbents and to find the ideal adsorption material, it is essential to establish the most appropriate adsorption equilibrium correlation, which is indispensable for reliable prediction of adsorption parameters and quantitative comparison of adsorbent behavior for different adsorbent types. So, in order to analyzing correctly the capabilities of adsorption of a material it's is fundamental to know is equilibrium curves, being that curves obtain at different conditions. Like, constant volume the isochoric curve, at constant pressures the isobaric curve and the most usual equilibrium curve at constant temperature the isotherm curve.

Theses curves are important tools for describing adsorption phenomena that occur at various types of interfaces, allowing characterize the types of porous of the material in study. Adsorption may occur by two distinguish types, physical or chemical, where the type of bonding between the adsorbate and the adsorbent depend the conditions of the system.

Chemical adsorption or chemisorption is a type of adsorption whereby a molecule adheres to a surface through the formation of a chemical bond. Generally occur at temperatures much higher than physical adsorption. The exceed of energy need in this types of adsorption, is due to the activation barrier needed to overcome in order to create a short and strong bond between adsorbate and the adsorbent. Because chemisorption occur whit the creation of a bond between adsorbate and the adsorbent, this is limited by a formation of a monolayer and often can become irreversible.

Physical adsorption or physisorption is a type of adsorption in which the adsorbate adheres to the surface mainly through Van der Waals interactions. This requires much less energy comparing to the chemisorption so the process of physisorption is a fast process, reversible and can form a multiplayer.

1.3.1 Adsorption equilibrium

Adsorption equilibrium is established when the chemical potential of the adsorbate in the bulk is equal to the chemical potential of the adsorbate in the adsorbent, whereas a ratio between the amount adsorbed with the remaining in the solution remains constant. There are many types of isotherm models that describe a variety of adsorbents: Langmuir; Freundlich; Sips; Brunauer–Emmett–Teller (BET), and many other. [12]

1.3.1.1 Langmuir isotherm model

Langmuir adsorption isotherm was originally developed to describe gas–solid-phase adsorption in activated carbon. In its formulation, the model assumes monolayer adsorption, having then a finite number of sites to adsorbed, this model can be also used for adsorbents where occurs chemisorption. Langmuir isotherm refers to homogeneous adsorption, which each molecule possess constant enthalpies and sorption activation energy (all sites possess equal affinity for the adsorbate).

Considering the fractional surface coverage or fractional filling of the micropore θ is the reason of the quantities adsorbed (q) over the quantity of saturation (q_S) and assuming a perfect gas, it's possible to related the adsorption rate with the desorption, obtaining the expression to the Langmuit model. [11] [13]

Adsorption:

$$\frac{d\theta}{dt} = k_a P * (1 - \theta) \qquad \textbf{Eq. 1.24}$$

Desorption:

$$\frac{d\theta}{dt} = k_d * \theta \qquad \textbf{Eq. 1.25}$$

In equilibrium both rates are equal, obtaining:

$$\theta = \frac{KP}{1+KP} \qquad \textbf{Eq. 1.26}$$

With:

$$\theta = \frac{q}{q_S} \qquad \textbf{Eq. 1.27}$$

and

$$K = \frac{k_a}{k_d} \qquad \textbf{Eq. 1.28}$$

The linearization of the expression 1.26, leads to:

$$\frac{1}{q} = \frac{1}{q_S} + \frac{1}{q_S * K} * \frac{1}{P} \qquad \textbf{Eq. 1.29}$$

1.3.1.2 Freundlich isotherm model

Freundlich isotherm is the earliest known relationship describing the non-ideal and reversible adsorption and can be applied to multilayer formation, with non-uniform distribution of adsorption, heat and affinities over the heterogeneous surface. At the beginning of the study of these models, it was proved that the ratio of the adsorbate for a given mass of adsorbent wasn't a constant at different solution concentrations.

The adsorption in this models is represent by the summation of adsorption on all sites, each having different bond energy, where the stronger sites are occupied first until adsorption energy exponentially decreased, completing the adsorption process. The Freundlich isotherm can be represented by the fouling expression: [13]

$$q = K_L * P^{\frac{1}{\eta}} \qquad \textbf{Eq. 1.30}$$

Where K_L is the Freundlich constant and 1/n depends on the linearity of the isotherm , varying between 0 and 1. These constants are related to adsorption capacity and adsorption efficiency, respectively.

Since the value of 1/n varies between 0 and 1, this models of isotherm maybe not the best to represent some systems, once at high pressures the value of q may surpass the quantity of saturation. The linear for of the Freundlich isotherm model can be represent by the following expression: [14] [11]

$$\ln(q) = \ln(K_L) + \frac{1}{n} * \ln(P) \qquad \textbf{Eq. 1.31}$$

1.3.1.3 Sips isotherm model

Sips or Langmuir-Freundlich model, it derives from a combination of the expressions Langmuir and Freundlich. This models ware deduced for a better predicting of the heterogeneous adsorption systems at any temperature, and to overcome the limitation of the rising adsorbate pressure associated with Freundlich isotherm model. At low adsorbate pressures, it reduces to Freundlich isotherm; while at high pressure, it predicts whit a better description the monolayer adsorption capacity characteristic of the Langmuir isotherm. As a general rule, the equation parameters are governed mainly by the operating conditions such as the alteration of pH, temperature, concentration or pressure.

The expression to the Sips isotherm model can be obtained considering that at equilibrium, the rate of desorption is equal to the rate of adsorption. The n parameter could be regarded as the parameter characterizing the system heterogeneity being higher than 1, so:

Adsorption:

$$\frac{d\theta}{dt} = k_a P * (1-\theta)^n \qquad \textbf{Eq. 1.32}$$

Desorption:

$$\frac{d\theta}{dt} = k_d * \theta^n \qquad \textbf{Eq. 1.33}$$

In equilibrium both rates are equal, obtaining:

$$\theta = \frac{(KP)^{\frac{1}{n}}}{1+(KP)^{\frac{1}{n}}} \qquad \textbf{Eq. 1.34}$$

Regarding temperature dependence on the terms K an n, it's have:

$$K = K_0 e^{\left[\frac{Q}{R_g T_0}\left(\frac{T_0}{T}-1\right)\right]} \qquad \textbf{Eq. 1.35}$$

$$\frac{1}{n} = \frac{1}{n0} + \alpha\left(1-\frac{T_0}{T}\right) \qquad \textbf{Eq. 1.36}$$

Where the K_0 is the affinity constant at a reference temperature, T_0, n_0 is the parameter n at the same reference temperature and α is a constant parameter. R_g is the ideal gas constant and Q is the heat of adsorption. [15]

1.3.1.4 BET isotherms

The Brunauer–Emmett–Teller (BET) isotherm was first introduced in the 1930s by Brunauer, Emmett and Teller is a theoretical equation, most widely applied in the gas–solid equilibrium systems. It was developed to derive multilayer adsorption systems with relative pressure ranges from 0.05 to 0.30

For the formulation of this isotherm it is consider Van-der-Waals forces, where each layer have a different quantity of energy, affecting the time and rate of absorption. Having then:

Adsorption into the i^{th} layer:

$$R_a^i = k_a^i * P * S_i \qquad \textbf{Eq. 1.37}$$

Desorption into the ith layer:

$$R_d^i = k_d^i * S_i * e^{-\frac{E_i}{RT}} \qquad \textbf{Eq. 1.38}$$

where S_i is the surface area and P the pressure; k_a and k_d correspond to the adsorption and desorption constants.

In this model is important to differentiate the monolayer from the other layers that are form above, in order to conjugate both expressions, Eq. 1.37 and Eq. 1.38, at equilibrium and obtain a more generic form of the expression for the monolayer and the layers that follows after:

Having for monolayer:

$$k_a^1 . P . S_0 = k_d^1 . S_1 . e^{-\frac{E_1}{RT}} \qquad \textbf{Eq. 1.39}$$

And for the other layers a more generic for:

$$k_a^{i+1} . P . S_i = k_d^{i+1} . S_{i+1} . e^{-\frac{E_{i+1}}{RT}} \qquad \textbf{Eq. 1.40}$$

By definition at equilibrium:

$$y = \frac{k_a^1}{k_d^1} . e^{\frac{E_1}{RT}} \quad \text{and} \quad x = P * \frac{k_d^n}{k_a^n} . e^{\frac{E_L}{RT}} \text{ with L>2} \qquad \textbf{Eq. 1.41}$$

Relating the energy with the surface area of the monolayer obtain an expression to the total area for each energy state. With that is possible to find an expression to the surface coverage (θ). Obtaining: [16] [17]

$$\theta = \frac{V_{total}}{V_{mono}} = \frac{(c.S_0.\sum_{i=1}^{L} i.x^i)}{S_0.(1+c.\sum_{i=1}^{L} i.x^i)} \qquad \textbf{Eq. 1.42}$$

Being:

$$c = y/x \qquad \textbf{Eq. 1.43}$$

Rearranging the expression into a more suitable form, obtain:

$$\frac{1}{V_{total}} . \left(\frac{x}{1-x}\right) = \frac{1}{c.V_{mono}} + \frac{(c-1)}{c} . \frac{1}{V_{mono}} . x \qquad \textbf{Eq. 1.44}$$

Substituting:

$$x = \frac{p}{p_0} \qquad \textbf{Eq. 1.45}$$

Finally arrive at the famous BET isotherm in the common form:

$$\frac{1}{V_{total}} \cdot \left(\frac{p}{p_0 - p}\right) = \frac{1}{c.V_{mono}} + \frac{(c-1)}{c} \cdot \frac{1}{V_{mono}} \cdot \frac{p}{p_0} \qquad \textbf{Eq. 1.46}$$

Combining some of this simple models, such as Langmuir and BET, and using their capability to express different types of phenomenon that occur during adsorption, other models where construct and improved to obtain other information and to express correctly the isotherm of different types of porous. Isotherm can be represented in six different types: [11] [12] [18] [19] [20]

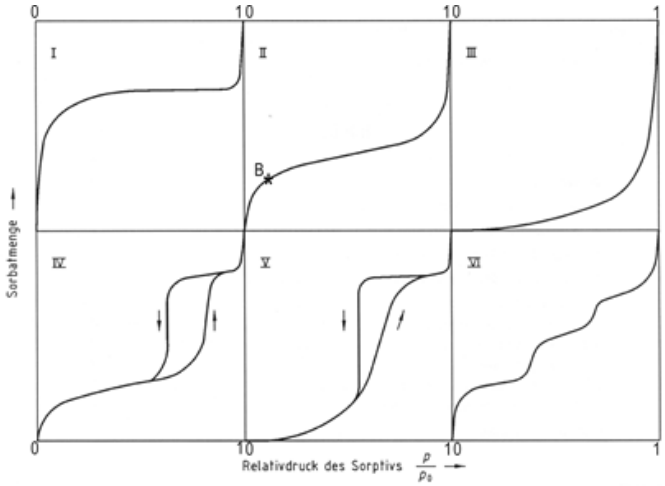

Figure 1.4 – The six types of adsorption isotherms, as classified by IUPAC. Specific amount adsorbed versus relative pressure P/P0, where P0 is the saturation vapor pressure. Adapted from [18]

Type I: Represent adsorption on microspores or adsorption in the monolayer. The rapid increases of the curve represent a rapid filling of the pores, enhanced on the microspores, by the overlapping of the interaction energy of the neighboring walls.

Type II: These types of isotherm are observed in multilayered adsorption on non-porous solids as well as microspores. Where point B represents the quantity on the monolayer of a microspore.

Type III: Represent adsorption on non-porous or macrospores solids, where are weak interactions gas-solid.

Type IV: The initial part of the isotherm is attributed to monolayer and multilayer adsorption. It is also possible to observe a hysteresis loop, which is associated with capillary condensation, taking place in mesopores. In the simplest cases this type of isotherm are very similar to Types II.

Type V: This type of adsorption may occur in mesoporous or microporous solids, and similar to the Type III isotherm week forces gas-solid are associated to adsorption.

Type VI: Represents stepwise multilayer adsorption on a uniform non-porous surface. Each step corresponds to the formation of a complete monomolecular adsorption layer.

Despite of the existence of many models that represent a series of compounds and their properties, those depend on experimental data or the solution of integral equation very hard to solve and calculate, and so the use of alternative methods, facilitate not only in the time consumed but also provides different types of experiences that can be tested.

That only was possible whit the implementation of the virial formalism in 1974, by Steele, and turn out to be the turning point in adsorption study. The numerical values of the second, third and fourth two-dimensional virial coefficients give qualitative information on the interactions between adsorbed molecules and adsorption sites as well as on the interactions with other adsorbed molecules, and there value are regardless if the adsorbent surface is homogeneous or heterogeneous.

The big handicap of the methods that uses the virial formalism is the present of a distribution function in the coefficients, being that function very hard to get by simple numeric methods. Only with the power of molecular simulation that's was possible to overcome some problems and obtained some results with very good precisions

Based directly on a microscopic model of the adsorption system, the computer simulation approach, both Monte Carlo as well as Molecular Dynamics, can provide then, an exact numerical solution of the model assumed. [12]

1.3.2 Adsorption Thermodynamics

In order to fully understand the adsorption phenomenon that occurs at surface of an adsorbent, it's fundamental to not only have into consideration the kinetic approach but also the thermodynamics that govern that process. The result is the understanding of the forces that governs adsorption, the types of binding between molecules and the variation of the energy of the system whit the change of is conditions and types of particles. [15]

Since adsorption is a spontaneous process, changes in the total energy of the systems must be considered. That change occurs mostly due to the tendency of transition between molecules in different phases. That transitions result usually in a loss of entropy ($\Delta S < 0$), once molecules that are in the gas phase have more degrees of freedom when comparing whit the ones that are adsorbed phase. Considering then a spontaneous process, it follows that adsorption must always be exothermic ($\Delta H_{ads} < 0$) since:

$$\mathbf{\Delta G_{ads}} = \boldsymbol{\Delta H_{ads}} - \boldsymbol{T\Delta S_{ads}} < \mathbf{0} \qquad \textbf{Eq. 1.47}$$

$$\mathbf{\Delta H_{ads}} = \boldsymbol{H_a} - \boldsymbol{H_g} \qquad \textbf{Eq. 1.48}$$

Where ΔH_{ads} represents the variation of enthalpy when a differential amount of adsorbate changes from the gas phase to the adsorbed phase. To achieve the equilibrium, the system tends to move the particles in the direction of the lower free energy state. At constant temperature and pressure, the equilibrium its obtain when the rate of particles, that goes from the gas phase to the adsorbate phase, is equal to the rate of particles that goes from the adsorbate phase to the gas phase, and so the variable to have into account is the chemical potential, since it's related whit the number of particles. The chemical potential in each phase is defined as: [22]

$$\boldsymbol{\mu_a = \left(\frac{\delta G_a}{\delta n_a}\right)_{T,P} = -s_a dT + v_a dP} \qquad \textbf{Eq. 1.49}$$

$$\boldsymbol{\mu_g = \left(\frac{\delta G_g}{\delta n_g}\right)_{T,P} = -s_g dT + v_g dP} \qquad \textbf{Eq. 1.50}$$

Where s_i and v_i are extensive properties of the systems:

$$\boldsymbol{s_i = \left(\frac{\delta S_i}{\delta n_i}\right)_{T,P}} \quad \boldsymbol{v_i = \left(\frac{\delta V_i}{\delta n_i}\right)_{T,P}} \qquad \textbf{Eq. 1.51}$$

When equilibrium is reached, the chemical potential of the gas phase and the adsorbed phase are equal, since:

$$\boldsymbol{dG = (\mu_a - \mu_g) dn_a = 0} \qquad \textbf{Eq. 1.52}$$

$$\boldsymbol{\mu_a = \mu_g} \qquad \textbf{Eq. 1.53}$$

$$\boldsymbol{-s_a dT + v_a dP = -s_g dT + v_g dP} \qquad \textbf{Eq. 1.54}$$

Taking the total derivative of temperature and pressure, on the previous equation, obtained the classic Clausius-Clapeyron relation:

$$\boldsymbol{\frac{dP}{dT} = \frac{s_a - s_g}{v_a - v_g}} \qquad \textbf{Eq. 1.55}$$

Considering that the volume of the gas phase is much larger than the adsorbed, this approximation is taken:

$$v_g - v_a \approx v_g$$

And so:

$$\boldsymbol{\frac{dP}{dT} = \frac{s_g - s_a}{v_g} = -(s_a - s_g)\rho_g = -\Delta S_{ads} * \rho_g} \qquad \textbf{Eq. 1.56}$$

Leading to:

$$\boldsymbol{\Delta S_{ads}(n_a) = -\frac{dP}{dT} * \rho_g^{-1}} \qquad \textbf{Eq. 1.57}$$

At equilibrium, the corresponding change in enthalpy upon adsorption is:

$$\mathbf{\Delta H_{ads}}(\boldsymbol{n_a}) = \mathbf{T} * \boldsymbol{\Delta S_{ads}}(\boldsymbol{n_a}) = -\boldsymbol{T} * \frac{\boldsymbol{dP}}{\boldsymbol{dT}} * \boldsymbol{\rho_g^{-1}} \qquad \textbf{Eq. 1.58}$$

Considering the ideal gas equation:

$$\boldsymbol{\rho_g} = \frac{\boldsymbol{n_g}}{\boldsymbol{V_g}} = \frac{\boldsymbol{P}}{\boldsymbol{RT}} \qquad \textbf{Eq. 1.59}$$

$$\mathbf{\Delta H_{ads}}(\boldsymbol{n_a}) = -\frac{\boldsymbol{RT^2}}{\boldsymbol{P}} * \left(\frac{\boldsymbol{dP}}{\boldsymbol{dT}}\right)_{\boldsymbol{n_a}} \qquad \textbf{Eq. 1.60}$$

Rearranging in the van't Hoff form obtained:

$$\mathbf{\Delta H_{ads}}(\boldsymbol{n_a}) = \mathbf{R} * \left(\frac{\boldsymbol{dln\ P}}{\boldsymbol{d\left(\frac{1}{T}\right)}}\right)_{\boldsymbol{n_a}} \qquad \textbf{Eq. 1.61}$$

The isosteric heat of adsorption Q_{st} (kJ/mol), a commonly reported thermodynamic quantity, is given as a positive value:

$$\mathbf{Q_{st}} = -\mathbf{\Delta H_{ads}}(\boldsymbol{n_a}) = -\mathbf{R} * \left(\frac{\boldsymbol{dln\ P}}{\boldsymbol{d\left(\frac{1}{T}\right)}}\right)_{\boldsymbol{n_a}} \qquad \textbf{Eq. 1.62}$$

1.3.2.1 Isosteric heat of adsorption

The decisive quantities when studying the adsorption process are the heat of adsorption, its coverage dependence on lateral particle–particle interactions, the kind and number of binding states and the nature of the surface of the adsorbent. The most relevant thermodynamic variable to describe the heat effects during the adsorption process is the differential isosteric heat of adsorption Q_{st}, (kJ mol^{-1}), that represents the energy difference between the state of the system before and after the adsorption for a differential amount of adsorbate on the adsorbent surface. It's also need to have into account is the electrostatics nature of some molecules.

For nonpolar molecules the heat of sorption is generally almost constant for low coverage, however it's shown a slightly increase as the coverage rises until reach saturation. That effect is often ascribed to the effect of intermolecular attraction. For the case of polar molecules, the heat sorption tends to decrease due to the power of polarization power. [23]

The study of the isosteric heat provides information about the type of adsorption, where variations in the heat of the adsorption heat lower than 80 kJ/mol, are considered as physisorption, and provides important information for kinetics studies once that the heat released can be transfers to the solid adsorbent or can be partly dissipated to the surrounding. [24] [25] [16]

There are many methods that can be used to estimate the isosteric heat, one frequently used is to measure various adsorption isotherms and to plot the data under the form of an isosteric plot. Another option is to fit the isotherm data to a temperature dependent adsorption model and then to derive the heat of adsorption by applying the Clausius-Clapeyron equation to the isotherm model. Two isotherm models that are usually used for this purpose are the Sips and Toth models. It is worth noting that the Sips models equation is not valid at very low pressure because it does not possess the correct Henry -aw type behavior. To proper calculate and represent those values, the Toth models is the most appropriated since this model describes well many systems with sub-monolayer coverage. [25] [23] [22] [15] [13]

1.3.2.2 Henry's Law

The Henry's Law, describe the system in a very simplest way, where it's used to describe the adsorption phenomenon at low occupancy. For very low pressures, at constant temperature, the relation between the pressure and the amount adsorbed can be express in the linear form, being the value of the slope the Henry constant. That value gives an insight of the affinity adsorbent and adsorbate, and gives also the possibility to compare the affinity of the adsorbent whit different types of adsorbates. If the chemical potential is sufficiently low, the loading q is proportional to the Henry coefficient K_H and the pressure and the henry constant can be obtain by the flowing expression.

$$\boldsymbol{q = K_H . P} \qquad \textbf{Eq. 1.63}$$

Where K_H is the henry constant, the q is the amount adsorbed and P is the pressure of the system. That equation can be easily obtained by a linear tendency line over the data obtain. [26]

For the last two decades the methods of molecular modeling of surface and interface phenomena have been widely developed. And with time other methods that are simplest and less time-consumers have been applied. The firsts, denominated as 'atomistic computer modeling', where based on the Schrodinger equation and in the advances made by Hartree FocK. Those type of models can be applied to any system regardless the availability of experimental data, obtaining properties prior to any synthesis and have a glimpse inside into materials behavior on the atomistic level.

In more complex systems the used of these types of methods is them limited by the computation power and time, and so there were the need to build much more minimalist technics, that use simple equation to predict microscopic properties, models like Monte Carlo as well as Molecular Dynamics. [27]

1.4 Simulation Tools

The use of simulation tools to describe some complex systems have become essential in science since it discovery. Despite of being a complicated tool to understand and used, the combination of statistical mechanics and thermodynamics, the use of the correct force fields, the use of the second law of Newton and the implementation of some algorism, make the Computer Simulation a very precise and helpful tool.

It emerge essential during and after the Second World War, for code breaking and to develop nuclear weapons and only after computer became available for nonmilitary uses, in the early 1950's, that has given a boom in this area. The first simulation performed in nonmilitary computer was carried out at the Los Alamos National Laboratories in United States by, Nicholas Metropolis, and many other scientists in 1952, on a computer called MANIAC (Mathematical Analyzer, Numerical Integrator, and Computer).

The use of computer simulation it only was possible with rapid increase of computer power and technology and today it's possible to perform simulation on any ordinary computer thanks to the internet.

In theory it's possible to simulate any system regardless of its size. However, even though of the remarkable computational power achieve today, the simulations performed goes around the number of atoms in the order of 10^6, representing fraction of a mole, in the order of 10^{-17}. Despite of those values be very small, the objective when performing molecular simulation is to obtaining many types of information and properties, for example density, free energy, specific heat, viscosity and average structure. Simulation can be performing for many different purposes like drug design, protein engineering, environmental processes and materials science.

Although computer simulation have a very important role in science, it should have into considerer that simulation is by no means ideal. Simulation provides statistical estimates rather than exact characteristics and performance measures of the model. Thus, simulation results are subject to uncertainty and contain experimental errors. It´s also important to consider that, no matter how precise, accurate, and impressive, the information obtain is, that it's only correct if the models is a valid representation of the system under study.

Computer simulation models can be classified in several ways:

- **Static versus Dynamic Models:** Where static models are the ones that are not time depend and therefor do not have a representation over the time. In contrast, dynamic models represent systems that evolve over time.
- **Deterministic versus Stochastic Models:** In a deterministic model, all mathematical and logical relationships between variables are fixed and not subject to uncertainty. They are often described by differential equations and solve by different numerical methods where a unique input leads to a unique output. In contrast, a model with at least one random input variable is called a stochastic model, where a unique input leads to different outputs.
- **Continuous versus Discrete Models:** In discrete simulation models, the state variable changes instantaneously at discrete points in time or space, whereas in continuous simulation models, the state changes continuously over time or space.

From the types of models present above, two major approaches ware construct. One, which uses discrete-event dynamic systems, is time depend and its often called Molecular Dynamics simulation (MD), the other one uses discrete-event static systems often call Monte Carlo simulation (MC). Those two approaches are strictly related with the ergodicyty hypothesis, where detonates that if it wish to compute averages of a function of the coordinates and momenta of many particle system, we can either compute that quantity by time averaging, the MD approach, or by ensemble averaging, the MC approach.

In both approach it is necessary to have into account the force field which describes the relation between the atoms. That force field is a summation of equations which analytically formulates the interaction of atoms between each other. These interaction potentials are usually classified in two groups; intermolecular and intramolecular. Intermolecular potentials are represented by two groups: the electrostatic and dispersive (Van der Waals) potentials. The intramolecular potentials are used for the atoms which belong to the same molecule.

To properly represent a force field as a function of the position of the atoms we revert to the Born-Oppenheimer approximation. The Born-Oppenheimer approximation is based on the fact that typical electronic velocities far exceed those of nuclei. Once nuclear motions are much slower than electron motion, the electronic wave function, or energy variations, can be calculated assuming a fixed position of the nuclei and nuclear motion can be considered assuming an average distribution of electron density. Without this approximation it is impossible to write the energy as a function of the nuclear coordinates. [28] [29] [30] [31]

1.4.1 ForceFields

The force field applied in simulation will have a major impact on the final results of the potential energy. The types of force field and the parameter chosen are determinant to a good representation of the real world. So it's important to understand correctly the force field. Being this divided in two major types, the intermolecular potentials, and the intramolecular potentials. In the image bellow it's possible to see the most common types of interactions that can be implemented to the system. [30]

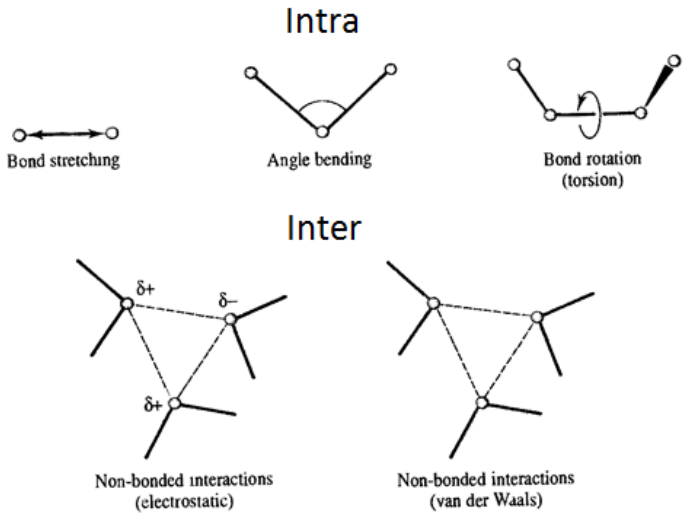

Figure 1.5 – Representation of the deferent types of interaction that occur intra and inter molecular level.

Being represented by the following expression:

$$\boldsymbol{U(r) = U_{VW} + U_{el} + U_{bond} + U_{bend} + U_{torsion}} \qquad \textbf{Eq. 1.64}$$

1.4.1.1 Intermolecular Potentials

1.4.1.1.1 Electrostatic Potentials

This type of potential is considered when an unequal charge distribution is over the atoms of a molecule. These charges must be determinate in order to represent correctly the electrostatic properties of a molecule. The electrostatic interaction between two atoms is calculated according to the Coulomb's law:

$$\boldsymbol{U_{el} = \sum_{i=1}^{N_A} \sum_{j=1}^{N_B} \frac{q_i \cdot q_j}{4\pi\varepsilon_0 r_{ij}}} \qquad \textbf{Eq. 1.65}$$

Where N_A and N_B are the number of point charges in the two molecules. [30] [28]

1.4.1.1.2 Van der Waals Potential

The other type of potential to represent intermolecular forces is the famous Van der Waals potential. These have into account the attractive and repulsive energy. Being the interaction energy zero, at an infinite distance between to atoms (at relatively short distances it is practical neglect), and with the approximation of those two atoms the energy can rapidly increases.

The repulsive contributions occur when the two atoms are close to each other in a way that is an overlap of their electronic clouds, having both clouds electrons with the same spin. The attractive contribution is due to the disperse forces. This principle was proved by London in 1930 using quantum mechanics. Where from the fluctuation in the electron clouds results in an instantaneous dipole in a molecule that can induce a dipole in neighboring atoms, giving rise to the attractive effect. [28]

Through the years many scientist have introduce many forms of this type of pair potential, ones that have better representation than other, but still very simple to compute. In the image below it is shown four types of potential developed in order to simulate liquid-state theory, being those potentials unrealistic and highly idealized.

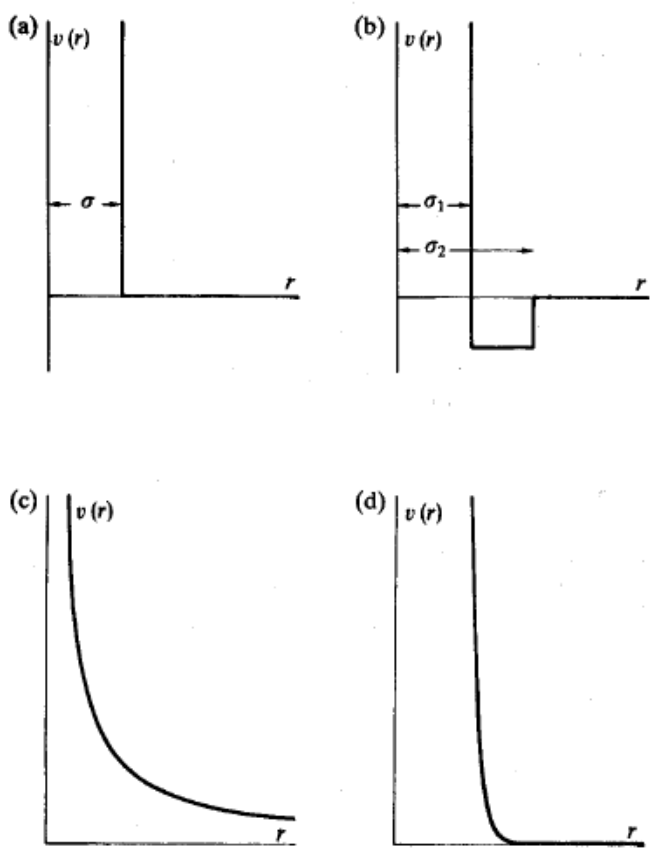

Figure 1.6 – a)The hard-sphere potential, b)The square-well potential; c and d) The soft-sphere potential with different repulsion parameter (v), whit v(c)>v(d). Adapted from [29]

Besides these models be unrealistic and highly idealized they don't have into account the attractive and repulsive contributions correctly, the best known of the Van der Waals potential is the Lennard-Jones 12-6 potential:

$$U_{VW} = 4\varepsilon * \left[\left(\frac{\sigma}{r}\right)^{12} - \left(\frac{\sigma}{r}\right)^{6}\right] \qquad \textbf{Eq. 1.66}$$

The Lennard-Jones 12-6 potential has two parameters, the collision diameter (σ), at which the energy is zero and the well depth ε, where the net force is zero. The repulsive term varies as r^{-12} and the attractive term varies as r^{-6}.

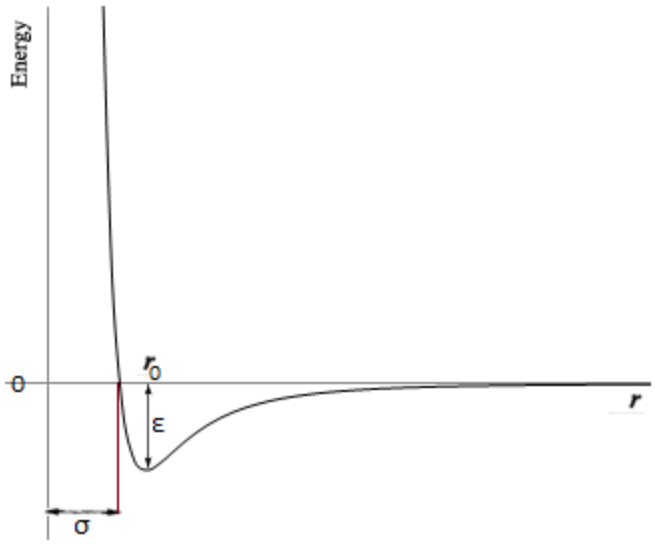

Figure 1.7 – Representation of a typical 12-6 Lennard Jones potential.

As shown in the figure above, at a r_0 distance the energy reach it lowest value, being this the most probable distance that two particles will be further apart. For molecular simulation of a physical adsorption phenomenon this type of potential has a very important role, since physical adsorption is ruled by week interactions, i.e., Van der Waals forces.

When dealing with a system that is from by more than two types of particles, it is necessary use combination rules to obtain the Lennar-Jones Parameters for the respective mixture, having into account parameters for each single particle. There are many types of combination rules that consider some other effects, like ionization potential, polarizability, deformation energies, and many others, but essential to tree main approaches are used: [32] [33]

- **Arithmetic:**

$$\boldsymbol{\sigma_{ij}} = \frac{\sigma_{ii}+\sigma_{jj}}{2} \qquad \boldsymbol{\varepsilon_{ij}} = \frac{\varepsilon_{ii}+\varepsilon_{jj}}{2} \qquad \textbf{Eq. 1.67}$$

- **Geometric:**

$$\boldsymbol{\sigma_{ij}} = \sqrt{\boldsymbol{\sigma_{ii}\sigma_{jj}}} \qquad \boldsymbol{\varepsilon_{ij}} = \sqrt{\boldsymbol{\varepsilon_{ii}\varepsilon_{jj}}} \qquad \textbf{Eq. 1.68}$$

- **Lorentz-Berthelot:**

$$\boldsymbol{\sigma_{ij}} = \frac{\sigma_{ii}+\sigma_{jj}}{2} \qquad \boldsymbol{\varepsilon_{ij}} = \sqrt{\boldsymbol{\varepsilon_{ii}\varepsilon_{jj}}} \qquad \textbf{Eq. 1.69}$$

1.4.1.2 Intramolecular Potentials

1.4.1.2.1 Bond Stretching

It is possible to relate the stretching of a bond with the extension of the spring bonding, bonding two atoms. Of many forms of models use to represent this energy, one widely used is the one suggested by Morse:

$$U_{bond} = D^{AB}\left(1 - e^{-\alpha\left(r^{AB} - r_0^{AB}\right)^2}\right)\sqrt{k/2D^{AB}} \qquad \textbf{Eq. 1.70}$$

Where r is distance between atoms, D^{AB} is the bond dissociation energy, $\alpha=\sqrt{k/2D^{AB}}$, and k is related to a spring constant. [32] [28]

1.4.1.2.2 Angle Bending

For this type of energy, it is commonly used the Hooke's law or a harmonic potential after being expressed by a Taylor expansion. It describes the deviation of the angles from the reference values of tree atoms:

$$U_{bend} = \frac{1}{2}k^{ABC}\left(\theta^{ABC} - \theta_0{}^{ABC}\right) \qquad \textbf{Eq. 1.71}$$

1.4.1.2.3 Bond Torsion

Four aligned atoms frequently will rotate along the central bond, as shown in following image:

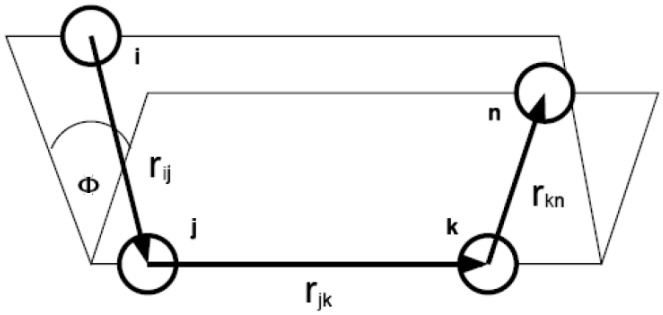

Figure 1.8 – Schematic representation of and Bond Torsion. Adapted from [30]

This type of interaction energy it's very important to understand the barriers to rotation on chemical bonds. The rotation along the bond is continuous so when the bond rotates by 360º the energy should return to the initial value, having a periodicity. The energy of torsional angle, is a function of the periodicity term n, the dihedral angle ϕ and the constant Vn representing the a barrier for rotation: [32]

$$U_{torsion} = \sum_n V_n \cos(n\varphi - \varphi_0) \qquad \textbf{Eq. 1.72}$$

In simulation it is always possible to use more precise models or add other types of interactions in order to represent the real system with better precision. When considering using this type of interaction it's very important to analyze the system and the problem, in order to understand if the used of each one of them is really significant. For the simplest models shown above the number of parameter used to specified for each atom is significant large, and the time to, not only find those parameter as also the time of simulation will not compensate the final results, since the simplest models have a significant error.

1.4.2 Molecular Dynamics

The first molecular dynamics simulation was performed by Alder and Wainwright in the mid fifties to study a condensed phase, with a hard-sphere model for intermolecular interactions. This type of simulation used the integrant of the second law of Newton's in order of time, being the force applied on a certain particle:

$$F_i = m_i . \frac{d^2 r_i}{dt^2} \qquad \textbf{Eq. 1.73}$$

Where m is the mass of the particle and r is the position of the particle. Whit this is possible to now the trajectory of all particles in the system, varying throw time.

In a molecular dynamics simulation a series of calculations are repeated every step to determine how the system evolves with time, until the properties of the systems no longer change. For this type of simulation tree major steps are taken, after choosing the initials conditions of the system:

1. **First:** Initials positions and velocities are selected. Where atoms are displaced in a lattice. The velocities are calculated according to the temperature desired based on Maxwell-Boltzmann distribution, using the relation:

$$\sum_{i=1}^{N} \frac{1}{2} m_i . v_i^2 = \frac{3}{2} N k_b T \qquad \textbf{Eq. 1.74}$$

2. **Second:** The force applied on each atom is calculated based on the interaction potentials:

$$\boldsymbol{F(r) = -\frac{dU(r)}{dr}} \qquad \textbf{Eq. 1.75}$$

And for the Lennard-Jones potential, with reduced units:

$$\boldsymbol{F(r) = \frac{48}{r}\left(\frac{1}{r^{12}} - 0.5.\frac{1}{r^{6}}\right)} \qquad \textbf{Eq. 1.76}$$

3. **Third:** Integration of the Equation of Motion. To do that numerous algorithms were proposed and the choice of a god algorithm is essential. They must ensure accuracy for large steps, good energy conservation and predict with accurately the trajectories of all particles. The most famous and perhaps most widely used is the Verlet algorithm. To derive it, it's done a Taylor expansion on the coordinate of the particle, around the independent variable, time:

$$\boldsymbol{r(t+\Delta t) = r(t) + v(t)\Delta t + \frac{1}{2}a(t)\Delta t^2 + \frac{1}{3!}b(t)\Delta t^3 + O(\Delta t^4)} \qquad \textbf{Eq. 1.77}$$

$$\boldsymbol{r(t-\Delta t) = r(t) - v(t)\Delta t + \frac{1}{2}a(t)\Delta t^2 - \frac{1}{3!}b(t)\Delta t^3 + O(\Delta t^4)} \qquad \textbf{Eq. 1.78}$$

Adding both expressions, obtain:

$$\boldsymbol{r(t+\Delta t) = 2r(t) + r(t-\Delta t) + a(t)\Delta t^2 + O(\Delta t^4)} \qquad \textbf{Eq. 1.79}$$

And form the integrating of Newton's equations, obtained:

$$\boldsymbol{a(t) = \frac{1}{m}\nabla U\big(r(t)\big)} \qquad \textbf{Eq. 1.80}$$

The concept behind the Molecular Dynamics approach it replicates with great precision the real world changes. In fact, if all fundamental steps where correctly implemented the mistakes that occur are very similar to those occurring in the laboratory, e.g., the sample is not prepared correctly, the measurement is too short, the systems undergoes an irreversible change during the simulation. [28] [30] [34]

1.4.3 Monte Carlo

In this chapter, it tries to give the fundamentals aspect about Monte Carlo Simulation. In order to fully understand how this type of simulation work, it's important to have into consideration some aspect that are the key, not to obtain a simulation, but to obtain experimental data via simulation and comparable to real data experiment. Although the algorithms applied are very simple, and base on a simple concept, that are other important features that are needed to understand and to consider, namely, the Markov chain, the type of sampling and the truncation of the interactions. [36]

Driven by the Second World War and the need to develop the atomic bomb, many studies where made to facilitate the analysis of larges systems. By traditional methods, those analyses where performed using the thermodynamics, statistical physics, and quantum mechanics that are inherently probabilistic and so complicated to obtain. [35] [29]

The solution to this problem was to simulate the results in the earliest computer made. At the end and after of the Second World War, and with more power full computers availed, von Neumann, Ulam and Metropolis crated this new method called Monte Carlo. [29] [35]

Although Molecular Dynamics and the Monte Carlo methods apply very distinguish ways to move one state to other, they are equivalent from the point of view of statistical mechanics, once the *ergodicity* hypothesis states, that time averages are equivalent to ensemble averages. So for the both methods, the results obtain, only are comparable with the real world data with the use of statistical thermodynamics and mechanics. [37]

1.4.3.1 Statistical Mechanics and the Boltzmann Distribution

Through statistical Mechanics it's possible to obtain the average behavior of a macroscopic system of interacting particles, from a microscopic point of view. This is only possible with the Boltzmann distribution. In this thesis it's briefly review the two thermodynamic ensembles that are interested in Monte Carlo simulations. [30] [28]

1.4.3.1.1 Canonical Ensemble

Having into account the equation 1.4 and 1.7 for the entropy presented at the chapter 1.1.6 and a system at constant V and N, it's possible to obtain the expression to the total multiplicity of states (Ω) in function of the total energy. Considering the classical statistical mechanics:

$$\boldsymbol{\Omega_i \propto e^{-\frac{E_i}{k_B T}}} \qquad \textbf{Eq. 1.81}$$

For such a macroscopic system in equilibrium at the temperature T, the probability Pi of finding the system in the particular state i is:

$$P_i = \frac{e^{-\frac{E_i}{k_B T}}}{\sum_i e^{-\frac{E_i}{k_B T}}} \qquad \textbf{Eq. 1.82}$$

So knowledge the distribution function of the energy it's possible to compute the average of the energy:

$$\overline{E} = \sum_i E_i . P_i \qquad \textbf{Eq. 1.83}$$

$$\Leftrightarrow$$

$$\overline{E} = \frac{\sum_i E_i . e^{-\frac{E_i}{k_B T}}}{\sum_j e^{-\frac{E_j}{k_B T}}} \qquad \textbf{Eq. 1.84}$$

Where the equation 1.84 can be writing as:

$$U(T,V,N) = \overline{E} = \frac{\delta ln Z}{\delta\left(\frac{1}{k_B T}\right)} \qquad \textbf{Eq. 1.85} \quad \text{Where} \quad Z = \sum_i e^{-\frac{E_i}{k_B T}} \qquad \textbf{Eq. 1.86}$$

Now comparing the expression for the average of energy with the thermodynamics relation:

$$U = \left[\frac{\delta\left(\frac{F}{T}\right)}{\delta\left(\frac{1}{T}\right)}\right]_{V,N} \qquad \textbf{Eq. 1.87}$$

Obtain the expression to the free energy of this system in function of the total multiplicity of states:

$$F = -k_B T ln(Z) \qquad \textbf{Eq. 1.88}$$

The calculus of the partition function Z is the central problem of statistical thermodynamics. That partition function can be written as a form of an integral having no analytical solution, and so in order to obtain the value for that partition function, numerical integration is needed. This, in principle, could be done by evaluating the integrand at many points inside the integration region and using the average value to obtain an approximated value of the integral. [37] However, this is not feasible in practice because of the huge number of points that would have to be calculated. Moreover, what is required in practice is the probability density of finding the system in a given configuration. This is shown below.

In a thermodynamics point of view, the partition function (Z) for a canonical ensemble of N particles has the form:

$$Q = \left(\frac{1}{\Lambda^{3N} N!}\right) \int e^{-\frac{H\left(r^N, p^N\right)}{k_B T}} dr^N dp^N \qquad \textbf{Eq. 1.89}$$

Where:

$$\boldsymbol{\Lambda = \sqrt{\frac{h^2}{2\pi k_B T}}} \qquad \textbf{Eq. 1.90}$$

Λ is the thermal Broglie wavelength, H is the Hamiltonian in function of momentum and position kB is the Boltzmann constant, and T is the temperature. The expression for the probability density obtained as the form of:

$$\boldsymbol{P_{i_{N,V,T}}(r^N, p^N) = \frac{e^{-\frac{H(r^N,p^N)}{k_B T}}}{\int e^{-\frac{H(r^N,p^N)}{k_B T}} dr^N dp^N}} \qquad \textbf{Eq. 1.91}$$

Notice that the Hamiltonian is a sum of the contribution of the kinetic energy and potential, if considering the system where the contribution of the kinetic energy is related with the ideal gas or the Born-Oppenheimer, those can be easily calculated by analytic methods and the contribution of the potential energy stays as a function of the position rN being the probability of finding configuration the following expression: [36]

$$\boldsymbol{P_{i_{N,V,T}}(r^N) \propto e^{\left[-\frac{U(r^N)}{k_B T}\right]}} \qquad \textbf{Eq. 1.92}$$

1.4.3.1.2 Grand-Canonical Ensemble

In a simulation of the grand-canonical ensemble, the chemical potential μ, volume V, and temperature T are fixed, where the number of particles N is allow changing. At constant volume and temperature, the chemical potential is the derivative of the Helmholtz free energy F with respect to particle number. For these situations, where the volume remains constant, the chemical potential is the amount by which the free energy will change if we add another particle, and so can be interpreted as the need to accept or not more particles.

The complete grand canonical partition function, given for a Hamiltonian $H(r^N,p^N)$, is:

$$\boldsymbol{Q\ (\mu, V, T) = \sum_{N=0}^{\infty} \left(\frac{1}{\Lambda^{3N} N!}\right) e^{\left[\frac{\mu N}{k_B T}\right]} \int e^{-\frac{H(r^N,p^N)}{k_B T}} dr^N dp^N} \qquad \textbf{Eq. 1.93}$$

In this type of ensemble the removing and adding of particles is assuming as an exchanging of a particle from a system to other, as shown in the flowing image:

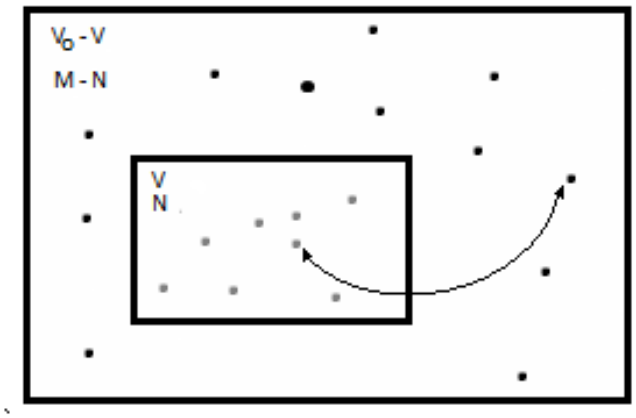

Figure 1.9 – Schetimatic GCMC simulation of an insertion/deletion move. Ideal gas (M – N particles, volume V0 – V) can exchange particle whit a N-particle system (volume V)

Considering that, in the subsystem of interest we have particles with the kinetic energy of an ideal gas, interacting with each other via a potential U(rN), it's is possible to obtain the total partition function as function of the reduced coordinates (sN), that include all possible distributions of M particle over the two subvolumes, when the limit of M/N tends to infinity, being: [36] [34]

$$\boldsymbol{Q}\ (\boldsymbol{\mu}, \boldsymbol{V}, \boldsymbol{T}) \equiv \sum_{\boldsymbol{N}=\boldsymbol{0}}^{\infty} \left(\frac{\boldsymbol{V}^{\boldsymbol{N}}}{\boldsymbol{\Lambda}^{\boldsymbol{3N}}\boldsymbol{N}!}\right) \boldsymbol{e}^{\left[\frac{\boldsymbol{\mu N}}{\boldsymbol{k_B T}}\right]} \int \boldsymbol{ds}^{\boldsymbol{N}} \boldsymbol{e}^{-\frac{\boldsymbol{U}\,(\boldsymbol{s}^{\boldsymbol{N}})}{\boldsymbol{k_B T}}} \qquad \textbf{Eq. 1.94}$$

And the corresponding probability density:

$$\boldsymbol{P}_{\boldsymbol{i}_{\boldsymbol{\mu},\boldsymbol{V},\boldsymbol{T}}}(\boldsymbol{r}^{\boldsymbol{N}}) \propto \frac{\boldsymbol{V}^{\boldsymbol{N}}.\boldsymbol{e}^{\left[\frac{\boldsymbol{\mu N}}{\boldsymbol{k_B T}}\right]}}{\boldsymbol{\Lambda}^{\boldsymbol{3N}}\boldsymbol{N}!} \boldsymbol{e}^{\left[-\frac{\boldsymbol{U}\left(\boldsymbol{r}^{\boldsymbol{N}}\right)}{\boldsymbol{k_B T}}\right]} \qquad \textbf{Eq. 1.95}$$

1.4.3.2 The Algorithm

The main challenge of designing an algorithmic to Monte Carlo molecular simulation lies in finding ways to adequately and efficiently sample the equilibrium distribution of the correct statistical mechanical ensemble, being that done using the Markov chain.

Markov chain is a collection of states where the probability of moving from one state to another depends only upon the state that the system is currently staying in, no matter how the system got into that current state. The trick is to select the probabilities of moving from one state to another in such a way that the system converges to a stationary distribution with the higher probabilities. That stationary distribution is reached according to the most probable state and because is reached with a Markov Chain by means of important sampling, it guarantees a fast and reliable simulation. [35]

Other important condition is that, once the equilibrium is reached, it must be not destroyed. This means that, in average, the probability of going to one state is equal to the probability of returning to that state, this is a very strong condition, namely, that in equilibrium the average of accepted moves from n state to n+1, is exactly canceled by the number of reverse moves. That condition implies, for a symmetric curve, the following: [34]

$$\boldsymbol{N(n).acc(n \rightarrow n+1) = N(n+1).acc(n+1 \rightarrow n)} \qquad \textbf{Eq. 1.96}$$

Where N(n) and N(n+1) are the probability density for the current state for the state after the perturbation, respectively, and acc(n→n+1) and acc(n+1→n) are the probability to accept a trial move from one state to other. From the equation 1.96:

$$\boldsymbol{\frac{acc(n \rightarrow n+1)}{acc(n+1 \rightarrow n)} = \frac{N(n+1)}{N(n)}} \qquad \textbf{Eq. 1.97}$$

If considering a canonical ensemble the probability of the density function is proportional to:

$$\boldsymbol{N(n) \propto e^{\left[-\frac{U(r^n)}{k_B T}\right]}} \qquad \textbf{Eq. 1.98}$$

Obtain:

$$\boldsymbol{\frac{acc(n \rightarrow n+1)}{acc(n+1 \rightarrow n)} = \frac{N(n+1)}{N(n)} = e^{\left[-\frac{1}{k_B T}.(U(r^{n+1}) - U(r^n))\right]}} \qquad \textbf{Eq. 1.99}$$

And so according to the choice of the metropolis et al, the probability of acceptance one move is:

$$\boldsymbol{acc(n \rightarrow n+1)} \begin{cases} \boldsymbol{1} & \boldsymbol{if\ \frac{N(n+1)}{N(n)} \geq 1} \\ \boldsymbol{\frac{N(n+1)}{N(n)}} & \boldsymbol{if\ \frac{N(n+1)}{N(n)} < 1} \end{cases} \qquad \textbf{Eq. 1.100}$$

If the probability of acceptance is equal or higher then 1, then the trial move perform in n+1, results in a potential energy lower than the previous n, and by that the trial move performed is automatically accepted. If the value obtain for the probability of acceptance is lower than 1, that trial move will be accepted regarding to a random number between 0 and 1. The Markov chain is then construct during the simulation where a large number of trial moves, the simulations steps, guarantee good results with a low variance. [39]

During simulation several types of perturbation can be made into to the system, some are restricted to the type of ensemble used and restricted to the numbers of the degrees of freedom of each molecule. The main perturbations made into to the systems can be grouped in tree types: [34]

- **Displacements:** This type of perturbation is allowed in the various types of ensembles, where a random particle is selected and then is coordinates are changed. The move is accepted with the probability:

$$\boldsymbol{acc(n \rightarrow n+1) = \min\left[1, e^{\left[-\beta.\left(U(r^{n+1})-U(r^{n})\right)\right]}\right]} \qquad \textbf{Eq. 1.101}$$

- **Volume changing:** A volume changing perturbation is done under a Isobaric-Isothermal ensemble, constant N,P,T, The move is accepted with the probability:

$$\boldsymbol{acc(n \rightarrow n+1) = \min\left[1,\ e^{\left[-\beta.\left(U(s^{N},V')-U(s^{N},V)\ P(V'-V)-N\beta^{-1}.\ln(\frac{V'}{V})\right)\right]}\right]} \qquad \textbf{Eq. 1.102}$$

Where sN is the reduced coordinates, Vn and Vn+1 are the volume of the system at a specific state and after the perturbation, respectively.

- **Insertion/Removal:** This type of perturbations only occur in the Grand-Canonical ensembles, where is allow the exchange of the number of particles (N) in the reservoir.
    - The acceptance probability of the perturbation that adds a particle as the form:

$$\boldsymbol{acc(N \rightarrow N+1) = \min\left[1, \frac{V}{\Lambda^{3}(N+1)} e^{[\beta.(\mu-U(N+1)+U(N))]}\right]} \qquad \textbf{Eq. 1.103}$$

    - The acceptance probability of the perturbation that removes a particle as the form:

$$\boldsymbol{acc(N \rightarrow N-1) = \min\left[1, \frac{\Lambda^{3}N}{V} e^{[-\beta.(\mu+U(N+1)-U(N))]}\right]} \qquad \textbf{Eq. 1.104}$$

Where the chemical potential can be related to the pressure of the reservoir. This can be made by simulation or true experimental data. Through simulation several simulations are performed under Canonical ensembles, where different sizes of the simulation box are chosen in order to represent different pressures at different temperatures. With the data collected, it's set a correlation between the chemical potential, the pressure and temperature, where's obtained an expression to the chemical potential in function of the pressure and the temperature. [40]

Other types of perturbations can be done in the system when it's given more degrees of freedom to the particles, namely, changes in the bond length, angle, torsions, regrowth's and others. The most suitable illustration of the mechanism of the algorithms can be presented by the following steps:

1. Select a molecule in the system at random.
2. Select a type of perturbation
3. Compute the potential energy change [U(rn+1) - U(rn)] caused by a perturbation in this particle from an old state to a new one.
4. Accept or reject the move according to the acceptance probability

The following algorithm shows the basic structure of a simulation in the Grand-Canonical ensemble.

Algorithm 1- [Basic Grand-Canonical Ensemble Simulation]	Comments
PROGRAM mc_gc	Basic μVT-ensemble simulation
do icycl=1,ncycl	Perform ncycl MC cycles
ran=int(ranf()*(npart+nexc))+1	
if (ran.le.npart) then	
call mcmove	Displace a particle
else	
call mcexc	Exchange a particle with the reservoir
endif	
if (mod(icycl,nsamp).eq.0)	
+ call sample	Sample averages
enddo	
end	

Comments:

1. This algorithm ensures that, after each MC step, detailed balance is obeyed. Per cycle we perform on average npart attempts to displace particles and nexc attempts to exchange particles with the reservoir.
2. Subroutine mcmove attempts to displace a particle (Algorithm 2), subroutine mcexc attempts to exchange a particle with a reservoir (Algorithm 3), and subroutine sample samples quantities every nsamp cycle.

Algorithm 2- [Attempt to Displace a Particle]	Comments
SUBROUTINE mcmove	Attempts to displace a particle
o=int(ranf()*npart)+1	Select a particle at random
call ener(x(o),eno)	Energy old conguration
xn=x(o)+(ranf()-0.5)*delx	Give particle random
call ener(xn,enn)	displacement
if (ranf().lt.exp(-beta + *(enn-eno)) x(o)=xn	Energy new conguration Acceptance rule (Eq 1.102)
return	Accepted: replace x(o) by xn
end	

Comments:

1. Subroutine ener calculates the energy of a particle at the given position.
2. Note that, if a conguration is rejected, the old conguration is retained.
3. The ranf() is a random number uniform in [0; 1].

Algorithm 3- [Attempt to Exchange a Particle with a Reservoir]	Comments
SUBROUTINE mcexc	Attempt to exchange a particle with a reservoir
if (ranf().lt.0.5) then	Decide to remove or add a particle
if (npart.eq.0) return	Test whether there is a particle
o=int(npart*ranf())+1	Select a particle to be removed
call ener(x(o),eno)	Energy particle o
arg=npart*exp(beta*eno))/(zz*vol)	Acceptance rule (Eq. 1.105)
if (ranf().lt.arg) then	
x(o)=x(npart)	
npart=npart-1	Accepted: remove particle o
endif	
else	
xn=ranf()*box	New particle at a random position
call ener(xn,enn)	Energy new particle
arg=zz*vol*exp(-beta*enn) /(npart+1)	acceptance rule (Eq. 1.104)
if (ranf().lt.arg) then	
x(npart+1)=xn	
npart=npart+1	
endif	Accepted: add new particle
endif	
return	
end	

Comment:

1. Where have defined: zz = exp(βμ)/Λ. The subroutine ener calculates the energy of a particle at a given position.

1.4.3.3 Truncation of Interactions

When considering a system that is rule by sort-range interaction, it's useful to truncate the intermolecular potential, at a critic distance of the particle i. That is done not only to decrease the time of the calculus of the intermolecular forces but also to avoid that the atom I encounter its self in the neighboring boxes. Macroscopic value are only obtain when considering a system that is organize as a repetition of the simulation box, this tries to simulate the bulk phase at a present of an infinite bulk surrounding, as it can see in the figure 1.10.

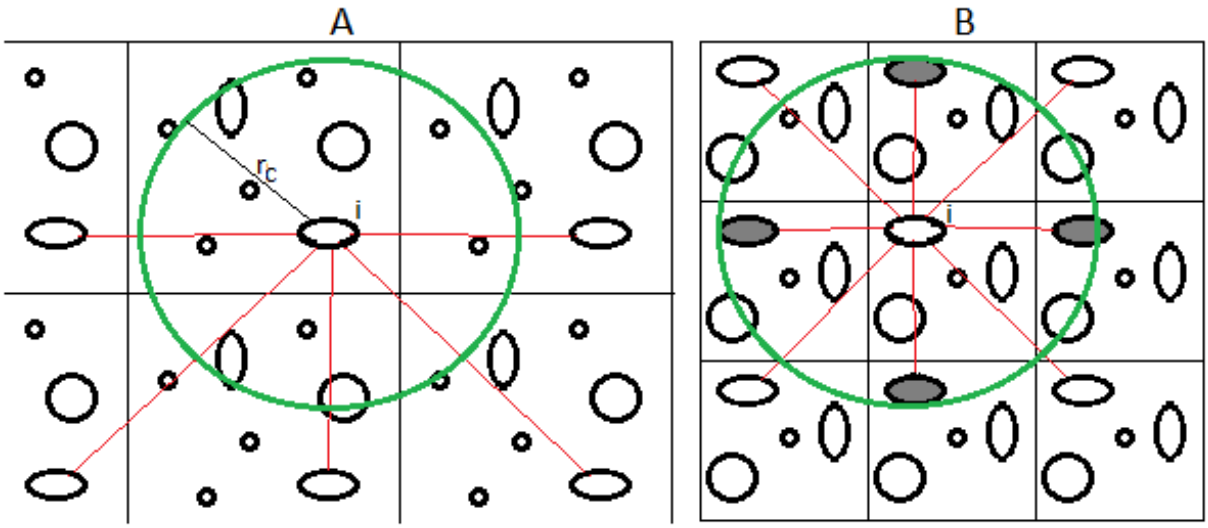

Figure 1.10 – Representation the simulated box and their naboring boxes. In A the cut radius is smaller than the simulation box length; In B the cut radius is larger than the simulation box length

In the two scenarios, A and B, the same critic distance for the truncation boundaries it's set for the particle I, the difference relies on the sizes of the boxes for the different scenarios. In the scenarios A, it is chosen a size large enough that the atom I will not encounter it's replica in the neighbors boxes. At the other hand, in the scenario B, it's is possible to observe that for a simulation box with a length smaller than the critic distance, the particle I will encounter its replicas, in other words the particle I will encounter itself in the bulk. So the scenario B must always be avoided, by changing the length of the simulation box or by changing the critic distance for the truncation.

The truncation used at the end of the critic distant was a very important role in simulation. The value for the LJ potential only is zero when the particles are at a considerable distance. For that and to correct that cut, mainly two types of truncation potential at the critic distance can be used, the Shift method and the Tail correlation. In this work tail corrections are used because that correspond to a better approximation of the full potential. This type of correction increases the attractive interactions in dense phases, such as the liquid phase (while having a similar, but smaller effect on the vapor phase) and, therefore, increases the critical temperature. [34]

1.5 Adsorbents

The study of many different types of porous materials revels to be of the most interest, because of their ability to interact with atoms, ions and molecules not only at their surfaces, but also throughout the bulk region. Porous solids are ubiquitous and utilized widely in many domestic, commercial or industry applications. Application that goes from storing, separating, ion exchange, and sensing molecular guests, as well as for their unique ability to act as host materials to promote organic reactions and act as heterogeneous catalysts. [41]

Adsorption may occur by tree different mechanisms: steric, equilibrium, and kinetics mechanism. The kinetics mechanism is related to the rates of adsorption and desorption of different species into the pores. Preferentially in an industrials process it's is used adsorbents with god adsorption/desorption kinetics, once the time of adsorption is a very important parameter to the process and so will affect the total efficiency of the factory, thus is need to have into consider the rates of desorption. If the process of desorption is very strong then, some problems may occur when regenerated the adsorbent, meaning additional cost. The equilibrium mechanism is based on the abilities of the solid to accommodate a certain quantities of different types of species. And the steric mechanism is related to the different pores dimensions in the solid, where it's allow to small molecules to enter while large molecules are excluded. Pores sizes and shapes of a particular material are directly related to its ability to do a particular function, where a uniform distribution of the pores size leads to selective adsorption.

Regarding pores size, deferent definitions were adopted by the IUPAC:

- Microporous have widths smaller than 2 nm.
- Mesoporous have widths between 2 and 50 nm.
- Macroporous have widths larger than 50 nm.

To obtain good adsorbent, whit good adsorption capabilities and with good kinetics some requirements bust be follow: [25]

- The solid must have reasonably high surface areas or microspores volume.
- The solid must have relatively large pore network for the transport of molecules to the interior.

Recently, many advances approaches have been done, not only to obtain new types of adsorbents, with exceptional properties as well with a uniform distribution, but also to obtain new types of adsorbents where theirs properties are tailored to specific applications like petrochemical, chemical, biochemical, biological, biomedical and others. For this thesis, two types of materials will be study: Carbon nanotubes, and Metal Organic Frameworks (MOFs) [42] [43]

1.5.1 Carbon Nanotubes

The study of materials at nanoscale revels to be of the most importance since at that scale those gain some distinct properties. Particularly materials like carbon materials have shown to be of the most relevance.

Carbon nanotubes are cylindrical structures with diameter in the range of the nanometer and with length that goes from a few microns to centimeters. Discovery in 1991 by Sumio Iijima, they have been target of many studies due to their innumerous fields of application, like electronics, biomedicine, textile industry, aeronautics, gas adsorption, and many others. [44]

Since carbon atom has four valence electrons, it has the capability to form different types of hybridization (sp1, sp2 e sp3), that provides the formation of four possible connections. One simple chance in that hybridization will have a drastic change in the properties of the material. For example, in the case of the diamond and graphite, the carbons atoms have a hybridization of sp3 and sp2, respectively, where in the graphite only three of the valence electrons participate in the connection. [45]

In the case of the carbon nanotubes, those revel to be in a state of hybridization sp2, and is due to the fact of those be in a cylindrical shape, whit very small diameters, that make carbon nanotubes very stiff and resilient, being stronger than diamond. Having high mechanic and thermics resistance, and depending of their symmetry, they can possess great electrical conduction, a ballistic effect, or can be turn into a semi-conduction material. [46]

The diameter of carbon nanotubes, can vary between one nanometer to a few hundreds, they can also be form by one single layer (Single Walled NanoTube – SWNT), ou by multiple layers (Multi Walled NanoTube – MWNT)

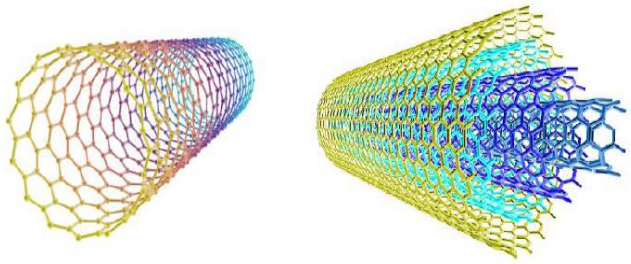

Figure 1.11 – Representation of SWNT at the left and of a MWNT at the right. Adapted from [45]

For the formation of the carbons nanotubes, several tactics can be employed. One process of creation the nanotube is associated to the instability of the graphite when encounter the right conditions and to eliminate those instabilities, the atom carbon that leave the surface of graphite and tends to close upon it self's forming then the nanotube. [47]

The classification of a carbon nanotube related with a sheet of graphite where nanotube is defined depending on the chiral vector (C_h) that he possess. Connecting the OA and BB' points in the image below, obtain a segment of the nanotube structure, where the chiral angle (θ) is obtain regarding the zigzag structure. So a nanotube that possess a θ=0º is denominated as a zigzag, one that have a θ=30º is denominated as an armchair, the others with a chiral angle varying between 0º≤θ≤30º are denominated as chiral nanotubes.

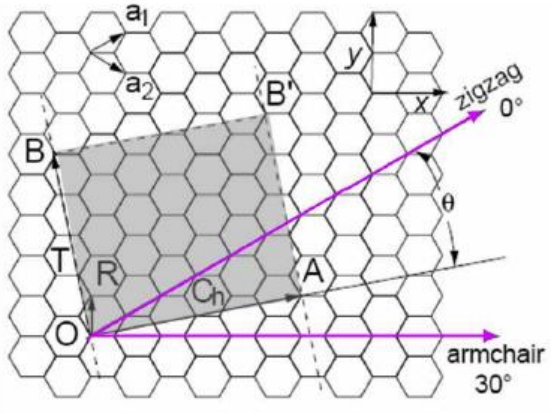

Figure 1.12 – Scheme of and hexagon grid structure. Adapted from [47]

The chiral angle can be express by two unitary vector, a1 and a2 that define the unit cell in the hexagonal structure on the grapheme sheet.

$$\boldsymbol{C_h = n * a_1 + m * a_2 \equiv (n, m)\ (\ 0 \leq n \leq m\ )} \qquad \textbf{Eq. 1.105}$$

So for each par (n,m) is generated a different structure with a certain chirality. In the limits of chirality, for a zigzag nanotube it has n≠0 and m=0 and the armchair tube it as n=m≠0. [46]

The diameter of the nanotube describe as the following:

$$\boldsymbol{d = \frac{L}{\pi} = \frac{|C_h|}{\pi} = \frac{\sqrt{3} * a_0}{\pi} * \sqrt{n^2 + m^2 + n * m}} \qquad \textbf{Eq. 1.106}$$

Where L is the perimeter of the circumference and a0=1.42Å is the length of the carbon-carbon connection in carbon nanotubes.

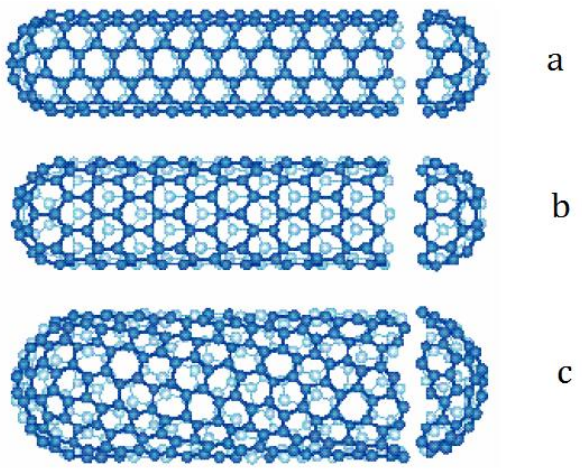

Figure 1.13 – (a) SWNT armchair, (b) SWNT zigzag e (c) SWNT quiral. Adapted from [46]

In the synthesis of the carbon nanotubes, all combination can be possible to form (n,m,θ) and in the case of the MWNT each cylinder can have different and complete distinct characteristics.

The quantic confinement along the circumference of the nanotube walls enables the change of conductivity depending on the configuration (n,m), if the difference between the par n and m, is a multiple of three, or zero the nanotube will present a metallic behavior, otherwise will describe an semiconductor behavior. [45]

1.5.1.1 Nanotubes Synthesis

The intensive study of the properties of the carbon nanotubes, began only after having established certain methods of synthesis. Being the most usual methods the arc discharge, laser ablation and chemical vapor deposition.

1.5.1.1.1 Arc discharge

Arc discharge belongs to the methods that use higher temperatures (above 1700ºC) for synthesis. This method causes the growth of CNTs with fewer structural defects in comparison with other techniques.

It's based on an electric discharged between two cylindrical electrodes of graphite, maintained at constant distance, 1 nm, from each other. The electric charge whit 50 to 120 ampers and with and voltage about 20 volts it's used to create a plasma, that guarantee good conditions to sublimate the carbon atoms in the graphite. The sublimated carbon then deposits in the cathode as form of nanotubes and other types of carbon particles. [47] [48]

This method presents a yield in order of 25 to 70%, and produces carbon nanotubes with diameter between 1.2 and 10 nm. To produce SWNT is necessary incorporates one or more catalytic metals, like cobalt, iron and niquel. [49]

1.5.1.1.2 Chemical vapor deposition (CVD)

This method have been widely used, it offers an alternative routes to obtain carbon nanotubes with the desired properties. It uses hydrocarbons in a presence of a catalyst, which acts as a support for the growth of the nanotube. [49]

Different technics can be used like CVD promoted by plasma, CVD on powder catalyst, CVD on catalyst laid on a plane support or CVD in gas phase. Those provide a synthesis with a high purity, and can be selective regarding to MWNT or SWNT, depending mostly of the catalyst and temperature decomposition of the hydrocarbon. [50]

This method has shown to be the most promisor in the fabrication of the carbon nanotubes since the parameters of synthesis are easily controlled. With the right adjustment on factors like the fraction of metal/catalyst, temperature and with the used of the right hydrocarbon it allows to obtain yields in order of the 70 80%, whit diameter that goes from 5 to 240 nm. [51]

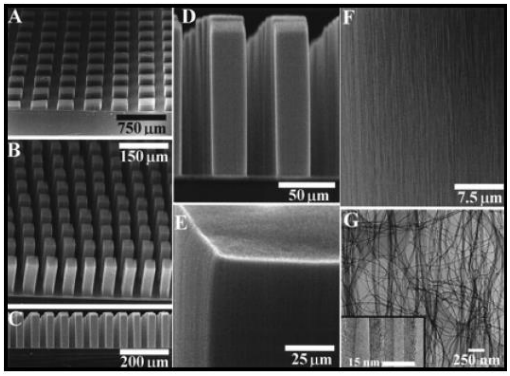

Figure 1.14 – Image of Scanning electron microscopy (SEM) of nanotubos a) Blocks of synthesize nanotubos on plate whit pores size, 250x250 µm, b) 38x38 µm. c) Lateral vision of the towers. d) Tower's top e) SEM image showing the carbon nanotubes perfect aliened. f) Image of a transmission electron microscope (TEM) of nanotubos growth in several towers g). Adapted from [46]

The figure above show, carbon nanotubes form by CVD on iron particles laid on a plane support. The particles are arranged in a nano pores formed on silica plate, obtaining tower's that are compost by many nanotubes aliened.

1.5.1.1.3 Laser ablation

This method is very similar to the Arc discharge method, where the sublimation of the atoms carbons from graphite occurs due to the incidence of a high-power laser.

With the use of the right catalyst and combination of one or more lasers, it's possible to obtain yields in the order of 70 to 90% of SWNT, with low variance in diameter and MWNT, that are compost by 4 a 20 nanotubes. [46]

1.5.1.2 Nanotubes Properties

The great interest of carbon nanotubes relies on is many different properties, like: the capability to be sime-conductors as well conductors, that transport electrons ate very high velocities; their very good capabilities of conduce heat without deforming; their elastic behavior and their physical and chemical properties.

Table 1.1 – Properties of the Carbon Nanotubes. [50] [51] [52] [53] [54] [55] [56] [57]

Material	Specific density (g/cm^3)	Young's modulus (TPa)	Tension (GPa)	Deformation of rupture (%)
Nanotubos	1.3 - 2	1.00	<60	10.00
Steel	7.8	0.20	4.10	< 10
Carbon Fibers	1.7 - 2	0.2 - 0.6	1.7 - 5	0.3 - 2.4
Kevlar* 49	1.4	0.13	3.6 - 4.1	2.80
Material	**Thermic conductivity (W/m.k)**		**Electric conductivity (1/Ω.m)**	
Nanotubos	> 3000		10^6 - 10^7	
Copper	400		6 x 10^7	
Carbon Fibers	1000		2 - 8.5 x 10^6	

For the interest of this thesis it's given a more detailed view of adsorption properties of carbon nanotubes. Adsorptions in nanotube have shown to be of great interest by the rapid increases of experimental and theoretical study.

1.5.1.2.1 Adsorption Properties

Gas adsorption in carbon nanotubes, particulary in SWNT and bundles is an important issue for both fundamental research and technical application of nanotubes. Since 1997, where carbon nanotubes were reported to store large amounts of hydrogen gas with uptake capacities in the range of 5–10% by weight (wt%) is observe a rapidly and intense research on this area. [58]

Adsorption in carbon nanotubes, offer many advantages, not only have an high surface areas, comparable to those of the activated carbons but their structure at the atomic scale is far more well-defined and uniform. So adsorption occurs in specific sites available to the adsorbate molecules. In any case the treatment of the sample of nanotubes must guaranty that open their ends and remove functional groups that block pore entry, and impurities such as carbon coated catalyst particles, graphitic carbons and other. [59] [60]

In the simplest case adsorption can occur in four different sites, as can be seen in the image below. Where the A is an interior site, B is an interstitial site, C is an exterior site and D is a groove site.

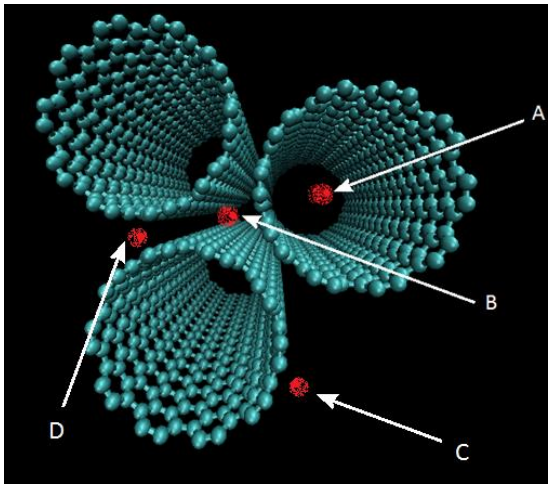

Figure 1.15 – Red dots represented possible sites for adsorption in a group of nanotubes.

The proximity of the interior wall, have a high impact on the binding energy toward adsorb molecules, once the attractive van der Waals interaction are maximize because of the small diameters of the tubes. On the other hand the curvature of the exterior wall's don't allow the overlapping of the van der Waals forces and so adsorption energy must be smaller compared to the interior. Other factors to have into account in the adsorption are the diameters of the tube and chirality due to the confinement. [61]

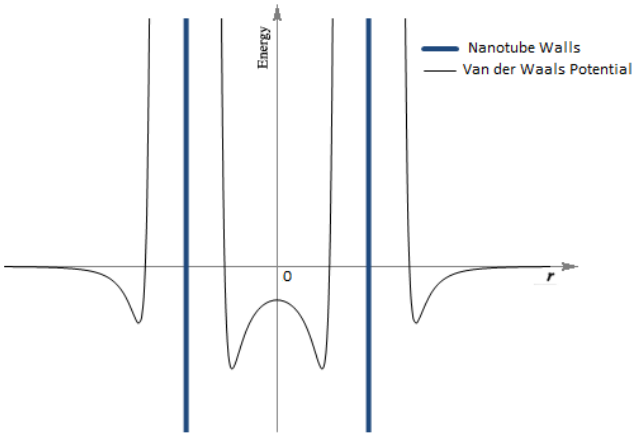

Figure 1.16 – Representation of the Lennad Jones potential, in and out of the nanotube walls.

Computational modeling of the adsorption of various types of gas in nanotubes is very an active area of research. Computational modeling studies show also that while H2, He and Ne particles can adsorb in the interstitial channels, other types of atom are too large to fit into such tiny spaces. The insight and studies given in this type of research has very important ramifications for the application of nanotechnology to gas-storage devices, molecular sieves and filtration membranes. [59]

1.5.1.3 Nanotubes Application

Since carbon nanotubes present a fascinating set of new properties, those open the doors to the nanotubes revolutionary the world. They have application that goes to the field of electronics to the field of composite materials.

In electronics they are used as transistors integrated in a nanocircuit, used as sensors, since they have the capability of change their electric properties with physical perturbations and used as super condenser. They are also used as additives to polymeric matrix, where provides stiffness and elasticity to membranes and can be used to create better materials that can handle with a lot of force. Can be incorporated in clothes as sensors and can also be applied in biomedicine, since they are biocompatible and finally, are used as an adsorbent of hydrogen and organic compounds, and function as a filter. [60] [62] [51]

1.5.2 Metal Organic Framework

Metal-organic frameworks (MOFs), also known as porous coordination polymers, are porous materials in which metal-containing nodes are connected by organic bridges. A larger variety of inorganic and organic components can be used to construct MOFs, and this versatility has enabled the design and assembly many materials, having new and exceptional properties.

The developed of MOF, start ate 1954 by Wells, and ware driven by the continues study on catalyst and their improvements, this, results in a compound whit high selectivity, high adsorption capacity, good adsorption/desorption rates and have the property of have low enough binding energy for total regenerability, and for that great interest in the chemical industry. [63]

They are usually crystalline compounds, built from organic ligands and metal ions that are held together by covalent bonds to form 1- 2- or 3-D structures. MOFs have exceptionally large surface areas and many have permanent porosity. The highest surface areas reported to date are over 6000 m2/g. They also display a vast chemical versatility and many possible structures, compared to conventional inorganic materials such as zeolites. Also have ability to withstand high pressures if necessary. As such, MOFs represent a unique class of ordered porous materials that have great potential as hosts in applications that require pore dimensions that exceed those of zeolites. [64] [65]

Because of their unique structure it's possible to design and control the architecture and functionalization of the porous. This only was possible when the synthesis, and the treatment after, occur at the right conditions. The initial MOFs exhibited a very poor stability, collapsing after drying, resulting in no permanent porosity. After the process of synthesis be well implemented the MOF obtain had extremely high surface areas and pore volumes, which can be chosen according to the specific applications. They also present, in some cases, flexible behaviors that allow the entry or exit of some specific compounds, being that phenomenon called of breathing or gate−opening phenomena and in this case, the porosity change according to some perturbation like changes in pressure, temperature, and guest molecules.

Different types of synthesis methods have been applied for construct MOF materials. Among them, classical hydro(solvo)thermal synthesis, microwave and electrochemical synthesis, diffusion and ultrasonic techniques. [66]

Similar to the synthesis of organic copolymers, the careful choice of the building blocks determines properties that are retained and exhibited by MOF, like is magnetic exchange, acentricity for non-linear optical (NLO – is the study of interaction of intense electromagnetic field with materials to produce modified fields that are different from the input one) applications, or the definition of large channels available for the passage of molecules. [67] [68]

MOF synthesis usually proceeds by self-assembly of a metal and an organic linker in solution. Where the metal is usually introduced in the form of salts, and organic solvent are typically used in the reaction. Typically the reaction in a batch reactor done at temperatures that goes from 100º to 200ºC for 12-48 hours. For large-scales production is used electrochemical, microwave assisted process, where those tries to give the best conditions for the self-assembling of the MOF, where low temperatures favor the growth of the MOF. [64] [41]

1.5.2.1 MOFs Application

Although porous MOFs have a fairly recent development, it is clear the number of advantages of this class of material.

Their synthesis process is relatively simple, and it's possible to design both the porous structure and the chemical environment of the active site, by carefully selecting the metal, the organic ligand and how they are connected. Selecting the right pours size it's possible to obtain different application for the MOF, with a majority of applications focusing on the sorption behavior and molecular sieving, like gas separation, or gas purification, membranes and coatings and lately gas chromatography.

Regarding other properties than pore size like pore topology, connectivity, and interactions (both van der Waals and electrostatic) of the guest molecules with the framework atoms, it's possible to separate wide variety of mixtures like CO_2–N_2, CO_2–CH_4, CO_2–CO–CH_4–H_2, CO_2–H_2, CH_4–H_2, O_2–N_2, natural gas, alkane–alkene, alkyne–alkene, and hydrocarbon isomers, reinforcing is importance in the chemistry industry. [69] [70] [71] [72] [73] [74] [75] [76] [77] [78]

Gas adsorption in MOF may occur, namely by gating and kinetic trapping. Gating occurs when the porous structure changes during adsorption process, going from non-porous to porous at a specific pressure. And kinetic trapping is due to the presence of narrow windows, which are considerably smaller than the pours, resulting in the kinetic trapping of sufficient smaller particles. That was shown by Zhao who reported the irreversible adsorption of hydrogen in some MOF at 77 K, as due to the kinetic trapping. [43] [79]

MOF also shown to have great capability to storage gases at low temperatures and high pressures, intense studies have been made in storage of hydrogen, methane and carbon dioxide. For example, it has been shown that MOFs are able to store high densities of hydrogen under relatively moderate pressures. The high accessible void volume in MOFs makes them one of the most promising materials to meet hydrogen storage standards set by the U.S. Department of Energy (DOE). Additionally MOFs offer the added advantage of having an organic component that can be tailored to accommodate a variety of reactive groups that can actively or passively participate in catalysis. That was shown by Hasegawa who used functionalized organics ligands with amide groups to demonstrate its ability to catalyze Knoevenagel condensation.

Because MOFs are biodegradable, they also are being studied as container materials for drug delivery. Horcajada have demonstrated MIL-53's ability for controlled release vehicle for drug ibuprofen. And regarding the capabilities of catalyst, MOFs with chiral framework architectures have been shown to catalyze reactions enantioselectively, in the studys of Wu and Lin. The great adsorption power, their large surface areas and pore dimension, also provides the MOF to be used as environmental remediation and purification. [64] [65] [80] [81] [82] [83] [84]

Other applications for MOF consist in their used in sensor devices, because of their magnetic and luminescence properties. Luminescence properties are obtained with the incorporation of luminescent inorganic metal centers being the most common choices lanthanide ions, especially Eu(III) and Tb(III).

Major breakthroughs in the development of MOFs have been done, resulting in a variety of MOF that can divide in classes such: Covalentorganic frameworks (COFs), which consist of light elements (B, C, N and O) resulting in various 2D and 3D porous framework; Zeolitic-Imidazolate Frameworks (ZIFs); Tetrahedral-Imidazolate Frameworks (TIFs); Boron-Imidazolate Frameworks (BIFs); Zeolitelike Metal-Organic Frameworks (ZMOFs). This type of MOFs, with topologies similar to the purely inorganic zeolites, exhibit unique properties when comparing to zeolites such, the presence of extra-large cavities, chemical stability, ion-exchange capability also having permanent porosity; and many others. [86]

Through this thesis only one class of MOF will be studied, namely the UiO-Zr.

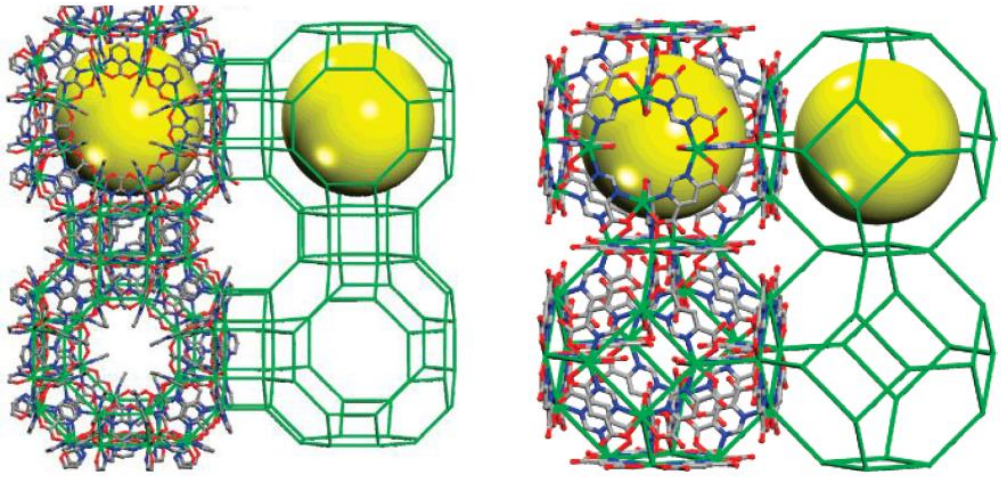

Figure 1.17 – Single-crystal structure of rho-ZMOF (left) and sod-ZMOF (right). Hydrogen atoms and quest molecules are omitted for clarity. In - green, C - gray, N - blue, O - red. The yellow sphere represents the largest sphere that can be fit inside the cage, considering the van der Waals radii. Adapted from the American Chemical Society. Adapted from [86]

1.5.2.2 UiO (Zr)

The UiO-series (UiO: Universitetet i Oslo) are a new type of MOF with new zirconium-based building brick that allows the synthesis of high surface area MOFs that goes up to 4170 m^2/g, and large pours with unprecedented stability. [86]

Group four elements can be used as inorganic component. They interact strongly with oxygen and are therefore obvious choices for stable inorganic cornerstones in combination with oxygen containing linkers. The linker can be of many different types, and their choice will not influence stability of the MOF, instead their selection will depend of the size of the pour pretended. Usually linkers with one, two, and three benzene rings, give openings corresponding to 6, 8, and 10 Å. [88]

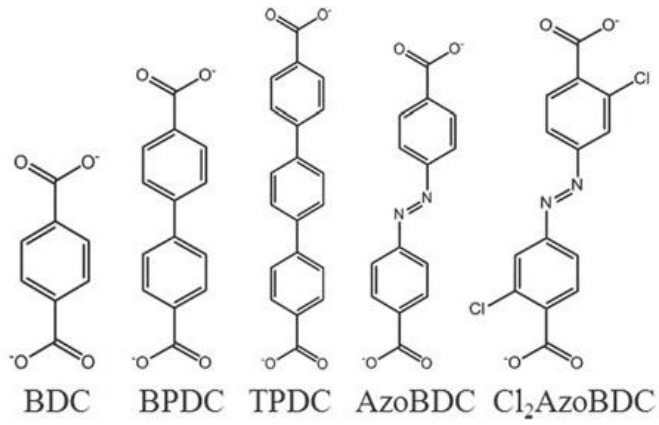

Figure 1.18 – Different type of organic linker.

For this thesis Zr-MOF with BDC and BPDC linker are used, commonly called of UiO-66 and UiO-67 respectively. The Access to the internal surface of Zr-MOFs is restricted by triangular windows. The main structure of the UiO-67 (Zr), and is crystal forma are represent in the images below.

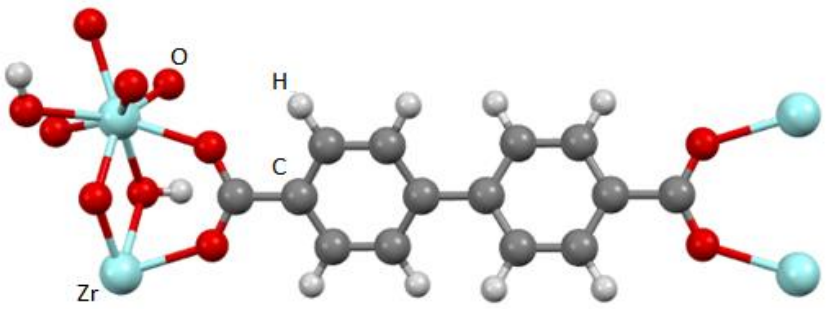

Figure 1.19 – Representation the main structure of the UiO-67Zr.

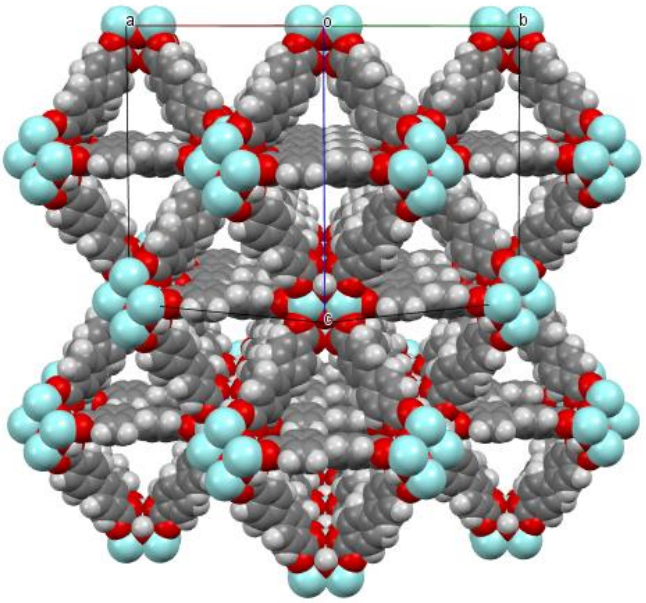

Figure 1.20 – Representation of eight molecules of UiO-67Zr.

Because of the stability provide by the elements in the Grup-4, the new Zr-MOFs series, have very high surface areas, the ability to adsorb large volumes of gas and have high thermal and chemical stability, especially water stability. Once the Zr metal can be in more than one oxidation state, this makes the Zr-MOFs ideal candidates for use as catalysts (e. g. in olefin polymerization), or more especially as electrodes in lithium batteries.

The chemical stability when exposure to Water, is a property rare in conventional MOFs and for that, other application can be given such as, new delivery release pharmaceutical formulations. The sustained release allows the effect of the drug to prolong in the system that occur due to a less fragment administration. For that they can be used as drug reservoirs for pharmaceuticals where the administration can be made by gastrointestinal tract or for depot placement subcutaneously. The thermal stability makes the Zr-MOFs particularly suited for gas storage since gas release is generally affected by raising the temperature on the MOF.

Their very high surface area and stability are also particularly suitable for containing gases. The types of gases of interest are principally fuel gases such as hydrogen, methane and acetylene, under raised temperature or reduced pressure. Also can be used to capture gaseous contaminants or to contained other gases such as nitrogen, carbon monoxide or carbon dioxide.

The Zr-MOFs may also be used as catalysts, where it's possible to control their catalyst power, by the catalytic activity of the metal, by using linkers with catalytic activity or by loading the MOF with a catalyst. [89]

1.6 Adsorbates

One main advantage of molecular simulation it's the capability of simulates any compound. In real experimental adsorption studies the time and the money spends on different types adsorbents is significant, and in some, there are some security related issues that are need to take into account. Nevertheless in molecular simulation, those problems are complete overtaking, and the choice of the adsorbents is done regarding the choice of the user. That choice must be done considering the types of adsorbents and their capabilities to adsorb the adsorbates chosen.

For the adsorbents presented, many different types of gaseous adsorbates can be used, where is given a greater emphasis in gases like carbon dioxide (CO_2), ethane (C_2H_6) and methane

1.6.1 Carbon Dioxide

Carbon dioxide (CO_2) is a colorless, odorless, non-flammable and nontoxic gas. It is assimilated by plants which in turn produce oxygen by photosynthesis. It is produced from the combustion of coal or hydrocarbons, the fermentation of liquids and the breathing of humans and animals. The resulting of the industrialization and the rise increase of burning and used of nonrenewable energies, such as fuel oil and is derivatives, cause an increase of 18% in the concentration of CO_2 between the years 1970 and 2010, according to the NOAA Climate.gov.

Carbon dioxide comprises two oxygen atoms double covalently bonded to a single carbon atom, with an O-C-O angle of 180°. It's a very stable gas and its used is confined as additives in food industry, commonly used in pneumatic systems (pressurized gas), fire extinguisher, used as a supercritical solvent, and others.

The continue increase of the concentration and the effects that carry after, led to many studies in technologies and new materials, to capture and storage the carbon dioxide. Currently three major technologies to capture CO_2 prevenient from coal fired power plant can be used: pós-combustion capture, which used a solvent that reacts with carbon dioxide and selectively removes it from the furnace outlet stream; oxyfuel combustion, which is based on the principle of combustion of coal in an oxygen rich nitrogen-free atmosphere; and pre-combustion capture, which is based on the combustion of hydrogen rich (Syngas) fuel created from coal or natural gas when carbon dioxide is removed to power a gas turbine.

For storage two approaches can used, long term store and temporary store. Where in temporary stage CO_2 it's used as an injection gas for Enhanced oil and gas recovery, being capable of be recovered and re-injected.

1.6.2 N-Alkanes and Alkenes

Hydrocarbons compounds are constituted essentially by carbon and hydrogen atoms. Those can be divided as saturated and unsaturated compounds. Alkanes are molecules that are completely saturated, generally be representing by the C_nH_{2n+2}, in contrast alkene are molecules that have at least one double bond and can be represented by C_nH_{2n}.

The most part of the hydrocarbons used in industry ware formed at high pressure, trough many years inside the Earth crust, and represent a very compact form of energy that can be used in many different and important applications. Through several different techniques it's is possible to obtain a grand variety of hydrocarbons from coal, oil and natural gas, that have high energy densities.

Typically with a decree on the number of carbon the energy/mass ration tends to increase, the problem is that light hydrocarbons are often found in the gas state and for that they have very low density, resulting in large volume reservoir, and high pressures conditions. One way to overcome these problems is to use adsorbent materials that guaranty good and safe conditions to storage large quantities of gases, typically gases like hydrogen and methane. [89]

From the series of alkanes and alkene available, this work will focus is studied in gases like methane (CH_4), ethane (C_2H_6), for storages and for separation. A separation of this kind of gases have a very important role in the petrochemical industry, since some of those gases are usually form at the same time and for that is require additional processes to separate them. Whit the study of new adsorbents whit high selectivity and that are easily restore it's possible to obtain a new viable and more economical process.

2 Experimental and Theoretical Studies

2.1 Theoretical studies of adsorption on the UiO-66Zr metal organic framework.

The study of the adsorption properties on MOF's it's a very important subject because of the advantages that they can offer, namely in storage and separation process. In the present work the two main gases study in UiO-66Zr adsortion are methane and carbon dioxide. Such gases have a high potential and importance of study, where Methane its point out as a new suitable and less polluting energy source and the store of Carbon Dioxide can have a significant impact on environment.

2.1.1 Methane

2.1.1.1 Introduction

Being a main component of the natural gas, methane had gain new interests in term of capture, storage and shipping methods. Where, the new upcoming form of obtaining natural gas true shale gas is set to have a significant impact on their uses. Until now, much of is used is restricted to industry and domestic uses, but continual increase of is extraction is lending producers to seek new markers, namely for transportation. Methane is a relatively clean-burning fuel, and it will continue to be an important part of the world economy and environment.

Comparing whit other fossil fuels, methane it has the lowest carbon intensity, emitting less CO_2 per unit of energy generated and it burns cleanly and efficiently. Unlike oil, natural gas also requires limited processing to prepare it for final use. These favorable characteristics have enabled him to penetrate many markets, including domestic and commercial heating, multiple industrial processes and electrical power. [90] [91]

On the other hand, since this is on the gaseous form have low energy density, being this a uniquely disadvantaged in terms of transport and storage. That has trigger tremendous studies with the aim to improve and created new technologies for that purposes.

One, related with physisorption process involving porous materials, show to have an efficient storage/capture with the ability to release the adsorbed gases by changing the conditions of the reservoir. Among the many materials study, such as activated carbons and zeolites, a new one, the metal–organic frameworks (MOFs) has shown suitable attention in adsorption/separation properties. [92] [93] [94] [95]

The simulations perform on the metal-organic framework UiO-66Zr, ware done by Monte Carlo method, where two different types of force field ware applied. Different types of force fields are used to represent the experimental data within a better fit; one force field, considers that the hydrogen's aren't explicit, that means that they are united in the major frame, called UiO-66-UA; the second one considers the explicitly of the hydrogen's, UiO-66-EH. That will give us an understanding on how important the hydrogen's are in the methane adsorption process on Ui-66Zr.

The different types of force fields ware obtain at three different temperatures, 298.15, 313.15 and 343.15 K at a pressure range that goes from 0.06 - 70 bar. The data obtain through simulation is them compared whit experimental data obtain by Jasmina H. Cavka et al..

2.1.1.2 Simulation

Many of the simulation perform on MOFs are under a classical type potential, where a broadly of force fields can be used. Different types of force fields have been constructed in order to represent the several types of atoms and molecules, not only in MOFs but also for a large number of adsorbents. The most often and commonly used force fields for MOFs are the UFF, DREIDING, OPLS and the TraPPE, those show to represent the experimental data whit very accuracy for materials like CU-BTC, various types of IRMOFs and MIL respectively. Combinations between force fields can also be applied where recently a combination between the UFF and the DREINING force field were studied by Qingyuan Yang et al. and applied in Zr type MOF's. [91] [96] [94] [97] [98]

As a simplification, we shall assume that the adsorbent under study, UiO-66Zr, has a rigid structure; this is a good simplification since the Zr-MOF has a very rigid structure and does not present conformational changes. For that reason the bond, angle, torsion and the improper torsion terms are cap as zero. For the parameterization of the solid-fluid dispersive interactions, the Lennard Jones parameter ware carefully selected taking into account the LJ's parameters of similar molecules. In the TraPPE force field, non-bonded interactions are governed by a 12-6 LJ, where in this case the electrostatic forces in the MOF are neglected since the methane molecule has no charges associated. For the parameterization of the adsorbate, is used a well-known force field the TraPPE-UA. The unlike LJ interactions are computed with Lorentz–Berthelot combining rules. The LJ parameters used for the united methane are presented in the table below.

Table 2.1 – LJ parameters for the pseudo-atom methane.

Label	σ (K)	ε/k_B (K)	Mass (g/mol)	Ref.
CH4	3.74	148	15.03	99

The used of two different force field applied, the force field denominated as UiO-66-UA and the force field denominated as UiO-66-EH, was done to obtain a more precise values when comparing whit the experimental data, where the difference between them relies on the explicit description of the hydrogen atoms. This results, in different but similar LJ parameters for both force fields. The crystallographic structure for the UiO-66Zr was obtained by Qingyuan Yang et al. by X-ray diffraction (XRPD). The resulting structure was further refined using a density functional theory (DFT) geometry optimization procedure.

- **UiO-66-UA**

The parameterization of the UiO-66Zr using an united atom force field uses seven pseudo-atoms: Zr, C25, C13, C1, O25, O1 and O29. The hydrogens H1 and H25 are united with the pseudo-atoms O25 and C25, respectively.

The LJ parameters for the aromatic carbons are taken from the parameterization TraPPE-UA of the toluene; the [CH]aro and the [C]aro-CHy correspond to the C25 and the C13 respectively. The C1 parameter was taken considering a nonbonded interaction. Regarding the oxygens parameters, for O1 and O29, they were taken from the TraPPE-UA for nonbonded interactions of an ether, where the LJ values correspond to a CHx-[O]-CHy. The values for the O25 were also obtained from the parameterization TraPPE-UA for nonbonded interactions of an alcohol being the parameters correspondent to a CHx -[CH2]-OH. The values for the Zr were obtained from the UFF force field.

Table 2.2 – LJ parameters of the UiO-66Zr molecule, for the UiO-66-UA force field.

Label	Site	σ (K)	ε/k_B (K)	Mass (g/mol)	Ref.
C25	[CH]aro	3.74	48.00	13.02	100
C1	C	3.90	41.00	12.01	101
C13	[C]aro-CHy	3.88	21.00	12.01	100
O1	TraPPE-UA	2.80	55.00	16.00	102
O25	CHx-[O]-H	3.02	93.00	17.01	102
O29	TraPPE-UA	2.80	55.00	16.00	102
Zr	UFF	2.78	34.72	91.22	103

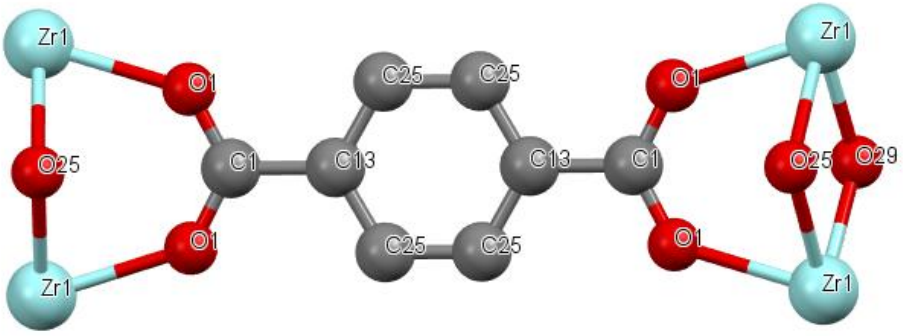

Figure 2.1 – United atom UiO-6Zr framework representation.

- **UiO-66-EH**

For the parameterization of the UiO-66Zr using the explicit hydrogen force field, we use nine atoms: Zr, C25, C13, C1, O25, O1, O29, H1 and H25. Regarding the atoms Zr, C13, C1, O1 and O29 the LJ parameters are the same as those for UiO-66-UA. The parameters of the atoms C25 and H25 are obtaining trough the parameterization TraPPE-EH of the benzene correspondent to a X(aro)-C-(aro)-X(aro) and H-C(aro), those value are been report by Neeraj Rai and J. Ilja Siepmann in their work on phase equilibrium, where they demonstrated to be within a good agreement with the experimental data. For the O25 and H25, their parameters are obtained from a parameterization TraPPE-UA of an alcohol, due to the lack of information. [100]

Table 2.3 – LJ parameters of the UiO-66Zr molecule, for the UiO-66-EH force field.

UiO-66	Site	σ (K)	ε/k_B (K)	Mass (g/mol)	Ref.
C25	[C]aro	3.60	30.70	12.01	104
C1	C	3.90	41.00	12.01	101
C13	[C]aro-CHy	3.88	21.00	12.01	100
O1	TraPPE-UA	2.80	55.00	16.00	102
O25	CHx-[O]-H	3.02	93.00	16.00	102
O29	TraPPE-UA	2.80	55.00	16.00	102
Zr	UFF	2.78	34.72	91.22	103
H1	H	2.36	25.45	1.01	104
H25	H	0.00	0.00	1.01	106

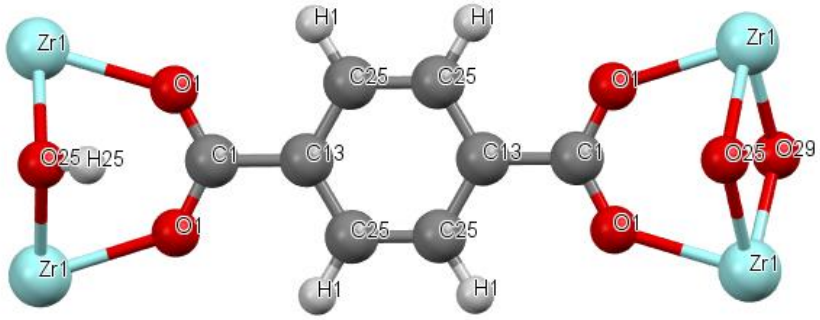

Figure 2.2 – Explicit hydrogens UiO-6Zr framework representation.

In this work the simulation box contains eight molecules of the MOF; this is required since a cut-off radius must be secured. The size of the cubic simulation box is Lx = 41.9568 Å, Ly = 41.9568 Å, and Lz = 41.9568 Å, whit a cell volume of 73859,6 Å3. In the image below, it is observed how the eight molecules of the MOF will be distributed in the simulation along the axis. [91]

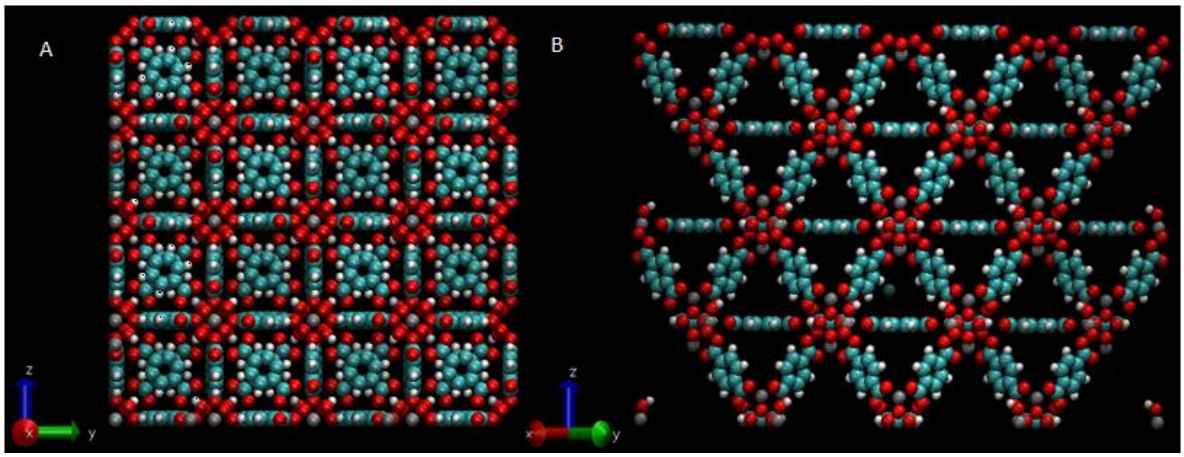

Figure 2.3 – A representation of the simulation box, whit the adsorbent built in, in different perspectives.

The potential radius cutoff (rcut) for solid fluid interaction is set for 14 Å. Conventionally, this should satisfy the following condition: rcut < min{(Lx)min (Ly)min, (Lz)min}/2. That is done to prevent interaction with replica atoms in the neighboring boxes. Since half the box size corresponds to 20.274 Å the condition is satisfies. Regarding the dispersive forces at the frontier of the rcut, we apply an analytical tail correction in all simulations.

Each Monte Carlo simulation consists in two runs. The first is to equilibrated the system and uses at least 10^5 steps, followed by a second run with at least 10^6 steps for the production period. The data is extract from the results of the second run and consists in the number of molecules, density of the adsorbate phase and the isosteric heat.

Regarding the types of perturbation allowed in the simulation, we only have to consider two types of moves for the methane molecules. The first, with a probability of attempt of 40% is an insertion/deletion perturbation; the second, with an attempt probability of 60% is a displacement perturbation. Finally, standard deviations of the ensemble averages were computed by breaking the production run into five blocks.

In the Grand Canonical Monte Carlo (GCMC) ensemble, the thermodynamic state of the system is defined by temperature, chemical potential and the extensive variable, box volume, that is fixed to all GCMC simulations performed in the UiO-66Zr.

In order to correctly relate the gas phase density and pressure values with the chemical potential in the simulation box, it is necessary to run a series of Canonical simulations (N,V,T) for the simulated temperatures, 298.15, 313.15 and 343.15 K. Considering 40 molecules of methane and taking eight different sizes of box length, from the canonical simulations we obtain the gas pressure and bulk gas density for each box size. With those values, a fitting to a polynomial equation is done for the independent variable P and ρ using the following relation:

$$\mu_i = \mu_0 + k_B T * \ln(\rho_i) \qquad \text{Eq. 2.1}$$

where:

$$\mu_{i0} = k_B T * \ln(\Lambda^3) \qquad \text{Eq. 2.2}$$

and:

$$\Lambda = \sqrt{\frac{h^2}{2\pi m k_B T}} \qquad \text{Eq. 2.3}$$

Λ is the thermal de Broglie wavelength, h is the Planck constant, m is the mass, k_B is the Boltzmann constant and T is the temperature. Combining the equation 2.1 and 2.2 it is obtain an expression for the relation between the μ vs ρ,T and μ vs P,T where:

$$\frac{\rho}{T^{\frac{3}{2}}} = f\left(\frac{\mu_{(\rho,T)}}{T}\right) \qquad \text{Eq. 2.4}$$

Considering the ideal gas equation:

$$\rho = \frac{P}{k_B T} \qquad \text{Eq. 2.5}$$

Obtain:

$$\frac{P}{T^{\frac{5}{2}}} = f\left(\frac{\mu_{(P,T)}}{T}\right) \qquad \text{Eq. 2.6}$$

Adjusting the values of the density bulk and pressure to the equation 2.4 and 2.6 respectively, to a linear equation, obtains the chemical potential calibration equations for methane:

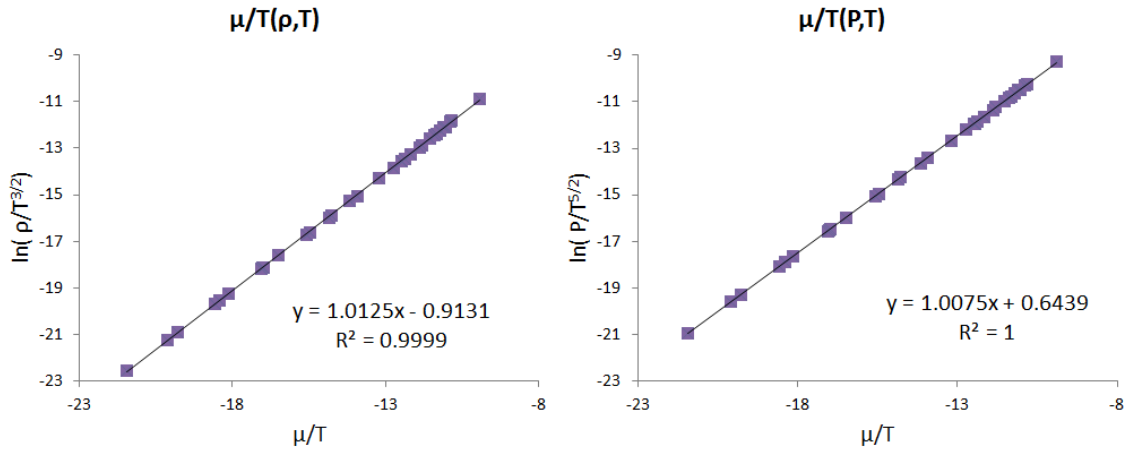

Figure 2.4 – Chemical potential calibration curves for methane, obtain through simulation.

As can be seen a linear equation adjust to the data whit a R^2 approximating the unit. Those equations are used to obtain, for a certain temperature, the pressure or density values in function of the chemical potential.

2.1.1.3 Results and Discussion

In order to compare the experimental data with the simulations, it is necessary to ensure the dimensionality of the system. The experimental data is present as the total amount adsorbed (q_T (mol/kg)) and so it is necessary to convert the simulation data to the same units. The simulation data obtained consist of the total number of adsorbate molecules in the box and the apparent density. Using the apparent density the flowing expression should be taken:

$$q_i = \frac{\rho_{a_i}}{MM_{MOF} * \rho_P} * 1000 \qquad \text{Eq. 2.7}$$

where q_i is the total amount of the absorbate in moles per kilograms of MOF for a certain pressure, ρ_{ai} correspond to the apparent density of the adsorbate phase. The ρ_{ai} can be obtained by direct extraction of the simulation data or by taking the total amount of methane molecules per box volume. Similarly, ρ_P corresponds to the apparent density of MOF.

Figure 2.5 compares the experimental adsorption isotherms obtained by Jasmina H. Cavka et al., with the simulated data for the tree distinct temperatures. These value are expressed in terms of the total amount adsorb q_T. As can been seen, there is good agreement between the simulated data and the experimental measurements for the two force fields. It is also seen that the UiO-66-UA force field gives slightly better predictions, although the differences between both force fields are not very significant. At pressures lower than 10 bar, figure 2.6 in a logarithmic scale, shows a slight discrepancy between the experimental data, where the simulated data overpredict the experimental loadings for all temperatures.

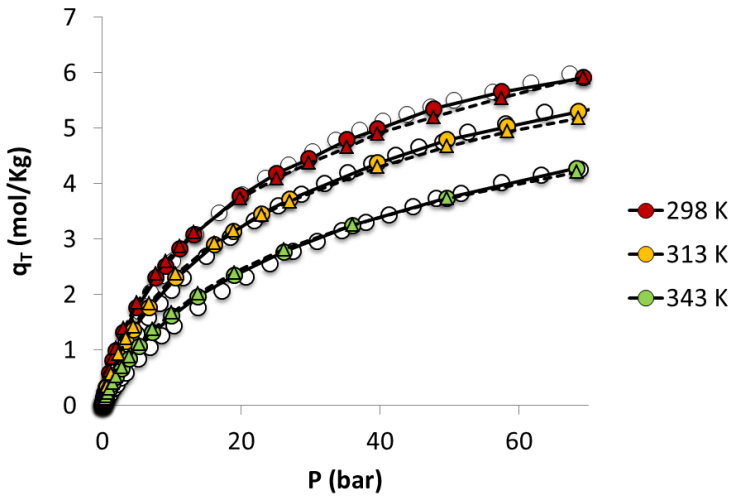

Figure 2.5 – Comparison between the two types of force fields applied for the simulation of methane on UiO-66Zr and the experimental data. The results are terms of total amount adsorbed in function of the pressure. The filled circles represent the UiO-66-UA, triangles the UiO-66-EH and empty circles the experimental data obtain by Jasmina H. Cavka et al, for the three distinct temperatures.

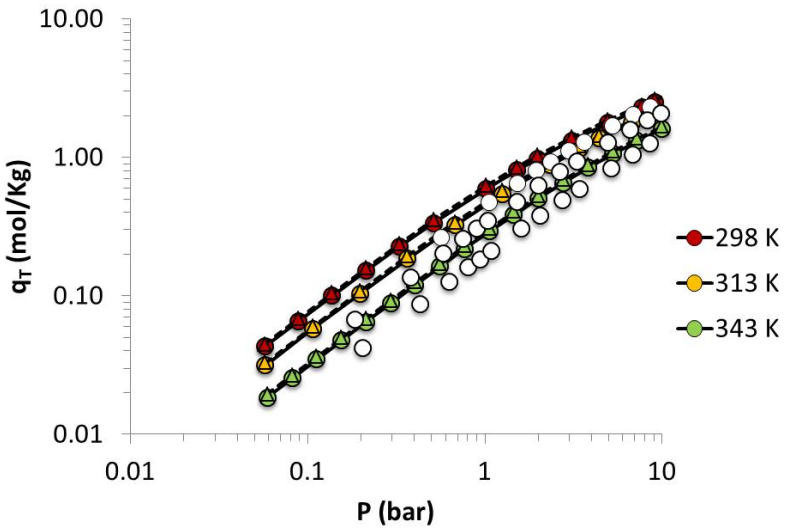

Figure 2.6 – Comparison between the two types of force fields applied for the simulation of methane on UiO-66Zr and the experimental data. The results are terms of total amount adsorbed in function of the pressure. The filled circles represent the UiO-66-UA, triangles the UiO-66-EH and empty circles the experimental data obtain by Jasmina H. Cavka et al, for the three distinct temperatures.

2.1.1.3.1 Isosteric heat of Adsorption

The isosteric heat (or differential enthalpy) of adsorption, Q_{st}, is the amount of heat released when an infinitesimal number of molecules is transferred at constant pressure from the bulk gas phase to the adsorbed phase. In this work, this quantity is calculated from statistical thermodynamics using the fluctuation formulas. In GCMC simulation, the isosteric heat is calculated from the partial derivative of average total energy concerning to adsorbate phase (U_{ads}) and the vapor phase (U_{gas}), with respect to the average number of adsorbed molecules.

$$\boldsymbol{Q_{st} = -\Delta H = k_B T - \frac{\delta\langle U_{ads}\rangle}{\delta\langle N\rangle} + \frac{\delta\langle U_{gas}\rangle}{\delta\langle N\rangle}} \qquad \textbf{Eq. 2.8}$$

And:

$$\left(\frac{\delta\langle U_{ads}\rangle_\mu}{\delta\langle N\rangle_\mu}\right)_\beta = \left(\frac{2\langle U\rangle_\mu}{2\langle N\rangle_\mu}\right)_\beta = \frac{\langle U.N\rangle_\mu - \langle U\rangle_\mu\langle N\rangle_\mu}{\langle N^2\rangle_\mu - \langle N\rangle_\mu\langle N\rangle_\mu} \qquad \textbf{Eq. 2.9}$$

Where the brackets ⟨…⟩μ denote an average in the grand canonical ensemble, N is the number of guest molecules, and μ is the chemical potential of the guest molecules. Considering that the gas phase behaves like an ideal gas, the last term in eq. 2.8 is negligible, leading to:

$$\boldsymbol{Q_{st} = -\Delta H = k_B T - \frac{\langle U.N\rangle_\mu - \langle U\rangle_\mu\langle N\rangle_\mu}{\langle N^2\rangle_\mu - \langle N\rangle_\mu\langle N\rangle_\mu}} \qquad \textbf{Eq. 2.10}$$

This method relies on many particle insertions and removals in the grand-canonical ensemble so long simulations in the grand-canonical ensemble are needed to obtain accurate statistics for the averages, especially in the limit of low chemical potential where the number of molecules is very low. [107]

The results, for the force field UiO-66-UA, are presented in the figure 2.7 where the values vary between 16 and 18.5 kJ/mol. A decrease is observed of the isosteric heat until reach a minimum at a loading of 2 mol/kg, changing is decrease tendency after. Such behavior is not unusual and has been observed for the C_{168} schwarzite by Ravichandar Babarao et. al. when studying methane adsorption. [85]

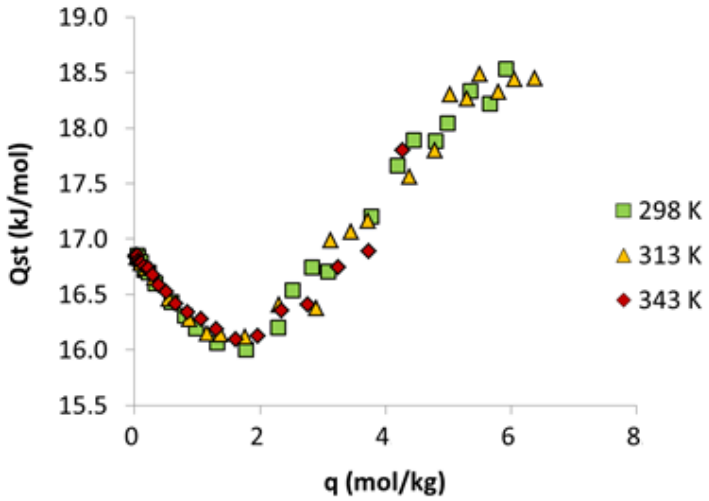

Figure 2.7 – Isosteric heat as a function of loading. The results ware obtains through the simulation of methane on UiO-66Zr, using the UiO-66-UA force field, for the three distinct temperatures.

2.1.1.3.2 Low-Coverage Adsorption Properties

For the calculus of the Henry's constant at low covered, five to six points were used that vary between 0.06 and 0.4 bar. The resulting linear tendency line and their corresponded square error are presented in the figure 2.8. As expected, the values for the Henrys constant get lower with the increase of the temperature.

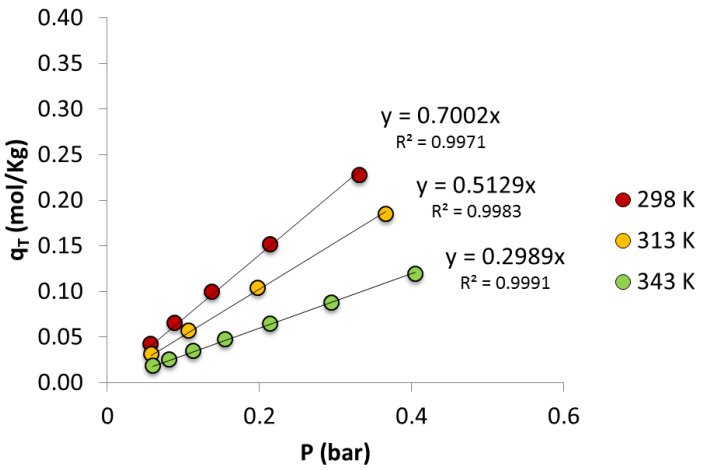

Figure 2.8 – Total amount adsorbed q_T in function of pressure, for the low pressure zone. The circles represent the results obtain through the simulation of methane on UiO-66Zr, using the UiO-66-UA force field, for the three distinct temperatures.

In the table 2.4 is presented the results of the Henrys constants for methane at the three temperatures in study.

Table 2.4 – Henry constants obtain for adsorption fot methane on UiO-66Zr, using the UiO-66-UA force field, for the three reference.

CH_4	289 K	313 K	343 K
K_H (mol/kg/bar)	0.7002	0.5129	0.2989
R^2	0.9971	0.9983	0.9991

2.1.2 Carbon dioxide

2.1.2.1 Introduction

The used and combustion of fossil fuels such coal and petroleum has generated a vast amount of CO_2 released to the atmosphere. This led to severely adverse impacts on environment like air pollution and global warming. In effort to reduce the amounts of CO_2 release to the atmosphere, new constrictions have been imposed to reduce those levels, namely in the industrial facilities. The current CO_2 separation technologies used constitute an energy penalty of 14–40% to those facilities and there is a need to study and develop new efficient and cheaper capture technologies. [108]

One of the technically feasible approaches for CO_2 captures is the use of a new porous material the MOFs. The use of different metallic centers and linking molecules has led to the creation of literally hundreds of different MOFs with many exciting possibilities for specialized functionality. Adsorption behavior can vary significantly between different MOFs due to differences in pore size, structural arrangement, and surface functionality.

Many studies of CO_2 adsorption have been made in three major different types of materials – silicalite, C_{168} schwarzite, and IRMOF-1 where IRMOF-1 revealed to have a great adsorption capacity for CO_2. More recently many studies are being made in the MIL and Zr-MOF. [85] [109]

The simulations perform on the Zr-MOF UiO-66Zr whit CO_2, ware done by Monte Carlo method, where 3 different types of force field were applied. Different types of force fields are used to represent the experimental data within a better fit; one force field, considers the explicitly the hydrogens and considers the electrostatic charges of the MOF, called UiO-66-EHq; the second one lumps the hydrogens to the connected carbon atoms and the charges of MOF, called UiO-66-UAq; the third, considers only the dispersive forces associated whit the pseudo-atoms used in the force field UiO-66-UA for the adsorption of methane, where only the electrostatic fluid-fluid interactions are consider, consider that the same label was maintained for the force field, the UiO-66-UA. That will give us an understanding on how important the hydrogens and the electric charges of the MOF are in the CO_2 adsorption process on Ui-66Zr.

The different types of force fields were obtained at three different temperatures, 298.15, 313.15 and 343.15 K at a pressure range that goes from 0.06 - 30 bar. The data obtained through simulation is then compared with the experimental data obtain by Jasmina H. Cavka et al..

2.1.2.2 Simulation

Similar to the simulation of methane adsorption, the adsorbent structured is assumed to be rigid. For the parameterization of the solid-fluid dispersive interactions, the Lennard Jones parameters for the MOF are the same used in the force fields applied to the adsorption of methane where differences relies on the charges that are consider for each force field. The non-bonded interaction are governed by a 12-6 LJ, being the unlike LJ interactions computed with Lorentz–Berthelot combining rules. For the computation of the Colombic electrostatic interactions we used Ewald summations that depends on constant number of inverse space vectors.

CO_2 is represented as a three-site molecule. The intrinsic quadrupole moment is described by base charge model. The CO bond length is 1.16 Å, and the bond angle OCO is 180°. The CO_2-CO_2 intermolecular interactions are modeled as a combination of LJ and Coulombic potentials given in Table 2.5.

Table 2.5 – LJ parameters for carbon dioxide.

Label	σ (K)	ε/k_B (K)	Mass (g/mol)	Base charge (e)	Ref.
C_C02	2.8	27.00	12.01	0.70	106
O_CO2	3.05	79.00	16.00	-0.35	106

Regarding the UiO-66-EHq and the UiO-66-UAq the same approximation done in the CH_4 adsorption is taken, where the explicit of the hydrogens is study. Regarding the force field UiO-66-UA, where no charges are considered, the purpose was to study the impact of the MOF charges in adsorption of CO_2. This results in similar LJ's parameters for all force fields.

- **UiO-66-EHq**

The MOF LJ parameters for this force field are equivalent to the UiO-66-EH. The electric charges were obtained by Qingyuan Yang et. al..

Table 2.6 – LJ parameters of the UiO-66Zr molecule, for the UiO-66-EHq force field.

Label	Site	σ (K)	ε/k_B (K)	Massa (g/mol)	Base Charge (e)	Ref.
C25	[C]aro	3.60	30.70	12.01	-0.121	104
C1	C	3.90	41.00	12.01	0.625	101
C13	[C]aro-CHy	3.88	21.00	12.01	-0.002	100
O1	TraPPE-UA	2.80	55.00	16.00	-0.582	102
O25	CHx-[O]-H	3.02	93.00	16.00	-1.179	102
O29	TraPPE-UA	2.80	55.00	16.00	-0.741	102
Zr	UFF	2.78	34.72	91.22	2.008	103
H1	H	2.36	25.45	1.01	0.127	104
H25	H	0.00	0.00	1.01	0.495	106

- **UiO-66-UAq**

For this force field, the LJ parameters for the UiO-66UA were used. The charges used correspond to the charges used in the UiO-66-EHq.

Table 2.7 – LJ parameters of the UiO-66Zr molecule, for the UiO-66-EAq force field.

Label	Site	σ (K)	ε/k_B (K)	Mass (g/mol)	Base Charge (e)	Ref.
C25	[CH]aro	3.74	48.00	13.02	-0.121	100
C1	C	3.90	41.00	12.01	0.625	101
C13	[C]aro-CHy	3.88	21.00	12.01	-0.002	100
O1	TraPPE-UA	2.80	55.00	16.00	-0.582	102
O25	CHx-[O]-H	3.02	93.00	17.01	-1.179	102
O29	TraPPE-UA	2.80	55.00	16.00	-0.741	102
Zr	UFF	2.78	34.72	91.22	2.008	103

- **UiO-66-UA**

For this unified force field, the LJ parameters remain the same and no charges for the MOF are considered.

Table 2.8 – LJ parameters of the UiO-66Zr molecule, for the UiO-66-UA force field.

Label	Site	σ (K)	ε/k_B (K)	Mass (g/mol)	Base Charge (e)	Ref.
C25	[CH]aro	3.74	48.00	13.02	0	100
C1	C	3.90	41.00	12.01	0	101
C13	[C]aro-CHy	3.88	21.00	12.01	0	100
O1	TraPPE-UA	2.80	55.00	16.00	0	102
O25	CHx-[O]-H	3.02	93.00	17.01	0	102
O29	TraPPE-UA	2.80	55.00	16.00	0	102
Zr	UFF	2.78	34.72	91.22	0	103

For those simulations, eight molecules of the MOF are used. The lattice parameters of the box are x=41.9568 Å, y=41.9568 Å, and z=41.9568 Å, with a box volume off 73859,6 $Å^3$.

The potential radius cutoff (rcut) for solid fluid interaction is set for 14 Å. regarding the dispersive forces at the frontier of the rcut it's applied an analytical tail correction in all simulations. The minimum bond length (rmin) is set to 0.8 Å due to fluid-fluid interactions.

For Monte Carlo simulation performed one box was used. Each simulation consist in two runs, the first is to equilibrated the systems and are used at least 10^5 steps followed by the second run whit at least 10^6 steps for the production period. The data is extract from the results of the second run and consists in the number of molecules, density of the adsorbate phase and the isosteric heat.

Regarding the types of perturbation allow in the simulation, four was consider to the adsorbate phase. The first, whit a probability of acceptance of 40% a insertion/deletion perturbation; the second, whit a probability of acceptance of 35%, is regarding to a displacement perturbation: the third, whit an acceptance probability of 10% is concerning a regrowth move; and the fourth, whit a probability of 15% is concerning rotational moves. The standard deviations of the ensemble averages were computed by breaking the production run into five blocks.

The calibration performer to the bulk carbon dioxide follows the same approach used to methane. The Canonical ensembles (N,V,T) ware done for the tree distinct temperatures, 298.15, 313.15 and 343.15 K, considering 40 molecules of carbon dioxide and take ten different sizes of box length. Obtaining value for the viral pressure (Pi) and bulk density (ρi) for each box size. Those values are adjusted the equation 2.4 and 2.6 respectively, to a third degree equation, obtains the chemical potential calibration equations for carbon dioxide:

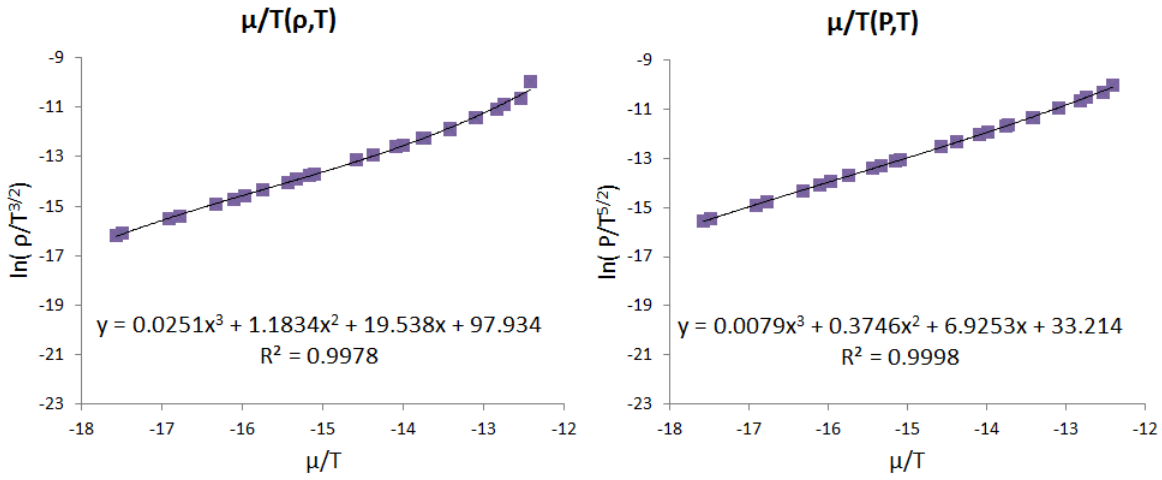

Figure 2.9 – Chemical potential calibration curves for methane, obtain through simulation.

As can be seen a third degree equation adjust to the data whit a R^2 approximating the unit. Those equations are used to obtain, for a certain temperature, the pressure or density values in function of the chemical potential.

2.1.2.3 Results and Discussion

Similar to the methane adsorption data the dimensionality of the data must be ensured using the equation 2.7.

The figure 2.10 compares the experimental adsorption isotherms obtain by Jasmina H. Cavka et al., whit the simulated data for the three distinct temperatures. Those value are express in terms of the total amount adsorb q_T. The figure 2.10 A), B) and C), represent the simulated results for the three force fields and for the three reference temperatures.

By the observation of those figures it is possible to observe that with the increase of temperature the simulation data starts to overlap the experimental avlues. However, it is interesting to observe that the force field UiO-66-UA, which has no charges for the solid, is the one that best fits the experimental data. For that reason it is important to observe how this force field behaves in the low-pressure region. This can be seen with a logarithmic scale, in the figure 2.10 D) at the three three temperatures, where very good agreement was obtained with a slightly increase of the q_T for higher temperatures.

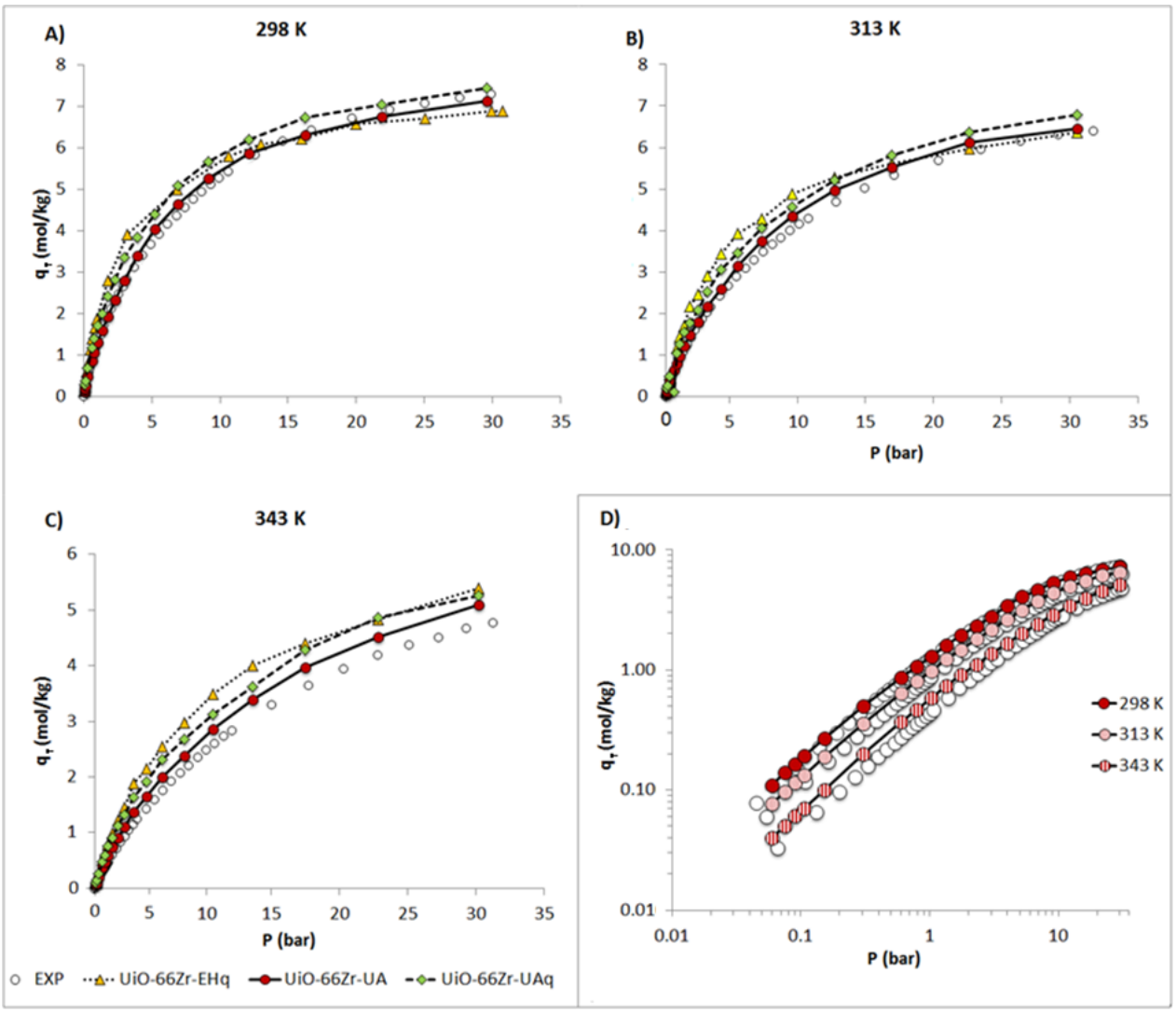

Figure 2.10 – A) B) and C) represents the comparison between the three types of force fields applied for the simulation of methane on UiO-66Zr and the experimental data for 298, 313 and 343 K respectively. The results are terms of total amount adsorbed in function of the pressure. The filled circles represent the UiO-66-UA, triangles the UiO-66-EHq, the rhombus the UiO-66-UAq and empty circles the experimental data obtain by Jasmina H. Cavka et al, for the three distinct temperatures. D) Comparison between the simulated results for the UiO-66-UA and the experimental data for 298, 313 and 343 K.

2.1.2.3.1 Isosteric heat of Adsorption

The isosteric heat Qst, is calculated by the same method used for the methane adsorption. The results can be seen in the figure 2.11. The values obtain vary between 20 and 27 kJ/mol. A constant value is observed until reach a loading of 2 mol/kg, after that, a steady increase is observed.

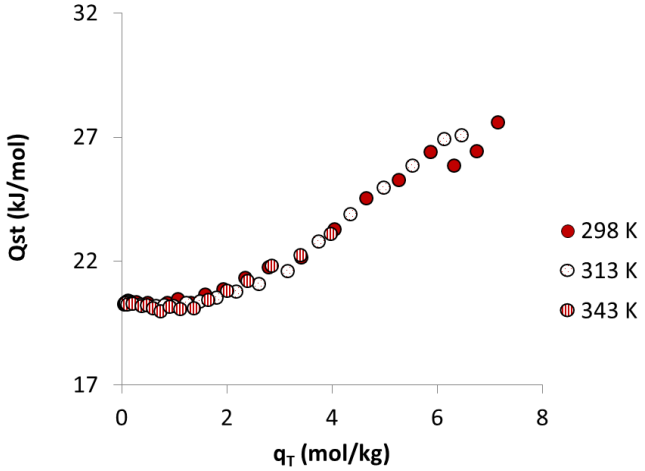

Figure 2.11 – Isosteric heat as a function of loading. The results ware obtains through the simulation of carbon dioxide on UiO-66Zr, using the UiO-66-UA force field, for the three distinct temperatures.

2.1.2.3.2 Low-Coverage Adsorption Properties

For the calculus of the Henry's constant at low covered, five points ware used that varies between 0.06 and 0.15 bar. The resulting linear tendency line and their corresponded square error are presented in the figure 2.12. As expected, the values for the Henrys constant get lower whit the increase of the temperature

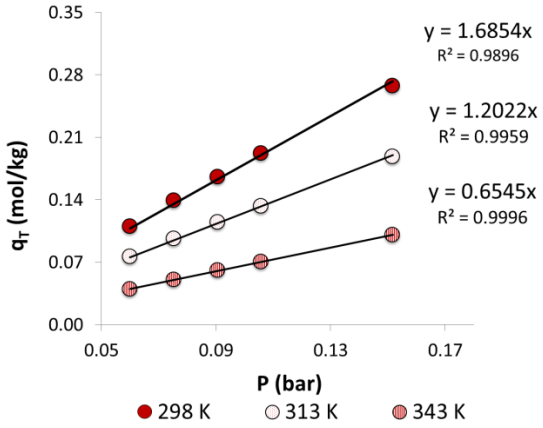

Figure 2.12 – Total amount adsorbed q_T in function of pressure, for the low pressure zone. The circles represent the results obtain through the simulation of carbon dioxide on UiO-66Zr, using the UiO-66-UA force field, for the three distinct temperatures.

In the table 2.9 is presented the results of the Henrys constants for carbon dioxide at the three temperatures in study.

Table 2.9 – Henry constants obtain for adsorption of carbon dioxide on UiO-66Zr, using the UiO-66-UA force field, for the three reference temperatures.

CO_2	289 K	313 K	343 K
K_H (mol/kg/bar)	1.6854	1.2022	0.6545
R^2	0.9896	0.9959	0.9996

2.2 Theoretical studies of adsorption in Carbon Nanotubes

The new and fascinating properties that carbon nanotubes possess, is setting them into one of the most important materials in the future. Having also innumerous applications in electronics, additives, composite materials and in adsorption process they are been seen as an important material to the larger industries. Their small nanometric size and their unique cylindrical shape, confers them larges surface area and great power of adsorption, doe to the overlap of the orbitals. For that reason the improvement of the knowledge of adsorption phenomenon on carbon nanotubes is fundamental.

Although the data from MC simulation on adsorption phenomenon, take much less time than the data taken experimentally, if large set of simulation runs is carry out, a good and a time efficient set of runs should be preferred. Choosing proper and/or simple models for the computation of the thermodynamics properties can improve by far the efficiency of the runs.

In this work, adsorption of ethane is carry out and it's study three types of runs, whit the purpose to find the faster and whit better predictions input file. The choice of the ethylene relies of mass production in the petrochemical industry and the types of process that are used nowadays to separate him from raw output stream.

Deriving mainly by the treatments and refining of crude oil and natural gas, ethane it's a very important compound in today economy. Having many applications, where can be used as an important material to the production of ethylene and vinyl chloride, used as a cryogenic refrigerator and also can be used as an energy source, a constant growing need to find new and more economical viable process for is production and separation are needed. Nowadays production of ethane occurs mainly by cracking of crude oil and is separation process is done by fractional distillation under very restrict conditions and under a very expensive and risky process. For those manners new materials have been actively sought to find ways to improve or replace the existing processes, being one of them the carbon nanotubes. [104] [105] [106]

Molecular simulation is one of the many options that can be taken to study such materials, providing innumerous form to obtain the data pretended at innumerous conditions. The input file apply in the Towhee software is a key factor for that studies and can be modulated as the will of the user in order to represent many different types of molecules. Many materials can be modulated at the atomic level i.e. the dispersive and electrostatic forces are calculated atom-by-atom representing tremendous calculations for more complex structures. To overcome those other types of modulations can be taken where a new set of equations is set.

In this work the three types of runs are tested, where two are related to the calculus of the forces atom by atom and the other consist in the simplification of the nanotube, where the Lennard-Jones 12-6 potential is calculated along the cylindrical shape of the nanotube.

2.2.1 Simulation

For the theoretical studies of adsorption on the Carbon Nanotubes, two types of runs with different input files were tested: ATOMIC force field and SMOOTH force field

For the GCMC simulation performed, some of the input file parameters are kept constant for the two force fields. The temperature is set for 303.15 K. One rigid carbon armchair nanotube is used with a chiral vector (10,10), composed by 16 cells, with a bond length of 1.418 Å and with a total length of 38.1224 Å. The carbon nanotube used, with a chiral vector of (10,10) has a radius of 6.78 Å, considering a cut-off of 14 Å the lattice parameters of the box are x=50.0 Å, y=50.0 Å guarantee the condition set for the box length. Regarding the z lattice parameter that was need to change depending on the type of run performed, we used z = 50 Å, and z = 38.1224 Å for the ATOMIC and SMOOTH runs, respectively. Concerning the dispersive forces at the frontier of the rcut, it's applied an analytical tail correction in all simulations. The minimum bond length (rmin) is set to 1 Å.

Each simulation consists of two runs; the first run is to equilibrate the system and uses 50000 steps; the second run with 250000 steps is the production period during which the statistical averages are computed. The data extract from the simulation results of the second run consist in the number of adsorbed molecules.

In these simulations there were four different types of trial steps to generate an equilibrated adsorbed phase. The first trial step, with an attempt probability of 40% is the insertion/deletion perturbation; the second trial step, with an attempt probability of 30% is a random displacement perturbation; the third trial step with an attempt probability of 15% is a configurational-bias regrowth move; and the fourth trial step, with an attempt probability of 15%, is a rotational move around the center of mass. The standard deviations of the ensemble averages were computed by breaking the production run into five blocks.

For the parameterization of the solid-fluid dispersive interactions, the Lennard-Jones parameters for the carbon nanotube (C_NT) have been intensely reported by many scholars. Regarding the adsorbent, ethane, its LJ parameters used are from de parameterization of the TraPPE-UA which consists of two CH3 pseudo-atoms connect by a bond length of 1.45 A. The unlike LJ interactions computed with Lorentz–Berthelot combining rules. The LJ parameters for the carbon nanotubes and for the adsorbate phase are presented in the table 2.10.

Table 2.10 – LJ parameters for the frame carbon nanotube and for pseudo-atom ethane.

Label	Site	σ (K)	ε/k_B (K)	Mass (g/mol)	Ref.
C_NT	[C]-C_3	3.40	28.00	12.01	113
C_2H_6	[CH_3]	3.75	98.00	15.03	99

- **ATOMIC run**

The ATOMIC run uses the standard configuration provided by the Towhee software for building an atomic nanotube. This configuration is called the ‘nanotube builder’ and requires the specification of a given number of parameters. These parameters are as follows:

- **forcefield:** The force field used is correspondent to the LJ parameter for the carbon of the nanotubes
- **atomname:** Correspond to the label given for the carbon the force field file
- **qqatom:** The atomic charge on each atom of the nanotube, in our works is set as 0.
- **nanotube_n:** The n index of the (n,m) chiral vector describing nanotube geometry, set as 10º.
- **nanotube_m:** The m index of the (n,m) chiral vector describing nanotube geometry, set as 10º.
- **nanotube_ncells:** The number of repeat cells to create for the nanotube, set as 16
- **nanotube_bondlength:** The atom bond length used to create the initial structure, set as 1.418 Å.

Given the above specifications, towhee generates a set of atoms fixed in space corresponding to atomic positions of the atoms along the nanotube wall. The interaction between an adsorbate molecule and the nanotube is computed as the summation of the LJ interaction between the molecule and all the nanotube atoms.

- **SMOOTH run**

The SMOOTH input file was built with the purpose of avoiding the summed summation of the LJ interactions with all the atoms of the nanotube wall. This code was developed jointly with Prof. José Paulo Mota. The code provides a handful of options that can be used to study many different types of features.

The SMOOTH run uses a modify Lennard-Jones 12-6 potential, which depends on the shortest distance between the adsorbate atom and the central axis of the cylindrical pore. It was obtained by integrating the LJ potential over the smooth wall of the nanotube.

For the correct mathematical expression for the LJ potential many parameter must be set, the figure 2.13 A, represent a cross-section along the axis of the nanotube where is present is geometric parameters.

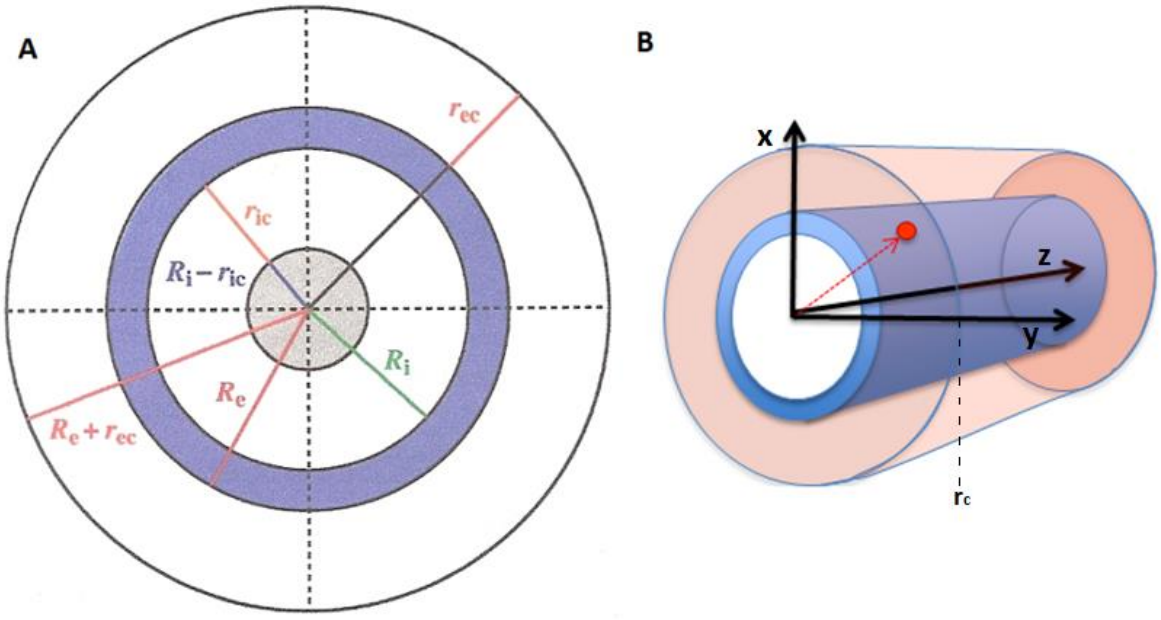

Figure 2.13 – A) cross-section along the axis of the nanotube. Where R_i is the interior radius of the nanotube, R_e is the exterior radius of the nanotube and R_e+r_{ec} represent the r_c distance. B) Representation of the SMOOTH modify LJ potential along the nanotube length, the red dot represent a particle in the range mod the LJ potential, and in this case only external interactions are taken.

With this parameterization the summation of the atom-atom interactions is simplified to a calculation that depends only the position of the adsorbate with regards to the nanotube. The name given to this type of run results of that simplification and can be represented as in figure 2.13 B. Here, rc is the cut-off radius for the Lennard-Jones interactions.

The SMOOTH run is modeled as an external field type for which the following parameters must be set:

- **nt_box:** Box where the nanotube resides.
- **nt_cx:** x-coordinate of the central axis of the nanotube, usually set as 0.5, to be in the middle of the box (expressed as a fraction of the box length).
- **nt_cy:** x-coordinate of the central axis of the nanotube, usually set as 0.5, to be in the middle of the box (expressed as a fraction of the box length).
- **nt_rw:** Radius of the innermost nanotube, set as 6.78 Å.
- **nt_nw:** Number of concentric nanotubes in the box. Set as 1.
- **nt_sw:** Spacing between concentric walls, by default set as 3.4 Å.
- **nt_rho:** Atomic surface density of the nanotube walls. Set as 0.457 Å-1.
- **nt_eps:** LJ epsilon parameters for carbon atoms in the nanotube. Set as 28.0 K.
- **nt_sig:** LJ sigma parameters for carbon atoms in the nanotube. Set as 3.4 K.
- **nt_liop:** If true, endohedral (internal) adsorption is allowed. Set as true.
- **nt_leop:** If true, exohedral (external) adsorption is allowed. Set as true.
- **nt_nisz:** Number of cubic hermit interpolation intervals for the endohedral potential. Set as 150 intervals for integration
- **nt_ncsz:** Number of cubic hermit interpolation intervals for the endohedral core potential. Set as 5 intervals for integration
- **nt_nesz:** Number of cubic hermit interpolation intervals for the exohedral potential. Set as 150 intervals for integration
- **nt_ric:** Maximun cut-off distance from the innermost nanotube towards the center beyond which the potential is switched to an infinitely repulsive core, i.e. there is a concentric solid cylinder with radius =nt_rw – nt_ric that is impenetrable to the fluid. By default set as nt_rw.
- **nt_rec:** Maximun cut-off distance from the outermost nanotube towards the external bulk beyond the potential is switched to an infinitely repulsive core, i.e. there as a concentric solid cylinder with radius =nt_rw + nt_swx(nt_nw – 1) + nt_rec that is impenetrable to the fluid. By default set as =10xnt_sigw.
- **nt_noff:** Number of atoms types that do not interact whit the wall atom. Set as 0.
- **nt_aname:** Name of noninteracting atom type.

With this set of parameters it is possible to study many different types of features, enabling to choose them according to the best describing scenario of the nanotubes sample. For example, usually the nanotube aggregates them self's into to bundles, where mostly, the internal surface area is the one availed for adsorption. Other feature that is possible to study with relative simplicity is the adsorption in multiwall nanotubes, where can be set the number of the nanotubes present in the box.

The calibration performed to the bulk ethane follows the same approach used to methane and carbon dioxide. The Canonical simulations (N,V,T) were done for four distinct temperatures, 303.15, 323.15, 353.15 and 373.15 K, considering 60 molecules of ethane and take eight different sizes of box length. The obtained values of the viral pressure (P_i) and bulk density (ρ_i) were recorded as a function of box size. Those values are adjusted whit the equation 2.4 and 2.6 respectively, to a third degree equation, obtains the chemical potential calibration equations for ethane:

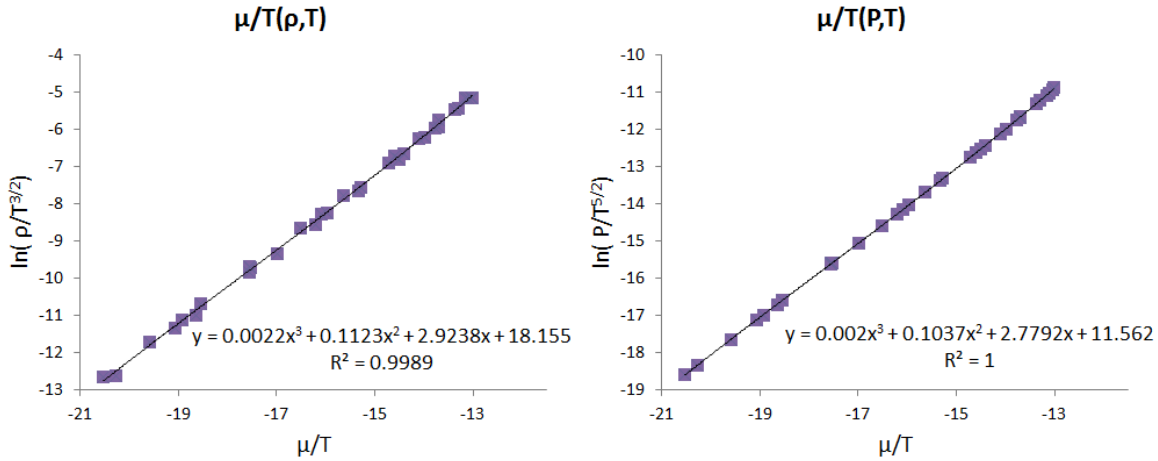

Figure 2.14 – Chemical potential calibration curves for ethane, obtain through simulation.

As can be seen, a third degree equation adjusts the data with a R^2 approximating the unit. Those equations are used to obtain, for a certain temperature, the pressure or density values in function of the chemical potential.

2.2.2 Results and Discussion

Figures 2.15 A and B, compare the data obtain for the two types of runs. The data is present as the number of ethane molecules per surface area of the nanotube, as a function of the pressure for a temperature set to 303.15 K.

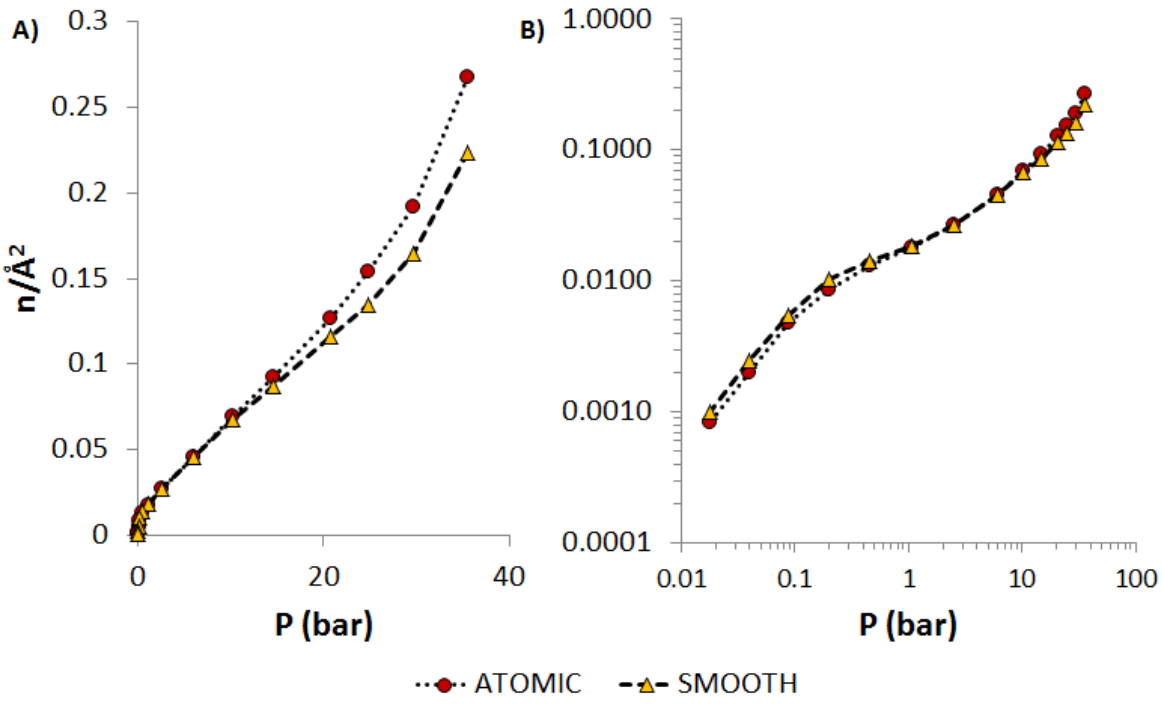

Figure 2.15 – Adsorption of ethane in a carbon nanotube present in number of particles per tube area, at 303.15 K. The circles represent the ATOMIC runs and the triangles de SMOOTH.

As can be seen in the figure 2.15 A, there is an increasing discrepancy of the data regarding the ATOMIC to the SMOOTH for the high pressures zone. However that is not observed in the low pressure zone as can be seen in the figure 2.15 B.

Regarding the simulation times for the runs, those can be seen in the flowing table:

Table 2.11 – Times of simulation for ATOMIC and SMOOTH runs.

Runs Type	Time (min)
ATOMIC	22.98
SMOOTH	13.95

Where the SMOOTH runs shown to be the fast ones, being 1.65 faster than the ATOMIC.

2.3 Conclusions

Regarding the results presented for UiO-66Zr, we have reported a combined experimental and theoretical study of the adsorption equilibrium properties of methane and carbon dioxide, over pressures in the range 0.06–70 MPa and temperatures in the 298–343 K regions. We demonstrated that the use of the TraPPE-UA force-field for modeling the solid–fluid interaction potential for both gases provides a good description of the experimental adsorption isotherms; concerning the isosteric heats obtained it was not possible to compare with other data, due to the lack of it.

When considering the hydrogen atoms in the MOF, the studies show that their explicit modeling does not appear to increase the accuracy of the simulated isotherms. This is observed more strongly in the studies performed with carbon dioxide, where clearly the isotherm of the UiO-66-EHq do not have the same tendency as the others.

It is also possible to conclude that the charges of the UiO-66Zr do not have a significant impact on the adsorption of carbon dioxide. The studies performed shown that, similar to the methane adsorption, the best force field that reply the experimental data is the UiO-66-UA.

Comparing the work done by Ravichandar Babarao et al. with the data obtained for the isosteric heat of methane adsorption, it is observed a similar decrease until a minimum is reached. That initial decrease as reported by Ravichandar Babarao et al. on the C168 schwarzite, results because of the heterogeneous character of the adsorbent, in which the more energetically favorable sites for adsorption are occupied first, and then the less favorable sites are occupied as the loading increases. However, in the adsorption studies perform for the isosteric heat whit carbon dioxide, that decrease is less obvious.

Today's technologies and software developments bring many advantages in terms of ways to study and understand phenomena and occurrences that are impossible to see and register experimentally. The fowling images were obtained through the visualization software VMD 1.9 (Visual Molecular Dimamics).

The image 2.16 A and B represents the interior of a UiO-66Zr molecule, with adsorbed methane molecules at 9.1 and 57 bar respectively. It is possible to see that methane molecules adsorb very close to the metallic center for both pressures and that this phenomenon is intensified whit the increase of the pressure. This leads us to conclude that these snapshots of the simulation box are consistent with the conclusions taken for isosteric heat.

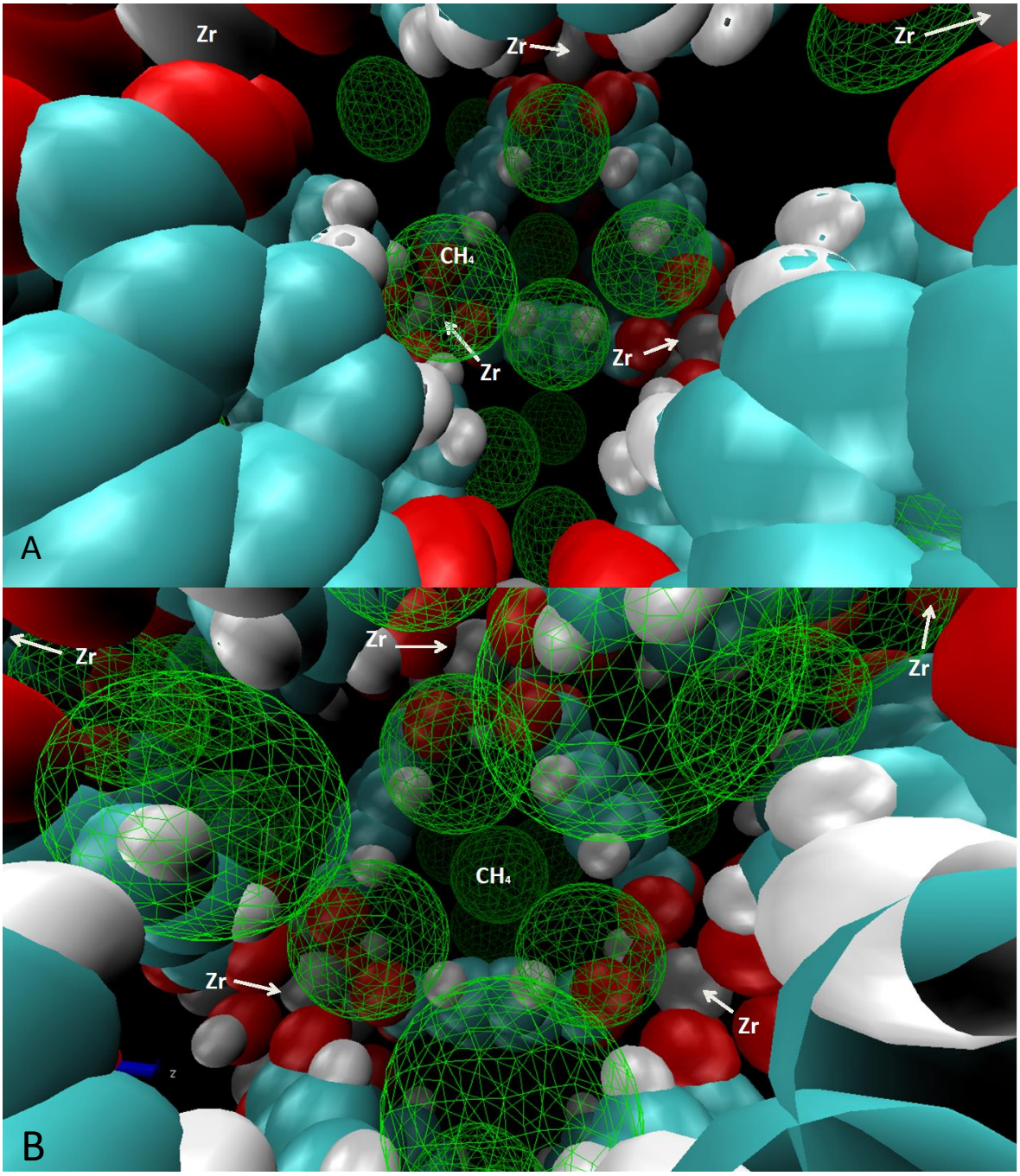

Figure 2.16 – 3D representation taken from the software VMD 1.9 of the adsorption of methane on UiO-66Zr. Figure A and B represents adsorption at 9.1 bar and 57 bar respectively at 298.15K.

Representations of carbon dioxide adsorption on UiO-66Zr are also taken using the VMD software. The figure 2.17 represents the adsorption of carbon dioxide at 2.3 bar, where it's also possible to observe some adsorption near the metallic center but less intensive as the adsorption of methane.

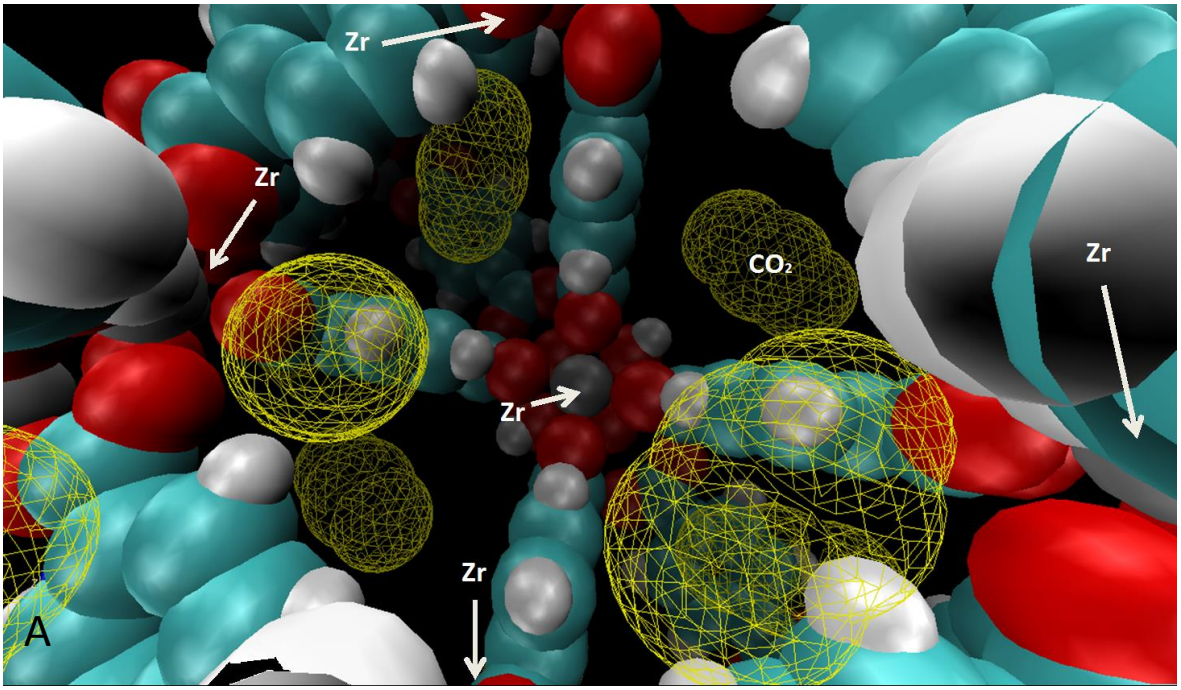

Figure 2.17 – 3D representation taken from the software VMD 1.9 of the adsorption of carbon dioxide on UiO-66Zr. Figure A adsorption at 2.3 bar at 298.15K.

Regarding the adsorption loading for the two gases in study, in the figure 2.18 A) it's possible to observe that the UiO-66Zr has more capacity to adsorb carbon dioxide than to adsorb methane, achieving loads of ≈6 and ≈7 mol/Kg of methane and carbon dioxide, respectively.

Considering that the best force field applied for the adsorption of carbon dioxide was the UiO-66-UA, we can conclude that the electrostatic parameterization obtained by Qingyuan Yang et. al. by quantum mechanics calculations are not suited to be combined with classical force fields such as TraPPE, UFF or Dreiding.

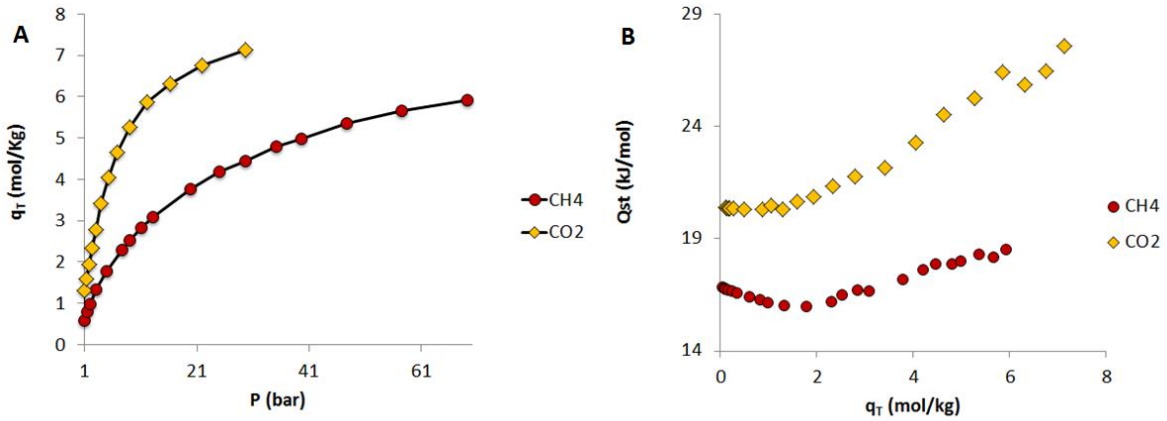

Figure 2.18 – Comparison between the adsorption of methane and carbon dioxide on UiO-66Zr using the uiO-66-UA force field. The Circles represents the data for the methane and the rhombus the data for the carbon dioxide. Figure A represents the total amount absorbed versus the pressure at 298.15 k and B the isosteric heat versus de total amount absorbed at 298.15 K

The Henry constants for both gases can be seen in the table below for the three temperatures study.

Table 2.12 – Henry constants obtain for adsorption of methane and carbon dioxide on UiO-66Zr, using the UiO-66-UA force field, for the three reference temperatures.

	CH_4	CO_2
	K_H (mol/kg/bar)	K_H (mol/kg/bar)
289 K	0.7002	1.6854
313 K	0.5129	1.2022
343 K	0.2989	0.6545

We can conclude that on average, carbon dioxide has an Henry constant 2.3 times larger than methane's. This shows that the studied MOF is selective for carbon dioxide than for methane

Regarding the results obtain for the studies perform for the adsorption of ethane on carbon nanotubes, two types of run ware study and it was observed the time for each run.

We conclude that the simplification done for the SMOOTH force field, gives good prediction regarding the experimental data. It's is observed grater contributions for adsorption for the ATOMIC runs at zone of high pressure; this is counter-intuitive since at high pressures the newly adsorbed molecules are placed at larger distances from the nanotube wall and thus less dependent on the local atomic structure of the nanotube.

Concerning the simulation time for each run, we conclude that the faster run type is the SMOOTH, which is 1.6 times faster than the ATOMIC. That will have a significant impact on the total time expend in the studies perform on carbon nanotubes, where it should be consider not only the time spend to obtain the final data, but also the time spend on testing the various types of parameters that can be change and implemented, i.e. different types of LJ parameters, used of the electrostatic contribution and many more.

3 Bibliography

[1] REN21, "Renewables 2013: Global Status Report," 2013.

[2] R. W. Howarth and R. Santoro, "Methane and the greenhouse-gas footprint of natural gas from shale formations," 2011.

[3] S. Cavenati, C. A. Grande and A. E. Rodrigues, "Adsorption Equilibrium of Methane, Carbon Dioxide, and Nitrogen on Zeolite 13X at High Pressures," Journal of Chemical and Engineering Data, vol. 49, pp. 1095-1101, 2004.

[4] J. Liu, . P. K. Thallapally and . B. P. McGrail, "Progress in adsorption-based CO2 capture by metal-organic frameworks," Chemical Society Reviews, vol. 41, no. 6, pp. 2308-2322, 2012.

[5] Y. H. Li, Y. M. Zhao, W. B. Hu and I. Ahmad, "Carbon nanotubes – the promising adsorbent in wastewater," Journal of Physics, vol. 61, pp. 698-702, 2007.

[6] M. Badino, "The Fundamentional Role of Ergodic Theory," Max Planck Institute for the History of Science, Department of Philosophy, University of Genoa, 2005.

[7] Y. Demirel, Nonequilibrium Thermodynamics: Transport and Rate Processes in Physical, Chemical and Biological Systems, University of Nebraska: Third Edition, Elsevier, 2013.

[8] J. M. Honig, Thermodynamics: Principles Characterizing, Physical and Chemical Processes, Purdue University, USA: Fourth edition, Elsevier, 2014.

[9] C. L. Tien and J. H. Lienhard, Statistical Thermodynamics, Washington, USA: Hemisphere Publishing Corporation, 1985.

[10] S. M. a. Thermodynamics, "Dr. Henry Glyde," 5 Feb 2010. [Online]. Available: http://www.physics.udel.edu/~glyde/PHYS813/Lectures/. [Accessed Oct 2014].

[11] K. Foo and B. Hameed, "Insights into the modeling of adsorption isotherm systems," Elsevier, vol. 156 , no. Chemical Engineering Journal, p. 2–10, 2010.

[12] A. Dabrowski, "Adsorption - from theory to practice," Elsevier, vol. 93, no. Advances in Colloid and Interface Science, pp. 135-224, 2001.

[13] M. Suzuki, Adsorption Engineering, University of Tokyo: Elsevier Science Publishers, 1990.

[14] C. A. Coles, "Estimanting Retardation From the Freundlich Isotherm for Modeling Contaminant transport," Memorial University of Newfoundland, Canada, 2008.

[15] S. M. Ali, "Adsorption and Desorption Surface Reactions," Singapore, 2013.

[16] K. Christmann, "Thermodynamics and Kinetics of Adsorption," Institut für Chemie und Biochemie, Freie Universität Berlin, 2012.

[17] F. Rouquerol, J. Rouquerol and K. Sing, Adsorption by Powders and Porous Solids, Universite de Provence, France: Academic Press , 1999.

[18] K. S. Sing, "Reporting Phisisorption Data with Special Reference to the Determination of Surface Area and Porosity," Pergamon, UK, 1982.

[19] N. S. Bibi, "Downstream process intensification by innovative material development," Bremen, 2012.

[20] T. Horikawa, D. Do and D. Nicholson, "Capillary condensation of adsorbates in porous materials," Elsevier, vol. 169, no. Advances in Colloid and Interface Science, p. 40–58, 2011.

[21] I. Hermann-Geppert, "Helmholtz-Zentrum Berlin," 2014. [Online]. Available: http://www.helmholtz-berlin.de/forschung/oe/ee/solare-brennstoffe/analytische-methoden/gassorptionsmessungen_en.html. [Accessed Sep 2014].

[22] N. Stadie, "Synthesis and Thermodynamic Studies of Physisortive Energy Storege Materials," California Institute of Thecnology Pasadena, California, 2013.

[23] D. M. Ruthven, "Principles of Adsorption and Adsorption Processes," John Wiley & Sons, Inc., USA, 1984.

[24] H. Delavari Amrei, M. R. Mehrnia, A. Ghanizadeh and M. M. Montazer-Rahmati, "Low pressure adsorption of CO2 on multi-wall carbon nanotubes," International Journal of Nanoscience and Nanotechnology, Iran, 2008.

[25] D. D. Do, Adsortion Analysis: Equilibria and Kinetics, University of Queensland, Australia: Imperial College Press, 1998.

[26] D. Dubbeldam, S. Calero, T. Vlught, R. Krishna, T. Maesen and B. Smit, "United Atom Force Field for Alkanes in Nanoporous Materials," The Journal of Physical Chemistry, vol. 108, no. B, pp. 12301-12313, 2004.

[27] S. E. Jalili, "Monte Carlo Simulation and Statistical Mechanics Modelling of Mixture Adsortion in Silicalite," University College London, UK, 2011.

[28] A. R. Leach, Molecular Modelling: Principles and Applications, UK: Pearson Education Limited, 2001.

[29] M. Allen and D. Tildesley, Computer Simulation of Liquids, USA: Clarendon Press, 1991.

[30] A. O. Yazaydin, "Molecular Simulation of the Adsorption of Organics From Water," Worcester Polytechnic Institute, UK, 2007.

[31] R. Y. Rubinstein, Simulation and the Monte Carlo Method, USA: Second Edition, John Wiley & Sons, 2008.

[32] T. Rodgers, "Soft Matter Simulation," 2012.

[33] T. Schnabel, J. Vrabec and H. Hasse, "Unlike Lennard-Jones Parameters for Vapor-Liquid Equilibria," Universität Stuttgart, Germany, 2007.

[34] D. Frenkel and B. Smit, Understanding Molecular Simulation: From Algorithms to Applications, First edition, Elsevier Science & Technology Books, 1996.

[35] J. Barry, "Monte Carlo Methods for Sampling Classical and Quantum," Swarthmore College, USA, 2007.

[36] M. Martin , "MCCCS Towhee: Tail correction VS shift truncation," 19 09 2012. [Online]. Available: http://ehc.ac/p/towhee/discussion/298241/thread/47def7d0/. [Accessed Sep 2014].

[37] M. Richey, "The Evolution of Markov Chain Monte Carlo Methods," Mathematical Association of America, USA, 2011.

[38] B. Widom, "The Boltzmann distribution law and statistical thermodynamics," Cambridge University Press, Cambridge University, UK, 2004.

[39] J. Merikanto, "Monte Carlo Simulations of Molecular Clusters in Nucleation," University of Helsinki, Finland, 2007.

[40] C. J. Geyer, "Introduction to Markov Chain Monte Carlo," 2001.

[41] A. Bétard, "Growth and Chemistry of Metal-Organic Framework Thin Films: Toward Functional Coatings," Ruhr-Universität Bochum, Germany, 2011.

[42] M. Hu, "Design, synthesis and applications of Metal Organic Frameworks," Worcester Polytechnic Institute, USA, 2011.

[43] B. Ravichandar, "Computational Study of Adsorption and Diffusion in Metal-Organic Frameworks," National University of Singapore, 2009.

[44] P. Ajayan, "Nanotubes from Carbon," Chemical reviews, vol. 99, pp. 1787-1799, 1999.

[45] F. M. Fernades, "Sintese de nanotubos de carbon orientados e aplicação na produção de pontas AFM," Universidade de São Paulo, Brasil, 2008.

[46] O. P. Ferreira, "Nanotubos de Carbono: Preparação e caracterização," Laboratória de Química do Estado Sólido, Brasil, 2005.

[47] I. Hammes, "Bundles de Nanotubos de Carbono: Teoria e Experimento," Departamento de Física - Universidade Federal Fluminense, Brasil, 2011.

[48] R. Saito, "Physical Properties of Carbon Nanotubes," Imperial College Press, vol. 35, pp. 73-81.

[49] M. Daenen, R. Fouw, B. Hamers and P. Janssen, "The Wondrous World Carbon Nanotubes," Eindhoven University of Technology, Netherlands, 2003.

[50] M. D. Lima, "Síntese de nanotubos de carbono por deposição química de vapor catalisada," Universidade Federal do Rio Grande do Sul, Brasil, 2007.

[51] Y. Wang, F. Wei and G. Luo, "The large-scale production of carbon nanotubes in a nano-agglomerate fluidized-bed reactor," Chemical physics, pp. 568-572, 2002.

[52] Y. Ohno, T. Shimada, S. Kishimoto, S. Maruyama and T. Mizutani, "Carrier transport properties in single-walled carbon nanotubes studied by photoluminescence spectroscopy," Journal of Physics, vol. 38, 2006.

[53] P. Bandaru, "Electrical properties and applications of carbon nanotube structures.," Journal of Nanoscience and Nanotechnology, vol. 7, pp. 1239-67, 2007.

[54] C. White and T. T.N., "Carbon nanotubes as long ballistic conductors," Nature, vol. 393, p. 240, 1998.

[55] J. Hone, "Phonons and termal Properties of Carbon Nanotubes," Springer, vol. 80, pp. 273-286, 2001.

[56] "Nanocyl. The Carbon Nanotube Specialist," [Online]. Available: http://www.nanocyl.com/CNT-Expertise-Centre/Carbon-Nanotubes. [Accessed Sep. 2014].

[57] A. Souza Filho and S. Fagan, "Funcionalização de nanotubos de Carbono," Quím. Nova, vol. 30, 2007.

[58] J. Zhao, A. Buldum, J. Han and J. P. Lu, "Gas molecule adsorption in carbon nanotubes and nanotube bundles," Institute of Physics, vol. 13, pp. 195-200, 2002.

[59] P. Kondratyuk, "Physical Adsorption on Single Wall Carbon Nanotubes," University of Pittsburgh, 2007.

[60] S. Agnihotri, M. J. Rood and M. Rostam-Abadi, "Adsorption equilibrium of organic vapors on single-walled carbon nanotubes," Elsevier, vol. 43, p. 2379–2388, 2005.

[61] D. Yi, Y. Xiao-bao and N. Jun, "Adsorption on the carbon nanotubes," Front. Phys. China, vol. 3, pp. 317-322, 2006.

[62] R. Bonadiman , "Nanotubos de Carbono como Adsorvente de Hidrogênio: Produção e Caracterização Comparativa com outros Materiais Carbonosos Adsorventes," Porto Alegre, Brasil, 2007.

[63] A. Ramos, S. Tanase and G. Rothenberg, "Redes Metalorgânicas e suas Aplicações em Catálise," Quimica Nova, Vols. 123-133, p. 37, 2014.

[64] L. Shen, "Synthesis, Characterization and application of Metal-Organic FrameWorks," University of Illinois, 2012.

[65] M. Hu, "Design, synthesis and applications of Metal Organic Frameworks," Worcester Polytechnic Institute, 2011.

[66] J. Alcañiz, "Engineering of Metal Organic Framework Catalysts," Universidad Politécnica de Valencia, 2013.

[67] S. Suresh and D. Arivuoli, "Nanomaterials for Nonlinear Optical (NLO) Applications: A review," Adv. Mater. Sci., vol. 30, pp. 243-253, 2012.

[68] J. L. Rowsell and O. M. Yaghi, "Metal–organic frameworks: a new class of porous materials," Elsevier, vol. 73, pp. 3-14, 2004.

[69] D. N. Dybtsev, A. Nuzhdin, H. Chun and K. Bryliakov, Angew. Chem., vol. 45, pp. 916-920, 2006.

[70] Z. Ni and R. Masel, J. Am. Chem. Soc., vol. 128, pp. 12394-12395, 2006.

[71] T. Chalati, P. Horcajada, R. Gref, P. Couvreur and C. Serre, J. Mater. Chem., vol. 21, pp. 2220-2227, 2011.

[72] P. Silva, A. Valente, J. Rocha and F. Paz, Cryst. Growth Des., vol. 10, pp. 2025-2028, 2010.

[73] W. Yuan, T. Friscic, D. Apperley and S. James, Angew. Chem., vol. 49, pp. 3916-3919, 2010.

[74] T. Friscic, D. Reid, I. Halasz, R. Stein and R. Dinnebier , Angew. Chem., vol. 49, pp. 712-715, 2010.

[75] A. Pichon and S. James, "CrystEngComm," vol. 10, pp. 1839-1847, 2008.

[76] U. Mueller, P. H. and M. Hesse, "WO," 2005/049892..

[77] Z. Wang and S. Cohen, Chem. Soc. Rev., vol. 38, pp. 1315-1329, 2009.

[78] R. Krishna and J. M. v. Baten, "Influence of adsorption thermodynamics on guest diffusivities in nanoporous crystalline materials," Phys. Chem. Chem. Phys, vol. 15, pp. 7994--8016, 2013.

[79] X. Zhao, A. Fletcher, K. Thomas and B. Bradshaw, Science, vol. 306, p. 1012, 2004.

[80] S. Hasegawa, S. Horike, R. Matsuda, S. Furukawa and S. Kitagawa, S. Journal of the American Chemical Society, vol. 129, p. 2607, 2007.

[81] J. Lee, F. O.K., J. Roberts, K. Scheidt and J. Hupp, Chem. Soc. Rev., vol. 38, p. 1450, 2009.

[82] M. Sabo, A. Henschel, H. Frode and E. Klemm, S. Journal of Materials Chemistry, vol. 17, p. 3827, 2007.

[83] P. Horcajada, C. Serre, G. Maurin, N. Ramsahye, M. Sebban and F. Taulelle, Journal of the American Chemical Society, vol. 130, p. 6774, 2008.

[84] C. Wu and W. Lin, Angewandte Chemie International, vol. 46, p. 1075, 2007.

[85] B. Ravichandar, H. Zhongqiao, J. Jianwen and C. Shaji, "Storage and Separation of CO2 and CH4 in Silicalite, C168 Schwarzite, and IRMOF-1: A Comparative Study from Monte Carlo Simulation," Langmuir, vol. 23, pp. 659-666, 2007.

[86] M. Gustafsson, "Metal−Organic Frameworks (MOFs) for Heterogeneous Catalysis," Stockholm University, 2012.

[87] J. Cavka, S. Jakobsen, U. Olsbye, C. Lamberti and K. Lillerud, "A New Zirconium Inorganic Building Brick Forming Metal Organic Frameworks with Exceptional Stability," J. Am. Chem. Soc., vol. 130, p. 13850–13851, 2008.

[88] J. Hafizovic, U. Olsbye, K. Lillerud and N. Guillou, "Metal Organic Framework". US Patent 8,653,292 B2, 18 Feb. 2014.

[89] J. Mason, M. Veenstra and . J. Long, "Evaluating Metal–Organic Frameworks for Natural Gas Storage," Chem. Sci., vol. 5, pp. 32-51, 2014.

[90] MIT, "The Future of Natural Gas," 2011.

[91] Q. Yang, V. Guillerm, F. Ragon, A. Wiersum and C. Serre, "CH4 storage and CO2 capture in highly porous zirconium oxide," The Royal Society of Chemistry, 2012.

[92] V. Gusev and J. O'Brien, "A Self-Consistent Method for Characterization of Activated Carbons Using Supercritical Adsorption and Grand Canonical Monte Carlo Simulations," Langmuir, vol. 13, pp. 2815-2821, 1997.

[93] P. Pascual, P. Ungerer, B. Tavitian, P. Perno and A. Boutin, "Development of a transferable

guest–host force field for adsorption of hydrocarbons in zeolites," Physical Chemistry Chemical Physics, 2003.

[94] M. Macedonia and E. Maginn, "Pure and binary component sorption equilibria of light hydrocarbons in the zeolite silicalite from grand canonical Monte Carlo simulations," Elsevier, vol. 160, pp. 19-27, 1998.

[95] T. Vuong and P. Monson, "Monte Carlo Simulation Studies of Heats of Adsorption in Heterogeneous Solids," Langmuir, vol. 12, pp. 5425-5432, 1996.

[96] Q. Yang and C. Zhong, "Molecular Simulation of Carbon Dioxide/Methane/Hydrogen Mixture Adsorption in Metal-Organic Frameworks," J. Phys. Chem., vol. 110, no. B, pp. 17776-17783, 2006.

[97] A. Martıín-Calvo, E. García-Pérez, J. Castillo and S. Calero, "Molecular simulations for adsorption and separation of natural gas in IRMOF-1 and Cu-BTC metal-organic frameworks," Physical Chemistry Chemical Physics, 2008.

[98] A. Skoulidas, "Molecular Dynamics Simulations of Gas Diffusion in Metal-Organic Frameworks: Argon in CuBTC," American Chemical Society, vol. 126, pp. 1356-1357, 2004.

[99] M. Martin and J. I. Siepmann, "Transferable Potentials for Phase Equilibria. 1. United-Atom Description of n-Alkanes," J. Phys. Chem., vol. 102, no. B, pp. 2569-2577, 1998.

[100] C. Wick, J. I. Siepmann, W. Klotz and M. Schure, "Temperature effects on the retention of n-alkanes and arenes in helium–squalane gas–liquid chromatography Experiment and molecular simulation," Elsavier, vol. 954, no. A, p. 181–190, 2002.

[101] G. Kamath, F. Cao and J. J. Potoff, "An Improved Force Field for the Prediction of the Vapor-Liquid Equilibria for Carboxylic Acids," J. Phys. Chem., vol. 108, no. B, pp. 14130-14136, 2004.

[102] J. M. Stubbs, J. J. Potoff and J. I. Siepmann, "Transferable Potentials for Phase Equilibria. 6. United-Atom Description for Ethers, Glycols, Ketones, and Aldehydes," J. Phys. Chem., vol. 108, no. B, pp. 17596-17605, 2004.

[103] A. Rappé, C. Casewit, K. Colwell, W. Goddard and W. Skiff, "UFF, a Full Periodic Table Force Field for Molecular," J. Am. Chem. Soc., vol. 114, pp. 10024-10039, 1992.

[104] N. Rai and J. I. Siepmann, "Transferable Potentials for Phase Equilibria. 10. Explicit-Hydrogen Description of Substituted Benzenes and Polycyclic Aromatic Compounds," J. Phys. Chem., vol. 117, p. 273−288, 2013.

[105] N. Rai and J. I. Siepmann, "Transferable Potentials for Phase Equilibria. 9. Explicit Hydrogen Description of Benzene and Five-Membered and Six-Membered Heterocyclic

Aromatic Compounds," J. Phys. Chem., vol. 111, no. B, pp. 10790-10799, 2007.

[106] J. J. Potoff and J. I. Siepmann, "Vapor-Liquid Equilibria of Mixtures Containing Alkanes, Carbon Dioxide, and Nitrogen," AIChE Journal, vol. 47, pp. 1676-1682, 2001.

[107] T. Vlugt, E. García-Pérez, D. Dubbeldam, S. Ban and S. Calero, "Computing the Heat of Adsorption using Molecular Simulations: The Effect of Strong Coulombic Interactions," J. Chem. Theory Comput., vol. 4, p. 1107–1118, 2008.

[108] C. M. Tenney, "Molecular Simulation of Carbon Dioxide Adsorption for Carbon Capture and Storage," University of Michigan, 2009.

[109] C. Serre, S. Bourrelly, A. Vimont, N. Ramsahye, G. Maurin, M. Daturi and O. Leynaud, "An Explanation for the Very Large Breathing Effect of a Metal–Organic Framework during CO2 Adsorption," Adv. Mater., vol. 19, p. 2246–2251, 2007.

[110] J. Wauquier, Crud Oil Petroleum Products Process Flowsheets, Technip, 1995.

[111] D. Jones and P. Pujadó, Handbook of Petroleum Processing, Netherlands.: Springer, 2006.

[112] J. Gary and G. Handwerk, Petroleum Refining Technology and Economics, Marcel Dekker, 2001.

[113] W. A. Steele, The Interaction of Gases with Solid Surfaces, Pergamon Press, 1974.

Appendix A: Tables of experimental and simulation data.

In this appendix, are presented all table related to experimental data used, and the data obtain through simulation for methane and carbon dioxide adsorption on UiO-66Zr. As well the data obtain for the simulation of ethane on carbon nanotubes.

A.1: Tables of the experimental and simulation data for adsorption on UiO-66Zr.

A.1.1: Methane adsorption.

Table 1 – Data of methane adsorption at 298.15 K on UiO-66Zr.

298.15 K

Experimental		Simulated				
				UiO-66-EH	UiO-66-UA	
P (bar)	q (mol/kg)	P (bar)	μ (K)	q (mol/kg)	q (mol/kg)	Q_{st} (kJ/mol)
0	0	0.057	-5250	0.045	0.043	16.849
0.56243	0.267	0.089	-5120	0.069	0.066	16.825
1.0568	0.477	0.138	-4990	0.104	0.100	16.786
1.5132	0.657	0.213	-4860	0.158	0.152	16.720
1.9502	0.81	0.331	-4730	0.237	0.227	16.696
2.3435	0.936	0.514	-4600	0.353	0.335	16.599
2.9709	1.124	1.011	-4400	0.621	0.589	16.429
3.6037	1.299	1.517	-4280	0.847	0.805	16.308
5.2277	1.7	1.988	-4200	1.033	0.979	16.190
6.8589	2.04	3.086	-4070	1.387	1.322	16.061
8.4951	2.341	4.954	-3930	1.857	1.769	16.006
10.124	2.607	7.688	-3800	2.376	2.295	16.198
13.446	3.085	9.104	-3750	2.597	2.515	16.534
16.782	3.479	11.151	-3690	2.868	2.825	16.741
20.097	3.815	13.205	-3640	3.116	3.079	16.708
23.44	4.101	19.813	-3520	3.727	3.774	17.206
26.754	4.353	25.103	-3450	4.092	4.186	17.658
30.189	4.59	29.727	-3400	4.373	4.449	17.889
33.579	4.793	35.202	-3350	4.654	4.793	17.885
36.928	4.966	39.624	-3315	4.900	4.982	18.045
40.331	5.142	47.721	-3260	5.204	5.349	18.331
43.756	5.262	57.474	-3205	5.542	5.659	18.219
47.177	5.387	69.220	-3150	5.917	5.914	18.529
50.507	5.511					
56.096	5.664					
61.68	5.82					
67.193	5.982					
72.736	6.12					
78.168	6.24					
83.582	6.409					

Table 2 – Data of methane adsorption at 313.15 K on UiO-66Zr.

313.15 K

Experimental		Simulated				
				UiO-66-EH	UiO-66-UA	
P (bar)	*q* (mol/kg)	P (bar)	μ (K)	q (mol/kg)	q (mol/kg)	Q_{st} (kJ/mol)
0	0	0.058	-5550	0.033	0.031	16.839
0.18412	0.067	0.107	-5358	0.060	0.058	16.839
0.38319	0.136	0.198	-5167	0.108	0.104	16.782
0.58057	0.202	0.366	-4975	0.194	0.186	16.733
0.75155	0.257	0.679	-4783	0.339	0.322	16.650
0.89703	0.306	1.258	-4592	0.572	0.543	16.464
1.0361	0.349	2.332	-4400	0.921	0.877	16.281
1.5099	0.48	3.432	-4280	1.205	1.150	16.149
2.002	0.622	4.440	-4200	1.426	1.365	16.143
2.6571	0.781	6.746	-4070	1.844	1.767	16.116
3.3034	0.933	10.587	-3930	2.368	2.299	16.405
4.9517	1.28	16.089	-3800	2.929	2.892	16.378
6.613	1.58	18.898	-3750	3.150	3.131	16.987
8.2576	1.843	22.925	-3690	3.432	3.452	17.066
9.9129	2.076	26.928	-3640	3.677	3.712	17.160
11.576	2.297	39.624	-3520	4.297	4.375	17.558
14.983	2.694	49.638	-3450	4.673	4.791	17.796
18.4	3.036	58.306	-3400	4.940	5.030	18.306
21.823	3.332	68.488	-3350	5.181	5.297	18.265
25.251	3.594	76.655	-3315	5.382	5.496	18.486
28.62	3.805	91.502	-3260	5.699	5.795	18.324
31.946	4.008	109.224	-3205	6.092	6.060	18.443
35.289	4.202					
38.731	4.365					
42.187	4.513					
45.606	4.66					
49.028	4.743					
52.543	4.935					
58.071	5.08					
63.604	5.281					

Table 3 – Data of methane adsorption at 343.15 K on UiO-66Zr.

343.15 K

Experimental		Simulated				
				UiO-66-EH	UiO-66-UA	
P (bar)	*q* (mol/kg)	P (bar)	μ (K)	q (mol/kg)	q (mol/kg)	Q_{st} (kJ/mol)
0	0	0.059	-6150	0.019	0.018	16.835
0.20423	0.042	0.082	-6041	0.027	0.025	16.853
0.43136	0.087	0.112	-5932	0.036	0.035	16.850
0.62642	0.126	0.155	-5823	0.050	0.047	16.854
0.80686	0.16	0.213	-5714	0.068	0.065	16.808
0.93903	0.183	0.294	-5605	0.092	0.088	16.790
1.0898	0.211	0.405	-5495	0.126	0.120	16.780
1.6096	0.305	0.558	-5386	0.170	0.162	16.752
2.0458	0.381	0.769	-5277	0.229	0.218	16.733
2.7344	0.489	1.060	-5168	0.306	0.292	16.677
3.4146	0.59	1.460	-5059	0.405	0.384	16.587
5.149	0.838	2.011	-4950	0.530	0.506	16.524
6.8467	1.053	2.771	-4841	0.688	0.654	16.416
8.5521	1.251	3.818	-4732	0.878	0.838	16.337
10.262	1.434	5.260	-4623	1.106	1.056	16.280
13.722	1.767	7.247	-4514	1.371	1.308	16.185
17.187	2.058	9.984	-4405	1.672	1.608	16.093
20.662	2.318	13.756	-4295	2.011	1.958	16.124
24.102	2.555	18.952	-4186	2.396	2.340	16.354
27.505	2.772	26.111	-4077	2.809	2.766	16.410
30.911	2.957	35.974	-3968	3.255	3.242	16.745
34.44	3.151	49.562	-3859	3.727	3.738	16.892
37.897	3.305	68.284	-3750	4.205	4.272	17.798
41.307	3.438					
44.662	3.583					
48.065	3.729					
51.593	3.817					
57.407	4.015					
63.14	4.146					
68.786	4.257					

Table 4 – Chemical potential calibration data for methane.

T (K)	m (K)	r (g/ml)	m / T	ln(r /$T^{3/2}$)	P (bar)	ln(P /$T^{5/2}$)
353.15	-6500	0.00002	-18.406	-19.541	0.040	-17.896
353.15	-6000	0.00009	-16.990	-18.125	0.163	-16.480
353.15	-5500	0.00037	-15.574	-16.705	0.675	-15.060
353.15	-5000	0.00152	-14.158	-15.289	2.779	-13.645
353.15	-4500	0.00637	-12.742	-13.857	11.570	-12.219
353.15	-4400	0.00850	-12.459	-13.568	15.392	-11.933
353.15	-4300	0.01137	-12.176	-13.277	20.549	-11.644
353.15	-4200	0.01523	-11.893	-12.985	27.373	-11.358
353.15	-4000	0.02767	-11.327	-12.388	49.135	-10.773
353.15	-3900	0.03741	-11.043	-12.086	65.966	-10.478
353.15	-3500	0.12479	-9.911	-10.881	219.190	-9.277
323.15	-6500	0.00000	-20.114	-21.246	0.006	-19.601
323.15	-6000	0.00002	-18.567	-19.699	0.027	-18.053
323.15	-5500	0.00008	-17.020	-18.152	0.127	-16.507
323.15	-5000	0.00036	-15.473	-16.603	0.598	-14.959
323.15	-4500	0.00169	-13.925	-15.051	2.821	-13.408
323.15	-4000	0.00813	-12.378	-13.480	13.433	-11.848
323.15	-3500	0.04268	-10.831	-11.821	67.132	-10.239
303.15	-6500	0.00000	-21.442	-22.573	0.001	-20.928
303.15	-6000	0.00000	-19.792	-20.924	0.007	-19.278
303.15	-5500	0.00002	-18.143	-19.274	0.035	-17.629
303.15	-5000	0.00012	-16.493	-17.624	0.184	-15.979
303.15	-4500	0.00061	-14.844	-15.973	0.958	-14.329
303.15	-4000	0.00321	-13.195	-14.312	5.013	-12.674
303.15	-3500	0.01779	-11.545	-12.600	26.950	-10.992
303.15	-3400	0.02556	-11.216	-12.238	38.198	-10.643
303.15	-3300	0.03715	-10.886	-11.864	54.343	-10.290
298.15	-5087	0.00006	-17.062	-18.198	0.099	-16.553
298.15	-4406	0.00064	-14.778	-15.896	0.992	-14.252
298.15	-3724	0.00652	-12.490	-13.579	9.910	-11.950
298.15	-3519	0.01340	-11.803	-12.859	20.218	-11.237
298.15	-3399	0.02034	-11.400	-12.441	30.142	-10.838
298.15	-3313	0.02860	-11.112	-12.101	41.663	-10.514

A.1.2: Carbon dioxide

Table 5 A – Data of carbon dioxide adsorption on UiO-66Zr.

Experimental		Simulated							
		UiO-66-Ehq q (mol/kg)					UiO-66-UAq q (mol/kg)		
P (bar)	q (mol/kg)	P (bar)	298 K	P (bar)	313 K	343 K	298 K	313 K	343 K
0.000	0.000	0.045	0.126	0.106	0.195	0.096	0.282	0.189	0.094
0.045	0.078	0.139	0.363	0.152	0.283	0.134	0.382	0.255	0.136
0.092	0.154	0.236	0.601	0.305	0.530	0.276	0.692	0.491	0.255
0.139	0.226	0.334	0.809	0.066	0.120	0.506	1.170	0.116	0.477
0.188	0.298	0.486	1.140	0.789	1.177	0.641	1.408	1.049	0.597
0.236	0.366	0.642	1.403	1.032	1.435	0.795	1.699	1.268	0.755
0.284	0.433	0.798	1.667	1.348	1.716	0.985	1.989	1.542	0.911
0.334	0.499	0.958	1.871	1.762	2.167	1.224	2.414	1.782	1.116
0.385	0.564	1.788	2.793	2.305	2.471	1.451	2.817	2.096	1.325
0.436	0.628	3.183	3.905	3.019	2.913	1.881	3.358	2.527	1.640
0.486	0.688	6.818	5.012	3.964	3.429	2.142	3.839	3.072	1.918
0.539	0.752	10.609	5.810	5.217	3.929	2.539	4.403	3.456	2.318
0.590	0.810	13.000	6.086	6.888	4.277	2.968	5.084	4.063	2.680
0.642	0.869	16.000	6.227	9.129	4.871	3.482	5.661	4.577	3.128
0.693	0.926	20.000	6.591	12.154	5.284	3.997	6.196	5.206	3.623
0.745	0.981	25.098	6.716	16.261	5.617	4.407	6.745	5.804	4.284
0.798	1.038	29.936	6.886	21.879	5.959	4.838	7.038	6.358	4.866
0.851	1.093	30.737	6.881	29.622	6.356	5.389	7.449	6.785	5.266
0.905	1.147								
0.958	1.200								
1.012	1.252								
1.264	1.486								
1.524	1.704								
1.788	1.912								
2.058	2.110								
2.332	2.295								
2.612	2.475								
2.896	2.650								
3.183	2.812								
3.767	3.121								
4.361	3.404								
4.964	3.667								
5.575	3.917								
6.192	4.149								
6.818	4.362								
7.437	4.562								
8.070	4.756								
8.705	4.935								
9.341	5.105								
9.978	5.265								
10.609	5.419								
12.617	5.818								
14.657	6.150								
16.724	6.414								
19.720	6.713								
22.502	6.924								
25.098	7.078								
27.633	7.207								
29.936	7.299								

Table 6 B – Data of carbon dioxide adsorption on UiO-66Zr.

Simulated						
UiO-66-UAq q (mol/kg)						
	298 K		313 K		343 K	
P (bar)	q (mol/kg)	Qst (kJ/mol)	q (mol/kg)	Qst (kJ/mol)	q (mol/kg)	Qst (kJ/mol)
0.060	0.110	20.410	0.076	20.339	0.040	20.268
0.075	0.139	20.367	0.096	20.332	0.050	20.294
0.091	0.165	20.359	0.115	20.376	0.061	20.305
0.106	0.192	20.361	0.133	20.320	0.070	20.304
0.152	0.267	20.364	0.188	20.288	0.100	20.250
0.305	0.496	20.331	0.358	20.253	0.198	20.283
0.603	0.869	20.324	0.643	20.182	0.368	20.207
0.789	1.064	20.471	0.801	20.230	0.468	20.226
1.032	1.304	20.315	0.982	20.194	0.587	20.112
1.348	1.588	20.665	1.218	20.327	0.736	19.987
1.762	1.932	20.884	1.477	20.386	0.909	20.151
2.305	2.339	21.328	1.795	20.537	1.111	20.072
3.019	2.789	21.761	2.174	20.783	1.363	20.110
3.964	3.405	22.153	2.606	21.082	1.644	20.432
5.217	4.045	23.287	3.155	21.618	2.006	20.806
6.888	4.643	24.538	3.740	22.793	2.388	21.203
9.129	5.269	25.275	4.343	23.912	2.853	21.818
12.154	5.862	26.412	4.972	24.962	3.395	22.249
16.261	6.319	25.873	5.526	25.860	3.970	23.116
21.879	6.748	26.451	6.128	26.923	4.510	
29.622	7.141	27.604	6.461	27.068	5.091	

Table 7 – Chemical potential calibration data for carbon dioxide.

T (K)	m (K)	r (g/ml)	m / T	ln(r /$T^{3/2}$)	P (bar)	ln(P/$T^{5/2}$)
298	-3700	0.24007	-12.416	-9.972	67.283	-10.034
298	-3800	0.09659	-12.752	-10.883	42.174	-10.501
298	-3900	0.05727	-13.087	-11.406	27.399	-10.932
298	-4000	0.03632	-13.423	-11.861	18.578	-11.321
298	-4100	0.02494	-13.758	-12.237	13.171	-11.665
298	-4200	0.01719	-14.094	-12.609	9.279	-12.015
298	-4500	0.00585	-15.101	-13.687	3.241	-13.067
298	-4600	0.00412	-15.436	-14.038	2.297	-13.411
298	-4800	0.00210	-16.107	-14.714	1.172	-14.084
298	-5000	0.00107	-16.779	-15.389	0.598	-14.757
313	-4100	0.05938	-13.099	-11.443	30.306	-10.954
313	-4300	0.02703	-13.738	-12.230	15.031	-11.655
313	-4500	0.01351	-14.377	-12.923	7.734	-12.320
313	-4800	0.00505	-15.335	-13.908	2.956	-13.282
313	-5000	0.00259	-15.974	-14.576	1.521	-13.946
313	-5500	0.00052	-17.572	-16.181	0.307	-15.545
343	-4300	0.14986	-12.536	-10.655	73.633	-10.295
343	-4400	0.09819	-12.828	-11.077	52.188	-10.639
343	-4600	0.04373	-13.411	-11.886	26.256	-11.326
343	-4800	0.02301	-13.994	-12.529	14.348	-11.931
343	-5000	0.01240	-14.577	-13.147	7.841	-12.535
343	-5200	0.00682	-15.160	-13.744	4.372	-13.119
343	-5400	0.00376	-15.743	-14.341	2.419	-13.711
343	-5600	0.00206	-16.327	-14.939	1.331	-14.308
343	-5800	0.00115	-16.910	-15.526	0.743	-14.892
343	-6000	0.00065	-17.493	-16.102	0.418	-15.466

A.2: Tables of the simulation data for adsorption of ethane on a SWNT.

Table 8 – Data of ethane adsorption on a SWNT.

303.15 K

				Number of Particles		Number of Particles / Å^2	
P (bar)	r_g (g/ml)	T (K)	m (K)	ATOMIC	SMOOTH	ATOMIC	SMOOTH
0.018	0.000022	303.15	-6000	1.41	1.70	0.0008	0.0010
0.039	0.000046	303.15	-5750	3.39	4.11	0.0020	0.0024
0.088	0.000102	303.15	-5500	8.07	9.27	0.0048	0.0055
0.200	0.000229	303.15	-5250	14.54	17.52	0.0087	0.0104
0.459	0.000531	303.15	-5000	21.77	23.90	0.0130	0.0143
1.069	0.001265	303.15	-4750	29.98	31.24	0.0179	0.0186
2.519	0.003091	303.15	-4500	45.19	45.13	0.0270	0.0269
6.010	0.007760	303.15	-4250	76.50	77.05	0.0456	0.0460
10.186	0.013653	303.15	-4100	116.47	113.46	0.0695	0.0677
14.516	0.020006	303.15	-4000	155.00	145.51	0.0925	0.0868
20.727	0.029440	303.15	-3900	212.87	194.40	0.1270	0.1160
24.786	0.035770	303.15	-3850	257.85	226.44	0.1538	0.1351
29.653	0.043508	303.15	-3800	322.01	276.00	0.1921	0.1646
35.495	0.052976	303.15	-3750	448.93	375.37	0.2678	0.2239
87.861	0.144076	303.15	-3500	1290.31	971.96	0.7697	0.5798

Table 9 – Chemical potential calibration data for ethane.

T (K)	m (K)	r (g/ml)	m / T	ln(r /$T^{3/2}$)	P (bar)	ln(P /$T^{5/2}$)
303.15	-3790.92	0.04681	-12.505	-5.141	30.885	-10.855
303.15	-3998.09	0.01801	-13.188	-5.945	13.825	-11.659
303.15	-4247.335	0.00710	-14.011	-6.823	5.746	-12.537
303.15	-4496.446	0.00300	-14.832	-7.665	2.475	-13.380
303.15	-4763.907	0.00122	-15.715	-8.557	1.015	-14.271
303.15	-4997.843	0.00056	-16.486	-9.333	0.467	-15.047
303.15	-5501.673	0.00011	-18.148	-10.996	0.088	-16.711
303.15	-5995.326	0.00002	-19.777	-12.625	0.017	-18.340
323.15	-4054.268	0.04681	-12.546	-5.140	34.025	-10.918
323.15	-4131.723	0.03288	-12.786	-5.432	25.401	-11.211
323.15	-4285.568	0.01801	-13.262	-5.971	14.830	-11.749
323.15	-4358.603	0.01387	-13.488	-6.213	11.640	-11.991
323.15	-4493.425	0.00873	-13.905	-6.647	7.542	-12.425
323.15	-4774.555	0.00349	-14.775	-7.544	3.076	-13.322
323.15	-4995.995	0.00173	-15.460	-8.237	1.537	-14.015
323.15	-5511.111	0.00035	-17.054	-9.837	0.310	-15.615
323.15	-6000.801	0.00008	-18.570	-11.354	0.068	-17.132
353.15	-4453.173	0.04681	-12.610	-5.148	38.570	-11.015
353.15	-4545.108	0.03288	-12.870	-5.449	28.531	-11.316
353.15	-4802.895	0.01387	-13.600	-6.245	12.881	-12.111
353.15	-5021.888	0.00710	-14.220	-6.888	6.768	-12.755
353.15	-5505.842	0.00173	-15.591	-8.280	1.682	-14.147
353.15	-6016.746	0.00040	-17.037	-9.732	0.394	-15.599
353.15	-6507.064	0.00010	-18.426	-11.122	0.098	-16.988
373.15	-4721.774	0.04681	-12.654	-5.155	41.589	-11.077
373.15	-4921.057	0.02397	-13.188	-5.753	22.877	-11.675
373.15	-5261.586	0.00873	-14.100	-6.713	8.762	-12.635
373.15	-5646.955	0.00300	-15.133	-7.765	3.059	-13.687
373.15	-5978.508	0.00122	-16.022	-8.659	1.251	-14.581
373.15	-6359.177	0.00044	-17.042	-9.681	0.450	-15.603
373.15	-6730.975	0.00016	-18.038	-10.678	0.166	-16.600
373.15	-7119.368	0.00006	-19.079	-11.720	0.059	-17.642
373.15	-7474.42	0.00002	-20.031	-12.672	0.023	-18.594

Appendix B: Input and Output towhee files.

In this appendix, are presented the various types of files related whit Towhee. It is present as an example the input files for methane adsorption on UiO-66Zr and for the adsorption of ethane on carbon nanotubes it's present the input files for the SMOOTH and ATOMIC runs. It is also present a standard output, in this case an output file od the adsorption of methane, as well fiel for the UiO-66-UA a force field.

B.1: Input files used in simulations.

B.1.1: CH4/MOF input file.

```
inputformat
'Towhee'
ensemble
'uvt'
temperature
298.15
nmolty
2
nmolectyp
0 5000
chempot
0.0 -3150.0
numboxes
1
stepstyle
'moves'
nstep
2000000
controlstyle
'manual'
printfreq
200000
blocksize
400000
moviefreq
-100
box
1
vclassic
1
molty
0 -1
runoutput
'blocks'
trmaxdispfreq
100
volmaxdispfreq
100
potentialstyle
'internal'
ffnumber
2
ff_filename
/home/jmaia/MOF/UiO-66/uVT/towhee_ff_UiO-66Zr
/home/jmaia/bin/ForceFields/towhee_ff_TraPPE-UA
```

```
classical_potential
'Lennard-Jones'
classical_mixrule
'Lorentz-Berthelot'
lshift
.false.
ltailc
.true.
rmin
1
rcut
14
rcutin
10
electrostatic_form
'none'
nfield
1
fieldtype
'Adsorbent'
ads_box
1
ads_imolty
1
ads_nuc
8
ads_filecoords
/home/jmaia/MOF/UiO-66/uVT/UiO.xyz
ads_ltailc
.true.
linit
.true.
initboxtype
'dimensions'
initstyle
'coords' 'coords'
initlattice
'none' 'none'
initmol
0 0
inix iniy iniz
2    2    2
hmatrix
41.9568 0.00000 0.00000
0.00000 41.9568 0.00000
0.00000 0.00000 41.9568
pmuvtcbswap
0.40            40% Configurational-bias grand-canonical
insertion/deletion
  pmuvtcbmt
  0.0 1.0       (0% MOF, 100% adsorbate)
pmtracm
1.0             60% Center-of-Mass Molecule Translation
  pmtcmt
  0.0 1.0       (0% MOF, 100% adsorbate)
  rmtrac
```

```
  2.0           (initial Center-of-mass translation maximum displacement,
Angstroms)
  tatrac
  0.5           (target acceptance rate for the center-of-mass
translation move = 50%)
# UiO-66(Zr) Chem. Commun. 48 (2012) 9831
input_style
'basic connectivity map'
nunit
344
nmaxcbmc
344
lpdbnames
F
forcefield
'UiO-66Zr'
charge_assignment
'manual'
unit ntype qqatom
  1  'Zr1'  0.0d0
vibration
0
improper
0
….
….
unit ntype qqatom
343  'C25'  0.0d0
vibration
0
improper
0
unit ntype qqatom
344  'C25'  0.0d0
vibration
0
improper
0
# METHANE (TraPPE-UA)
input_style
'basic connectivity map'
nunit
1
nmaxcbmc
1
lpdbnames
F
forcefield
'TraPPE-UA'
charge_assignment
'manual'
unit ntype     qqatom
1    'CH4'     0.0
vibration
0
improper torsion
0
```

B.1.2:C2H6/SWNT input file.

- **SMOOTH**

```
inputformat
'Towhee'
ensemble
'uvt'
temperature
303.15
nmolty
1
nmolectyp
5000
chempot
-6000
numboxes
1
stepstyle
'moves'
nstep
50000
controlstyle
'manual'
printfreq
10000
blocksize
10000
runoutput
'blocks'
pdb_output_freq
50000
trmaxdispfreq
100
volmaxdispfreq
0
potentialstyle
'internal'
ffnumber
1
ff_filename
/home/jmaia/bin/ForceFields/towhee_ff_TraPPE-UA
classical_potential
'Lennard-Jones'
classical_mixrule
'Lorentz-Berthelot'
lshift
.false.
ltailc
.true.
rmin
1
rcut
14
rcutin
10
electrostatic_form
'none'
```

```
nfield
1
fieldtype
'Smooth MWNT'
nt_cx
0.5
nt_cy
0.5
nt_rw
6.78
nt_nw
1
nt_sw
3.41
nt_liop
.true.
nt_leop
.true.
nt_nisz
150
nt_ncsz
10
nt_nesz
150
nt_rec
55
linit
.true.
initboxtype
'dimensions'
initstyle
'coords'
initlattice
'none'
initmol
0
inix iniy iniz
20   20   20
hmatrix
 55.0   0.0   0.0
  0.0  55.0   0.0
  0.0   0.0  38.1224
pmuvtcbswap
0.40            40% Configurational-bias grand-canonical
insertion/deletion
  pmuvtcbmt
  1.0           (100% adsorbate)
pmcb
0.55            15% Configurational-Bias Partial Molecule Regrowth
  pmcbmt
  1.0           (100% adsorbate)
  pmall
  0.0           (probability of regrowing the entire molecule = 0% MOF &
0% adsorbate)
pmtracm
0.85            30% Center-of-Mass Molecule Translation
  pmtcmt
```

```
  1.0           (100% adsorbate)
  rmtrac
  2.0           (initial Center-of-mass translation maximum displacement,
Angstroms)
  tatrac
  0.5           (target acceptance rate for the center-of-mass
translation move = 50%)
pmrotate
1.0             15% Rotation about the Center-of-Mass
  pmromt
  1.0           (0% MOF, 100% adsorbate)
  rmrot
  1.57          (initial molecular rotation maximum displacement, pi/2
radians)
  tarot
  0.5           (target acceptance rate for the rotation move = 50%)
# ETHANE (TraPPE-UA)
input_style
'basic connectivity map'
nunit
2
nmaxcbmc
2
lpdbnames
F
forcefield
'TraPPE-UA'
charge_assignment
'manual'
unit ntype    qqatom
1    'CH3*(sp3)' 0.0
vibration
1
2
improper torsion
0
unit ntype    qqatom
2    'CH3*(sp3)' 0.0
vibration
1
1
improper torsion
0
```

- **ATOMIC**

```
inputformat
'Towhee'
ensemble
'uvt'
temperature
303.15
nmolty
2
nmolectyp
15 000
chempot
0.0 -6000.0
numboxes
1
stepstyle
'moves'
nstep
50000
printfreq
10000
blocksize
10000
moviefreq
100
backupfreq
100
runoutput
'full'
pdb_output_freq
50000
potentialstyle
'internal'
ffnumber
2
ff_filename
/home/jmaia/bin/ForceFields/towhee_ff_TraPPE-UA
/home/jmaia/CNT/ATOMIC/towhee_ff_TraPPE-CNT
classical_potential
'Lennard-Jones'
classical_mixrule
'Lorentz-Berthelot'
lshift
.false.
ltailc
.true.
rmin
1
rcut
14
rcutin
10
electrostatic_form
'none'
linit
.true.
```

```
initboxtype
'dimensions'
initstyle
'nanotube' 'full cbmc'
initlattice
'simple cubic' 'simple cubic'
initmol
1 0
inix iniy iniz
20    20    20
hmatrix
55.0   0.0    0.0
 0.0  55.0    0.0
 0.0   0.0   50.0
pmuvtcbswap
0.40            40% Configurational-bias grand-canonical
insertion/deletion
  pmuvtcbmt
  0.0 1.0           (100% adsorbate)
pmcb
0.55            15% Configurational-Bias Partial Molecule Regrowth
  pmcbmt
  0.0 1.0           (100% adsorbate)
  pmall
  0.0 0.0           (probability of regrowing the entire molecule = 0%
MOF & 0% adsorbate)
pmtracm
0.85            30% Center-of-Mass Molecule Translation
  pmtcmt
  0.0 1.0           (100% adsorbate)
  rmtrac
  2.0           (initial Center-of-mass translation maximum displacement,
Angstroms)
  tatrac
  0.5           (target acceptance rate for the center-of-mass
translation move = 50%)
pmrotate
1.0             15% Rotation about the Center-of-Mass
  pmromt
  0.0 1.0           (0% MOF, 100% adsorbate)
  rmrot
  1.57          (initial molecular rotation maximum displacement, pi/2
radians)
  tarot
  0.5           (target acceptance rate for the rotation move = 50%)
#nanotube
input_style
'nanotube builder'
forcefield
'TraPPE-CNT'
atomname
'NT_C'
qqatom
0
nanotube_n
10
nanotube_m
```

```
10
nanotube_ncells
16
nanotube_bondlength
1.418d0
# ETHANE (TraPPE-UA)
input_style
'basic connectivity map'
nunit
2
nmaxcbmc
2
lpdbnames
F
forcefield
'TraPPE-UA'
charge_assignment
'manual'
unit ntype    qqatom
1    'CH3*(sp3)' 0.0
vibration
1
2
improper torsion
0
unit ntype    qqatom
2    'CH3*(sp3)' 0.0
vibration
1
1
improper torsion
0
```

B.2: CH4/MOF output file.

```
MCCCS Towhee - Version 7.0.4   (September 18 2012)
 EXTENDED **** <2012> Jose P. B. Mota
 Copyright (C) <2012> Marcus G. Martin
 Code Contributors for 2012: Marcus G. Martin;
 Copyright (C) <2011> Marcus G. Martin
 Code Contributors for 2011: Fred James; Marcus G. Martin; Suleiman
Oloriegbe;
 Copyright (C) <2010> Marcus G. Martin
 Code Contributors for 2010: Rene Haber; Andrej Lajovic; Marcus G.
Martin; Loukas Peristeras;
 Copyright (C) <2009> Marcus G. Martin
 Code Contributors for 2009: Rene Haber; Marcus G. Martin; Loukas
Peristeras;
 Copyright (C) <2008> Marcus G. Martin
 Code Contributors for 2008: Rene Haber; Iyad A. Hijazi; Marcus G.
Martin; Loukas Peristeras; Craig Tenney;
 Copyright (C) <2007> Marcus G. Martin
 Code Contributors for 2007: Bernhard Eckl; Frank Heilmann; Jianhui Li;
Marcus G. Martin; Craig M. Tenney; Ozgur Yazaydin
 Copyright (C) <2006> Marcus G. Martin
 Code Contributors for 2006: Alan A. Chen; Arben Jusufi; Christian D.
Lorenz; Marcus G. Martin; Jeffrey J. Potoff; Vincent K. Shen; Matthew A.
Wyczalkowski; Ozgur Yazaydin
 Copyright (C) <2005> Marcus G. Martin
 Code Contributors for 2005: Marcus G. Martin; Alan A. Chen; Christian D.
Lorenz; Matthew A. Wyczalkowski
 Copyright (C) <2004> Marcus G. Martin
 Code Contributors for 2004: Marcus G. Martin; Christian D. Lorenz; Peter
A. Schultz; Aidan P. Thompson; Jeffrey J. Potoff; Steve R. Lustig; Paul
S. Crozier; Nicholas du Preez
 Copyright (C) <2003> Marcus G. Martin
 Code Contributors for 2003: Marcus G. Martin; Christian D. Lorenz; David
B. Ritch; Michael L. Greenfield; Yogesh Srivastava; Evangelos A Coutsias
 Copyright (C) <2002> Marcus G. Martin
 Code Contributors for 2002: Marcus G. Martin; Christian D. Lorenz; Aidan
P. Thompson; Allen G. Sault
 Copyright (C) <2000-2001> Marcus G. Martin
 Copyright (C) <1999> J. Ilja Siepmann and Marcus G. Martin
 Code Contributors for 1999: J. Ilja Siepmann; Marcus G. Martin; Bin
Chen; Collin D. Wick; John Stubbs

 Direct comments about this code to Marcus G. Martin
(marcus_martin@users.sourceforge.net)
 See the MCCCS Towhee web site for more information and the users manual.
 http://towhee.sourceforge.net

 We would like to thank the following agencies for providing funding used
to develop MCCCS Towhee
 -Department of Energy Industrial Technologies Program (MGM)
 -National Science Foundation (JIS)
 -Department of Energy Computational Science Graduate Fellowship
(MGM,CDW)

 This program is free software; you can redistribute it and/or modify
```

```
 it under the terms of the GNU General Public License as published by
 the Free Software Foundation; either version 2 of the License, or
 (at your option) any later version.
 This program is distributed in the hope that it will be useful,
 but WITHOUT ANY WARRANTY; without even the implied warranty of
 MERCHANTABILITY or FITNESS FOR A PARTICULAR PURPOSE. See the
 GNU General Public License for more details.

 You should have received a copy of the GNU General Public License
 along with this program; if not, write to the Free Software
 Foundation, Inc., 59 Temple Place, Suite 330, Boston, MA  02111-1307
USA

 Reading from towhee_input file: towhee_input1
 in directory: current directory
 inputformat: Towhee
 ensemble: uvt
 temperature:  298.150
 nmolty:            2
 nmolectyp:           0         5000
 chempot:  0.00000    -3150.00
 numboxes:          1
 stepstyle: moves
 nstep:      2000000
 controlstyle: manual
 printfreq:       200000
 blocksize:       400000
 moviefreq:         -100
 box:           1
 vclassic:            1
 molty:  0 -1
 runoutput: blocks
Output running block averages
 trmaxdispfreq:          100
 volmaxdispfreq:          100
 potentialstyle: internal
 ffnumber:            2
 ff_filename:
/home/jmaia/MOF/UiO-66/uVT/towhee_ff_UiO-66Zr
/home/jmaia/bin/ForceFields/towhee_ff_TraPPE-UA
 classical_potential: Lennard-Jones
 READCLASSICAL: pot_num:     1 potential name: Lennard-Jones
 classical_mixrule: Lorentz-Berthelot
 lshift:  F
 ltailc:  T
 rmin:  1.00000
 rcut:  14.0000
 rcutin:  10.0000
 electrostatic_form: none
 Setting up force field parameters from files
 opening forcefield file:    1
 opening forcefield file:    2
 Lorentz-Berthelot Mixing rules
 Arithmetic mean of sigma terms
 Geometric mean of epsilon term
default max_bond_length:  3.00
 nfield:            1
```

```
Field:     1 fieldtype: Adsorbent
 ads_box                        :            1
 ads_imolty                     :            1
 ads_nuc                        :            8
 ads_filecoords                 : /home/jmaia/MOF/UiO-66/uVT/UiO.xyz
 No. atom coordinates in file  :         2753
 ads_ltailc                     :  T
 No solvation model used
 linit:  F
 initboxtype: dimensions
initstyle Box:    1
 coords               coords
Box:  1 initlattice: none                none
Box:  1 initmol:         0          0
Box:  1 inix,iniy,iniz:          2          2          2
Box idim hmatrix:    1 1   41.95680    0.00000    0.00000
Box idim hmatrix:    1 2    0.00000   41.95680    0.00000
Box idim hmatrix:    1 3    0.00000    0.00000   41.95680
 pmuvtcbswap: 0.400000
 pmuvtcbmt:  0.00000     1.00000
 pmtracm:  1.00000
 pmtcmt:  0.00000     1.00000
 rmtrac:  2.00000
 tatrac: 0.500000
cbmc_formulation: Martin and Frischknecht 2006
 Coupled to pre-nonbond formulation from
 M.G. Martin; A.L. Frischknecht; Mol. Phys. 104 2439-2456 (2006)
cbmc_setting_style: Martin and Frischknecht
 input_style: basic connectivity map
 nunit:          344
 nmaxcbmc:           344
 lpdbnames:  F
   using the UiO-66Zr   force field
 charge_assignment: manual
   Building the input file for molecule type:     1
unit:    1 name:Zr1        charge:   0.00000
unit:    2 name:C25        charge:   0.00000
unit:    3 name:O1         charge:   0.00000
unit:    4 name:C1         charge:   0.00000
….
….
unit:  340 name:C25        charge:   0.00000
unit:  341 name:C13        charge:   0.00000
unit:  342 name:C1         charge:   0.00000
unit:  343 name:C25        charge:   0.00000
unit:  344 name:C25        charge:   0.00000
 input_style: basic connectivity map
 nunit:            1
 nmaxcbmc:             1
 lpdbnames:  F
   using the TraPPE-UA  force field
 charge_assignment: manual
   Building the input file for molecule type:     2
unit:    1 name:CH4        charge:   0.00000
 Verifying input structures are consistent
Determining CBMC bond distributions
     for molecule type     2
```

```
Determining Autofit Gaussian bend A parameters
Determining Autofit Gaussian bend B parameters
Determining Autofit Gaussian dihedral parameters
 Determining cyclic subunits for molecule type          1
 Determining cyclic subunits for molecule type          2
Default total charge on molecule   1 is   0.00000
Default total charge on molecule   2 is   0.00000
Total charge in the simulation system:   0.00000
Bond Types
   No Bond Types
Angle Types
   No Angle Types
Torsion Types
   No Torsion Types
Improper Torsion Types
   No Improper Types
 Grand Canonical ensemble
 3-dimensional periodic box
 Additional Center-of-Mass cutoff
 Dual Cutoff Configurational-bias Monte Carlo
 Coupled-decoupled Configurational-bias MC
 External fields specified

Molecular mass for molecule type     1 is  6656.2429 g/mol
Molecular mass for molecule type     2 is    16.0426 g/mol
 Reading in initial conformation from towhee_inital
Initial version:    7
Restarting random number generator DX-1597-2-7 from integer seed array
 new maximum displacements read from towhee_initial
box:     1
molecule type:     1
 Max displacement for Atom translate:   0.500000
 Max displacement for COM translate:   2.000000
 Max displacement for rotation:   0.500000
molecule type:     2
 Max displacement for Atom translate:   0.500000
 Max displacement for COM translate:   1.008265
 Max displacement for rotation:   0.500000
 Max disp. for unit cell perturbation

 new box dimensions read from towhee_initial
 Box  1 hmatrix(1,x):       41.95680       0.00000       0.00000
 Box  1 hmatrix(2,x):        0.00000      41.95680       0.00000
 Box  1 hmatrix(3,x):        0.00000       0.00000      41.95680

Energies exclusively from internal potentials
Nonbonded Force Field
Lennard-Jones 12-6 potential
    with tail corrections
u(r) = 4*epsilon[(sigma/r)^12 - (sigma/r)^6] - shift
Num. Atom(i)    Num. Atom(j)         sigma    epsilon      shift     1-
4sig     1-4eps
   1 Zr1           1 Zr1            2.7830    34.7240     0.0000
0.0000     0.0000
   1 Zr1           2 O25            2.9015    56.8272     0.0000
0.0000     0.0000
```

```
   1 Zr1           3 O1             2.7915    43.7015     0.0000
0.0000     0.0000
   1 Zr1           4 C25            3.2615    40.8259     0.0000
0.0000     0.0000
….
….
   6 C1            9 CH4            3.8150    77.8974     0.0000
0.0000     0.0000
   7 O29           7 O29            2.8000    55.0000     0.0000
0.0000     0.0000
   7 O29           9 CH4            3.2650    90.2219     0.0000
0.0000     0.0000
   9 CH4           9 CH4            3.7300   148.0000     0.0000
0.0000     0.0000

Number of MC moves:              2000000
Number of molecules:                5000
Temperature [K]:       298.15000

Initial Energies for Box     1
Total molecules in this box        304
Molecules of type   1 :          0
Molecules of type   2 :        304
 total vibration            0.000 [K]         0.00000 [kcal/mol]
    regular                 0.000 [K]         0.00000 [kcal/mol]
    bond-bond(1-2)          0.000 [K]         0.00000 [kcal/mol]
 total angle                0.000 [K]         0.00000 [kcal/mol]
    regular                 0.000 [K]         0.00000 [kcal/mol]
    angle-angle             0.000 [K]         0.00000 [kcal/mol]
 total torsion              0.000 [K]         0.00000 [kcal/mol]
    regular                 0.000 [K]         0.00000 [kcal/mol]
    improper                0.000 [K]         0.00000 [kcal/mol]
 total nonbond         -57544.341 [K]      -114.35303 [kcal/mol]
    intramolecular          0.000 [K]         0.00000 [kcal/mol]
    2-body nonbond     -56021.910 [K]      -111.32763 [kcal/mol]
    3-body nonbond          0.000 [K]         0.00000 [kcal/mol]
    tail correct.       -1522.431 [K]        -3.02540 [kcal/mol]
 external field       -481732.023 [K]      -957.30551 [kcal/mol]
 solvation                  0.000 [K]         0.00000 [kcal/mol]
 total classical           -539276.3638 [K]         -1071.658534
[kcal/mol]

 +++++ start of markov chain +++++

Move       Box   Energy [K]  Volume [A^3] Press. [kPa] Molecules
    200000 B: 1 -0.5909E+06  0.7386E+05          0.0     0  332
    400000 B: 1 -0.5761E+06  0.7386E+05          0.0     0  330
Block Averages (BA) for block     1
BA Box: 1 Volume [A^3] 0.73859621E+05
BA Box: 1 V^2 [A^6] 0.54552436E+10
BA Box: 1 Specific density [g/ml] 0.11373475E+00
BA Box: 1 Virial Pressure      [kPa] 0.00000000E+00
BA Box: 1 Total Classical -.55400291E+06
BA Box: 1 Inter vdw       -.62749724E+05
BA Box: 1 Angle           0.00000000E+00
BA Box: 1 Torsion         0.00000000E+00
BA Box: 1 Intra vdw       0.00000000E+00
```

```
BA Box: 1 External Field  -.49125319E+06
BA Box: 1 Vibration       0.00000000E+00
BA Box: 1 Coulomb         0.00000000E+00
BA Box: 1 Tail vdw        -.16395251E+04
BA Box: 1 Solvation       0.00000000E+00
BA Box: 1 u (Gibbs Total) [K] Type   1 0.00000000E+00
BA Box: 1 u (Gibbs Total) [K] Type   2 -.31566696E+04
BA Box: 1 Number density [nm-3] Type   1 0.00000000E+00
BA Box: 1 Number density [nm-3] Type   2 0.42693566E+01
BA Box: 1 Mol Fraction Type   1 0.00000000E+00
BA Box: 1 Mol Fraction Type   2 0.10000000E+01
BA Box: 1 Stress Tensor Virial S_xx          [kPa] 0.00000000E+00
BA Box: 1 Stress Tensor Virial S_yy          [kPa] 0.00000000E+00
BA Box: 1 Stress Tensor Virial S_zz          [kPa] 0.00000000E+00
BA Box: 1 Stress Tensor Virial S_xy          [kPa] 0.00000000E+00
BA Box: 1 Stress Tensor Virial S_xz          [kPa] 0.00000000E+00
BA Box: 1 Stress Tensor Virial S_yz          [kPa] 0.00000000E+00
BA Box: 1 Stress Tensor Virial P_tail        [kPa] 0.00000000E+00
BA Box: 1 Radius of Gyration Type:  1        0.00000
BA Box: 1 Radius of Gyration Type:  2        0.00000
    600000 B: 1 -0.5742E+06  0.7386E+05          0.0     0  324
    800000 B: 1 -0.5415E+06  0.7386E+05          0.0     0  310
Block Averages (BA) for block     2
BA Box: 1 Volume [A^3] 0.73859621E+05
BA Box: 1 V^2 [A^6] 0.54552436E+10
BA Box: 1 Specific density [g/ml] 0.11409175E+00
BA Box: 1 Virial Pressure      [kPa] 0.00000000E+00
BA Box: 1 Total Classical -.55661973E+06
BA Box: 1 Inter vdw       -.62054791E+05
BA Box: 1 Angle           0.00000000E+00
BA Box: 1 Torsion         0.00000000E+00
BA Box: 1 Intra vdw       0.00000000E+00
BA Box: 1 External Field  -.49456494E+06
BA Box: 1 Vibration       0.00000000E+00
BA Box: 1 Coulomb         0.00000000E+00
BA Box: 1 Tail vdw        -.16492286E+04
BA Box: 1 Solvation       0.00000000E+00
BA Box: 1 u (Gibbs Total) [K] Type   1 0.00000000E+00
BA Box: 1 u (Gibbs Total) [K] Type   2 -.31347820E+04
BA Box: 1 Number density [nm-3] Type   1 0.00000000E+00
BA Box: 1 Number density [nm-3] Type   2 0.42827573E+01
BA Box: 1 Mol Fraction Type   1 0.00000000E+00
BA Box: 1 Mol Fraction Type   2 0.10000000E+01
BA Box: 1 Stress Tensor Virial S_xx          [kPa] 0.00000000E+00
BA Box: 1 Stress Tensor Virial S_yy          [kPa] 0.00000000E+00
BA Box: 1 Stress Tensor Virial S_zz          [kPa] 0.00000000E+00
BA Box: 1 Stress Tensor Virial S_xy          [kPa] 0.00000000E+00
BA Box: 1 Stress Tensor Virial S_xz          [kPa] 0.00000000E+00
BA Box: 1 Stress Tensor Virial S_yz          [kPa] 0.00000000E+00
BA Box: 1 Stress Tensor Virial P_tail        [kPa] 0.00000000E+00
BA Box: 1 Radius of Gyration Type:  1        0.00000
BA Box: 1 Radius of Gyration Type:  2        0.00000
   1000000 B: 1 -0.5730E+06  0.7386E+05          0.0     0  322
   1200000 B: 1 -0.5483E+06  0.7386E+05          0.0     0  313
Block Averages (BA) for block     3
BA Box: 1 Volume [A^3] 0.73859621E+05
BA Box: 1 V^2 [A^6] 0.54552436E+10
```

```
BA Box: 1 Specific density [g/ml] 0.11478985E+00
BA Box: 1 Virial Pressure      [kPa] 0.00000000E+00
BA Box: 1 Total Classical -.56122499E+06
BA Box: 1 Inter vdw       -.63194565E+05
BA Box: 1 Angle           0.00000000E+00
BA Box: 1 Torsion         0.00000000E+00
BA Box: 1 Intra vdw       0.00000000E+00
BA Box: 1 External Field  -.49803042E+06
BA Box: 1 Vibration       0.00000000E+00
BA Box: 1 Coulomb         0.00000000E+00
BA Box: 1 Tail vdw        -.16704327E+04
BA Box: 1 Solvation       0.00000000E+00
BA Box: 1 u (Gibbs Total) [K] Type   1 0.00000000E+00
BA Box: 1 u (Gibbs Total) [K] Type   2 -.31378566E+04
BA Box: 1 Number density [nm-3] Type   1 0.00000000E+00
BA Box: 1 Number density [nm-3] Type   2 0.43089626E+01
BA Box: 1 Mol Fraction Type   1 0.00000000E+00
BA Box: 1 Mol Fraction Type   2 0.10000000E+01
BA Box: 1 Stress Tensor Virial S_xx          [kPa] 0.00000000E+00
BA Box: 1 Stress Tensor Virial S_yy          [kPa] 0.00000000E+00
BA Box: 1 Stress Tensor Virial S_zz          [kPa] 0.00000000E+00
BA Box: 1 Stress Tensor Virial S_xy          [kPa] 0.00000000E+00
BA Box: 1 Stress Tensor Virial S_xz          [kPa] 0.00000000E+00
BA Box: 1 Stress Tensor Virial S_yz          [kPa] 0.00000000E+00
BA Box: 1 Stress Tensor Virial P_tail        [kPa] 0.00000000E+00
BA Box: 1 Radius of Gyration Type:  1        0.00000
BA Box: 1 Radius of Gyration Type:  2        0.00000
   1400000 B: 1 -0.5248E+06  0.7386E+05          0.0     0  304
   1600000 B: 1 -0.5842E+06  0.7386E+05          0.0     0  330
Block Averages (BA) for block     4
BA Box: 1 Volume [A^3] 0.73859621E+05
BA Box: 1 V^2 [A^6] 0.54552436E+10
BA Box: 1 Specific density [g/ml] 0.11331738E+00
BA Box: 1 Virial Pressure      [kPa] 0.00000000E+00
BA Box: 1 Total Classical -.55129817E+06
BA Box: 1 Inter vdw       -.61176482E+05
BA Box: 1 Angle           0.00000000E+00
BA Box: 1 Torsion         0.00000000E+00
BA Box: 1 Intra vdw       0.00000000E+00
BA Box: 1 External Field  -.49012169E+06
BA Box: 1 Vibration       0.00000000E+00
BA Box: 1 Coulomb         0.00000000E+00
BA Box: 1 Tail vdw        -.16270622E+04
BA Box: 1 Solvation       0.00000000E+00
BA Box: 1 u (Gibbs Total) [K] Type   1 0.00000000E+00
BA Box: 1 u (Gibbs Total) [K] Type   2 -.31645400E+04
BA Box: 1 Number density [nm-3] Type   1 0.00000000E+00
BA Box: 1 Number density [nm-3] Type   2 0.42536892E+01
BA Box: 1 Mol Fraction Type   1 0.00000000E+00
BA Box: 1 Mol Fraction Type   2 0.10000000E+01
BA Box: 1 Stress Tensor Virial S_xx          [kPa] 0.00000000E+00
BA Box: 1 Stress Tensor Virial S_yy          [kPa] 0.00000000E+00
BA Box: 1 Stress Tensor Virial S_zz          [kPa] 0.00000000E+00
BA Box: 1 Stress Tensor Virial S_xy          [kPa] 0.00000000E+00
BA Box: 1 Stress Tensor Virial S_xz          [kPa] 0.00000000E+00
BA Box: 1 Stress Tensor Virial S_yz          [kPa] 0.00000000E+00
BA Box: 1 Stress Tensor Virial P_tail        [kPa] 0.00000000E+00
```

```
BA Box: 1 Radius of Gyration Type:  1        0.00000
BA Box: 1 Radius of Gyration Type:  2        0.00000
   1800000 B: 1 -0.5758E+06  0.7386E+05          0.0     0  321
   2000000 B: 1 -0.5864E+06  0.7386E+05          0.0     0  331
Block Averages (BA) for block     5
BA Box: 1 Volume [A^3] 0.73859621E+05
BA Box: 1 V^2 [A^6] 0.54552436E+10
BA Box: 1 Specific density [g/ml] 0.11501965E+00
BA Box: 1 Virial Pressure      [kPa] 0.00000000E+00
BA Box: 1 Total Classical -.56177825E+06
BA Box: 1 Inter vdw       -.63318764E+05
BA Box: 1 Angle           0.00000000E+00
BA Box: 1 Torsion         0.00000000E+00
BA Box: 1 Intra vdw       0.00000000E+00
BA Box: 1 External Field  -.49845949E+06
BA Box: 1 Vibration       0.00000000E+00
BA Box: 1 Coulomb         0.00000000E+00
BA Box: 1 Tail vdw        -.16766001E+04
BA Box: 1 Solvation       0.00000000E+00
BA Box: 1 u (Gibbs Total) [K] Type   1 0.00000000E+00
BA Box: 1 u (Gibbs Total) [K] Type   2 -.31562297E+04
BA Box: 1 Number density [nm-3] Type   1 0.00000000E+00
BA Box: 1 Number density [nm-3] Type   2 0.43175889E+01
BA Box: 1 Mol Fraction Type   1 0.00000000E+00
BA Box: 1 Mol Fraction Type   2 0.10000000E+01
BA Box: 1 Stress Tensor Virial S_xx          [kPa] 0.00000000E+00
BA Box: 1 Stress Tensor Virial S_yy          [kPa] 0.00000000E+00
BA Box: 1 Stress Tensor Virial S_zz          [kPa] 0.00000000E+00
BA Box: 1 Stress Tensor Virial S_xy          [kPa] 0.00000000E+00
BA Box: 1 Stress Tensor Virial S_xz          [kPa] 0.00000000E+00
BA Box: 1 Stress Tensor Virial S_yz          [kPa] 0.00000000E+00
BA Box: 1 Stress Tensor Virial P_tail        [kPa] 0.00000000E+00
BA Box: 1 Radius of Gyration Type:  1        0.00000
BA Box: 1 Radius of Gyration Type:  2        0.00000

 +++++ end of markov chain +++++

 Final hmatrix (general box dimensions)
Box:     1
  hmatrix(1,x)      41.95680       0.00000       0.00000
  hmatrix(2,x)       0.00000      41.95680       0.00000
  hmatrix(3,x)       0.00000       0.00000      41.95680

* Grand Canonical Ensemble SWAP Moves *
Molecule type:     1
Molecule type:     2
  From box  1 to box  0 Attempted:  401227 Grown:  401227 Accepted:
32744
  From box  0 to box  1 Attempted:  399864 Grown:  399864 Accepted:
32771

* COM Translation Moves *
Molecule:  2 Box: 1 Attempts:        1198909. Accepted:         606864.
Accepted:  50.618 %

Final Energies for Box     1
Total molecules in this box        331
```

```
Molecules of type   1 :          0
Molecules of type   2 :        331
 total vibration            0.000 [K]         0.00000 [kcal/mol]
    regular                 0.000 [K]         0.00000 [kcal/mol]
    bond-bond(1-2)          0.000 [K]         0.00000 [kcal/mol]
 total angle                0.000 [K]         0.00000 [kcal/mol]
    regular                 0.000 [K]         0.00000 [kcal/mol]
    angle-angle             0.000 [K]         0.00000 [kcal/mol]
 total torsion              0.000 [K]         0.00000 [kcal/mol]
    regular                 0.000 [K]         0.00000 [kcal/mol]
    improper                0.000 [K]         0.00000 [kcal/mol]
 total nonbond         -66216.674 [K]      -131.58682 [kcal/mol]
    intramolecular          0.000 [K]         0.00000 [kcal/mol]
    2-body nonbond     -64411.803 [K]      -128.00015 [kcal/mol]
    3-body nonbond          0.000 [K]         0.00000 [kcal/mol]
    tail correct.       -1804.872 [K]        -3.58667 [kcal/mol]
 external field       -520146.261 [K]     -1033.64289 [kcal/mol]
 solvation               0.000 [K]         0.00000 [kcal/mol]
 total classical      -586362.9351 [K]         -1165.229714
[kcal/mol]
Averages                Units Type       Box  1
 Volume                  nm^3       0.73860E+02
 Volume^2                nm^6       0.54552E+04
 Molecule Number                1        0.000
 Molecule Number                2      316.597
 Molar Volume          ml/mol       0.14049E+03
 Specific Density        g/ml        0.11419068
 Number Density          nm-3    1      0.00000
 Number Density          nm-3    2      4.28647
 Mole Fraction                   1    0.0000000
 Mole Fraction                   2    1.0000000
 Radius of Gyration        A     1    0.0000000
 Radius of Gyration        A     2    0.0000000
 Ideal Pressure          kPa       0.17650E+05
 Ideal p_i <N/V>kT       kPa     1 0.00000E+00
 Ideal p_i <N/V>kT       kPa     2 0.17650E+05
 Total Classical           K       -0.5570E+06
 Inter vdw                 K       -0.6250E+05
 Angle                     K        0.0000E+00
 Torsion                   K        0.0000E+00
 Intra vdw                 K        0.0000E+00
 External Field            K       -0.4945E+06
 Vibration                 K        0.0000E+00
 Coulomb                   K        0.0000E+00
 Tail vdw                  K       -0.1653E+04
 Solvation                 K        0.0000E+00
 u (Density)               K     2    -2856.922
 u (NVT Insertion)         K     2     -293.360
 u (NpT Insertion)         K     2     -293.360
 u (Den. + NVT Insert)     K     2    -3150.282
 u (Den. + NpT Insert)     K     2    -3150.282
 u (Gibbs Total)           K     2    -3150.244
 G: Sum{<u_i><N_i>}   kJ/mol       -0.8292E+04
 U                    kJ/mol       -0.4631E+04
 Henry Law (Residual)    MPa     1 0.17645E+02
```

```
Block Averages (  5 blocks) Units Type Box Average      Standard
Deviation
 Specific Density            g/ml        1  0.11419E+00  0.63663E-03
 Total Classical                K        1 -0.55698E+06  0.40576E+04
 Inter vdw                      K        1 -0.62499E+05  0.79562E+03
 Angle                          K        1  0.00000E+00  0.00000E+00
 Torsion                        K        1  0.00000E+00  0.00000E+00
 Intra vdw                      K        1  0.00000E+00  0.00000E+00
 External Field                 K        1 -0.49449E+06  0.34016E+04
 Vibration                      K        1  0.00000E+00  0.00000E+00
 Coulomb                        K        1  0.00000E+00  0.00000E+00
 Tail vdw                       K        1 -0.16526E+04  0.18593E+02
 Solvation                      K        1  0.00000E+00  0.00000E+00
 u (Gibbs Total)                K    2   1    -3150.016       11.608
 u (NpT Insertion)              K    2   1     -293.157       10.946
 u (NVT Insertion)              K    2   1     -293.157       10.946
 Number Density              nm-3    1   1  0.00000E+00  0.00000E+00
 Number Density              nm-3    2   1  0.42865E+01  0.23898E-01
 Mole Fraction                       1   1    0.0000000    0.0000000
 Mole Fraction                       2   1    1.0000000    0.0000000
 Molarity                       M    1   1  0.00000E+00  0.00000E+00
 Molarity                       M    2   1  0.71204E+01  0.39697E-01
 Radius of Gyration             A    1   1      0.00000      0.00000
 Radius of Gyration             A    2   1      0.00000      0.00000

 -----block averages ------
Box:    1
Block Energy         Density        Virial Press.  Mol fracs
    1 -.55400291E+06 0.11373475E+00 0.00000000E+00 0.00000000 1.00000000
    2 -.55661973E+06 0.11409175E+00 0.00000000E+00 0.00000000 1.00000000
    3 -.56122499E+06 0.11478985E+00 0.00000000E+00 0.00000000 1.00000000
    4 -.55129817E+06 0.11331738E+00 0.00000000E+00 0.00000000 1.00000000
    5 -.56177825E+06 0.11501965E+00 0.00000000E+00 0.00000000 1.00000000
Please see towhee_citations for a list of suggested citations for this
simulation
```

B.3: UiO-66-UA force field file.

```
towhee_ff Version
          14
Number of Nonbonded Types
          7
Potential Type
Lennard-Jones
Classical Mixrule
Lorentz-Berthelot
Atom Type Number
           1
Nonbond Coefficients
    2.783
   34.724
    0.0
    0.0
Mass
    91.224
Element
 Zr
Bond Pattern
null
Base Charge
    0.0
Polarizability
    1.0
Force Field Name
UiO-66Zr
Atom Names
Zr1
none
none
none
Atom Type Number
           2
Nonbond Coefficients
     3.88
    21.0
     0.0
     0.0
Mass
    12.011
Element
 C
Bond Pattern
null
Base Charge
    0.0
Polarizability
    1.0
Force Field Name
UiO-66Zr
Atom Names
C13
```

```
none
none
none
Atom Type Number
           3
Nonbond Coefficients
     3.74
    48.0
     0.0
     0.0
Mass
    12.011
Element
 C
Bond Pattern
null
Base Charge
    0.0
Polarizability
    1.0
Force Field Name
UiO-66Zr
Atom Names
C25
none
none
none
Atom Type Number
           4
Nonbond Coefficients
     2.925
    66.5
     0.0
     0.0
Mass
    15.999
Element
 O
Bond Pattern
null
Base Charge
    0.0
Polarizability
    1.0
Force Field Name
UiO-66Zr
Atom Names
O1
none
none
none
Atom Type Number
           5
Nonbond Coefficients
     3.02
    93.0
     0.0
```

```
     0.0
Mass
    15.999
Element
 O
Bond Pattern
null
Base Charge
    0.0
Polarizability
    1.0
Force Field Name
UiO-66Zr
Atom Names
O25
none
none
none
Atom Type Number
           6
Nonbond Coefficients
     3.2
    80.0
     0.0
     0.0
Mass
    15.999
Element
 O
Bond Pattern
null
Base Charge
    0.0
Polarizability
    1.0
Force Field Name
UiO-66Zr
Atom Names
O29
none
none
none
Atom Type Number
           7
Nonbond Coefficients
     3.95
    46.0
     0.0
     0.0
Mass
     1.0078
Element
 C
Bond Pattern
null
Base Charge
    0.0
```

```
Polarizability
    1.0
Force Field Name
UiO-66Zr
Atom Names
C1
none
none
none
Number of Bonded Terms
          0
Number of Angle Terms
          0
Number of Torsion Terms
          0
Number of Improper Terms
          0
Number of Angle-Angle Terms
          0
Number of One-Five Types
          0
Number of Bond Increments
          0
```